FLEXURAL RESPONSE OF MASONRY ELEMENTS STRENGTHENED WITH EPOXY-BONDED ELASTOMERIC FIBER REINFORCED FILMS

A Thesis
Presented to
The Academic Faculty

By

Melanie Ann Parker

In Partial Fulfillment
Of the Requirements for the Degree
Master of Science in Civil Engineering

Georgia Institute of Technology
December 2006

FLEXURAL RESPONSE OF MASONRY ELEMENTS STRENGTHENED WITH EPOXY-BONDED ELASTOMERIC FIBER REINFORCED FILMS

Approved by:

Dr. David W. Scott , Chair
School of Civil and Environmental Engineering
Georgia Institute of Technology

Dr. Stanley Lindsey
School of Civil and Environmental Engineering
Georgia Institute of Technology

Dr. Cameron Coates
School of Computing
Armstrong Atlantic State University

Date Approved: August 22, 2006

ACKNOWLEDGEMENTS

First, I would like to thank my thesis advisor, Dr. David Scott, for his patience, encouragement, and support throughout the duration of this research program. His complete confidence in my abilities was essential to the successful completion of this work. I would also like to express my gratitude to Dr. Stanley Lindsey and Dr. Cameron Coates for serving on my thesis committee, and to Carol Johnson and the other ERDC personnel that made this research possible.

I would also like to sincerely thank my good friends and colleagues, Evan Bennett and Kevin Smith, for their assistance and friendship during the early stages of my research. Without them, many aspects of this study would have been overwhelming. I would also like to extend deep gratitude to Heather Wilburn, Justin Hodges, Ryan Purvis, and Neil McKenzie for their contributions to this work.

In addition, I would like to thank all of my friends and family who have helped me through all the difficult times along the way. I owe much of my success to my wonderful parents that have supported me in all of my endeavors. I love and appreciate them very much.

Finally, my heartfelt thanks go to my Lord and Savior, Jesus Christ. There are many times throughout this study that I felt overwhelmed and turned to Him for comfort and strength. I could not have been successful without His guidance.

TABLE OF CONTENTS

LIST OF TABLES

LIST OF FIGURES

NOMENCLATURE

A_0	original cross-sectional area of coupon
A_1	cross-sectional area of coupon at ultimate or proportional limit
A_e	cross-sectional area of epoxy bond layer
A_f	cross-sectional area of film reinforcement
b_f	width of film reinforcement
b_m	width of masonry block
c	neutral axis depth
C_m	compressive force in masonry
COV	coefficient of variation
d_m	depth of masonry block
d_t	depth of trowel grooves
E	modulus of elasticity
f_e	tensile stress in epoxy bond layer
$f_{e,avg}$	average tensile stress in epoxy bond layer
$f_{e,max}$	epoxy ultimate tensile strength
f_e*	effective tensile stress in epoxy bond layer
f_f	tensile stress in film reinforcement
f_{fe}	effective tensile stress in film reinforcement
$f_{f,required}$	required tensile stress in film reinforcement

$f_{f=PL}$	tensile stress in film reinforcement at proportional limit
$f_{f=PL,true}$	true stress in film reinforcement at proportional limit
$f_{f,true}$	true stress in film reinforcement
$f_{f,max}$	ultimate tensile strength of film reinforcement
f'_m	compressive strength of masonry
M_n	nominal moment capacity
M_{max}	maximum experimental moment capacity
t_0	original thickness of tensile test coupon
t_1	thickness of tensile test coupon at ultimate or proportional limit
t_e	thickness of epoxy bond layer
t_{rf}	thickness of reinforced film
t_{uf}	thickness of unreinforced film
T_e	epoxy component of total tensile force
T_f	film reinforcement component of total tensile force
T_T	total tensile force
w_0	original width of tensile test coupon
w_1	width of tensile test coupon at ultimate or proportional limit
ε_e	tensile strain in epoxy bond layer
ε_{mu}	limiting compressive strain in masonry
φ	proposed strength reduction factor

SUMMARY

This thesis presents results from an experimental investigation pertaining to the structural response of masonry elements reinforced with hybrid elastomeric/fiber materials. Material characterization was performed on various reinforced and unreinforced elastomeric materials to identify those materials that were best suited for use as structural retrofits. A new test fixture was developed for tensile testing in order to overcome problems encountered with traditional wedge grips due to the extreme deformation capacity of the tested materials. After material characterization was completed, the three most promising material systems were selected for further investigation. Static four-point bending tests were performed on two-span masonry elements joined with a central mortar joint and strengthened with the three selected material systems. The three reinforcing schemes examined included an unreinforced film, a reinforced film with fibers oriented at 0/90º, and a reinforced film with fibers oriented at +/- 45º. Retrofit materials were adhered to the masonry with a two-part epoxy applied using a trowel. Strain gages were applied to the tension and compression sides of selected specimens of each reinforcing scheme to estimate the strain distribution through the heterogeneous cross section. A linear variable displacement transducer (LVDT) and a load cell were employed to obtain load-deformation data for each tested specimen. The experimental load-deformation response was used, along with material characterization results, in the development of a semi-empirical model to predict the static moment

capacity of the strengthened masonry system. It is expected that this model will be used in the development of reliable design criteria for masonry walls strengthened with these advanced materials.

CHAPTER I

INTRODUCTION

1.1 INTRODUCTION

Recent history has shown a marked increase in the necessity for heightened security in civilian structures as well as federal buildings and military installations. Events such as the bombing of the Murrah building in Oklahoma City have illuminated the need for structures that have a greater resistance to non-traditional loading regimes such as air blast. Where new construction is taking place, the dimensions of critical structural elements may be increased, or the overall structural design may be modified to enhance the survivability of the structures from these types of loadings. However, these measures are not applicable to structures already in service. As such, effective technologies must be developed to retrofit existing structures to better withstand the effects of short-duration shock events, which can involve impact loading or air blast.

In developing these technologies, the most common method involves the use of externally applied reinforcement to increase the static and dynamic load capacity of critical structural elements. Steel plates and post-tensioned rods and cables have been employed with varying degrees of success. Installation time, maintenance and aesthetic challenges have prompted researchers to investigate the use of advanced materials such as fiber-reinforced polymers (FRP) as an alternative to traditional construction materials. The term “fiber reinforced polymer” refers to a class of materials that consist of a combination of a polymer matrix and a reinforcing agent that combine to perform a discernable reinforcing function in one or more directions. FRPs are useful in civil infrastructure because of their light weight, high strength, non-corrosive, and non-

magnetic characteristics. This technology is already employed in the civilian sector for the static strengthening of bridges, buildings, and other structures. With this as a starting point, several researchers have undertaken exploratory investigations to evaluate the effectiveness of the use of these materials for retrofit against blast loading.

Recently, researchers with the U.S. Air Force and U.S. Army have begun to investigate elastomeric rather than polymeric materials for use in protective retrofits. Since one of the most dangerous aspects of blast response is debris hazard, retrofit techniques that lend ductility to the structure instead of simply strengthening the structure may be more beneficial. (Johnson, et al, 2003)

1.2 SCOPE AND OBJECTIVES

This thesis presents results from an experimental investigation pertaining to the structural response of masonry elements reinforced with hybrid elastomeric/fiber materials. Material characterization was performed on various reinforced and unreinforced elastomeric materials to identify those materials that were best suited for use as structural retrofits. A new test fixture was developed for tensile testing in order to overcome problems encountered with traditional wedge grips due to the extreme deformation capacity of the tested materials. After material characterization was completed, the three most promising material systems were selected for further investigation. Static four-point bending tests were performed on two-span masonry elements joined with a central mortar joint and strengthened with the three selected material systems. The three reinforcing schemes examined included an unreinforced film, a reinforced film with fibers oriented at 0/90º, and a reinforced film with fibers oriented at +/- 45º. Retrofit materials were adhered to the masonry with a two-part epoxy

applied using a trowel. Strain gages were applied to the tension and compression sides of selected specimens of each reinforcing scheme to estimate the strain distribution through the heterogeneous cross section. A linear variable displacement transducer (LVDT) and a load cell were employed to obtain load-deformation data for each tested specimen. The experimental load-deformation response was used, along with material characterization results, in the development of a semi-empirical model to predict the static moment capacity of the strengthened masonry system. It is expected that this model will be used in the development of reliable design criteria for masonry walls strengthened with these advanced materials.

CHAPTER II

PREVIOUS WORK

Numerous studies have been performed investigating both the static and dynamic out-of-plane response of fiber reinforced polymeric and elastomeric materials used as structural retrofits. Reviewed in the current study are a number of investigations pertaining to the static out-of-plane capacity of masonry retrofits, the dynamic out-of-plane capacity of concrete retrofits, and the dynamic out-of-plane capacity of masonry retrofits.

2.1 STATIC TESTING OF MASONRY RETROFITS

Gilstrap, Dolan, and Christensen (1995) evaluated the use of aramid fabric reinforcement for masonry walls. Kevlar 49® fabric was adhered to brick beams that were supported at their ends and loaded to failure with a center point load. Two brick mortar walls simply supported on all sides were also reinforced and tested under quasi-static uniform loading. The ultimate flexural strength of both the beams and walls were recorded and compared to strength calculations made using the yield line theory. Researchers determined that the actual crack patterns observed during testing were consistent with theoretical crack patterns and that using Kevlar fabric reinforcement is highly effective for seismic upgrade of masonry walls.

Triantafillou (1998) studied the strengthening of unreinforced masonry structures using epoxy-bonded FRP laminates. The effects of FRP reinforcement on masonry strength were examined for out-of-plane bending with axial force, in-plane bending with axial force, and in-plane shear with axial force. A total of 12 small-scale wall specimens were constructed using perforated clay units and tested statically in four-point bending.

Six walls were tested in-plane and six were tested out-of-plane. Four of the six walls in each type of loading were reinforced with epoxy-bonded unidirectional CFRP laminates while the other two were used as unreinforced control specimens. Reinforcing of the walls tested in out-of-plane bending consisted of either two or four CFRP laminates bonded to their tension face. The walls were loaded to failure using a hydraulic testing system.

All four CFRP-reinforced walls tested out-of-plane failed by crushing of the masonry in the compression zone. Theoretical predictions of the failure load were made using the area fraction in the vertical direction and mechanical properties determined in tension and compression tests performed on the masonry units and FRP strips prior to the wall tests. The area fraction in one direction is defined as the total cross-sectional area of the FRP divided by the corresponding wall area.

The increase in out-of-plane bending capacity depends on the product of the area fraction and the elastic modulus of the FRP. Therefore, laminates with higher stiffnesses were found to be more efficient in masonry reinforcement. The experimental failure loads of the strengthened specimens were approximately 10 times the failure loads of the unreinforced control specimens. This difference demonstrates the effectiveness of the CFRP strengthening technique.

Gilstrap and Dolan (1998) examined the use of high-performance fibers for reinforcing masonry structures with an emphasis on out-of-plane bending. Two phases of testing were conducted. The first phase evaluated adhesives using small-scale brick beam tests. The second phase involved the retrofit and testing of unreinforced masonry walls. For the second phase of testing, different sizes of walls were reinforced using

various types of FRP reinforcement and adhesives. A total of seven walls were tested, including six reinforced walls and one control specimen.

Two walls, blanketed with full sheets of Aramid fabric and simply supported on all sides, were placed horizontally on a test frame with the reinforcement on the bottom. A vertical static load was applied through a loading plate at the center of the wall, and foam pad was used to distribute the load throughout the wall.

The second set of tests was performed on two walls reinforced with Kevlar tapes. The tapes were adhered at third points on each of the two walls in the transverse and longitudinal directions using similar high viscosity adhesives. These two walls were subjected to the same loading as the first two walls but they were simply supported. The failure mode was rupture of the tape followed by a secondary compressive failure.

Carbon reinforcements were used on the remaining two walls. The first wall had a carbon tow sheet applied in two layers. The second wall had carbon straps applied at the third points of the wall along its width. Failure was governed by the compression strength of the wall because the walls were over-reinforced.

The predicted values for the moment capacity were determined using yield line analysis or simple bending theory based on the tensile capacity of the composite. The failure mode that actually occurred sometimes differed from the failure mode used to predict the moments. This resulted in over and under-predictions of up to approximately 800%.

Ehsani, Saadatmanesh, and Velazquez-Dimas (1999) examined the behavior of retrofitted unreinforced brick masonry walls subjected to cyclic out-of-plane loading. Three half-scale unreinforced masonry walls, constructed with solid clay brick, were used

for the testing. Each of the walls were retrofitted on both the north and south faces with three vertical composite strips of E-glass fabric, bonded using a two-component epoxy resin. The spacing of the vertical fabric strips remained constant and the height-to-thickness ratio of each wall was 14. Varying percentages of composite reinforcement with respect to the balanced condition were applied to each face. A balanced condition is assumed to occur when the masonry reaches its compressive capacity at the same time that the composite material reaches its tensile capacity. The walls were simply supported at the top and bottom, and the other two sides remained free. Each wall was designated with the letter 'S' followed by the reinforcement ratio of the north and south faces of the wall, respectively.

A steel test frame consisting of two identical reaction frames was constructed for this experimentation. One reaction frame was located to the north and one was located to the south of the wall being tested. An airbag confined in a plywood box was used for applying the out-of-plane pressure to the wall surfaces. The load sequence consisted of a large number of cyclic displacements.

Wall S75/25 was first tested as a control specimen with no reinforcement. Under this condition, the wall failed by splitting in two pieces. The wall was then retrofitted and tested again. The south face was subjected to 21 cycles, while the north face supported 23 cycles. As the applied pressure increased with the cycles, both faces experienced progressive bed joint cracking and gradual delamination of the composite strips. Severe damage caused by delamination in the strips on the south face resulted in the test being terminated prior to failure. The load was stopped at a pressure of 259psf and a deflection of 0.63 inches, which was the maximum deflection observed in this study. This was done

in order to continue the test on the north face. Delamination also occurred on the north face, and peeling controlled failure in both faces. The north face supported a pressure of 648psf and deflected 0.60 inches before failing. This was the maximum pressure resisted by any of the specimens.

Failure occurred in the north face of wall S20/40 during the 16th cycle while the south face of the wall supported a total of 18 cycles. On the south face, the bottom half of the east and west strips, as well as the top half of the central strip peeled off completely. On the north face, the top half of the east strip peeled off, and the central and west strips delaminated almost 50% of their own areas. No tensile failure on the fabric was observed.

Wall S30/30 was retrofitted in a more efficient manner because of the excessive delamination observed in the first two wall tests. The fabric density was decreased by 50% in the tested direction and the width of the strips was increased by a factor of two. This helped to prevent delamination and resulted in a tensile failure of the fabric. Failure occurred during the 17th cycle on the south face, when the wall split into two pieces due to a wide horizontal crack that developed along the central bed joint. No failure occurred on the north face prior to the wall splitting.

The authors concluded that the ultimate flexural capacity of the tested walls was significantly increased. Deflections almost 14 times the maximum allowable deflection according to code specifications were recorded during testing. It was also concluded that GFRP composite strips are a good alternative for retrofitting masonry walls against lateral loads.

Albert, Elwi, and Cheng (2001) conducted an experimental program to determine the effectiveness of externally applied fiber reinforce polymers in increasing the load-carrying capacity of unreinforced masonry subjected to out-of-plane flexural loads. The effects of the type, amount, and layout of the fiber reinforcement, as well as the effects of a compressive axial load and cyclic behavior were all investigated. Ten masonry walls reinforced with externally applied FRP were subjected to primarily monotonically increasing lateral out-of-plane loads, and one wall was loaded cyclically. Each wall was simply supported and loaded using a hydraulic jack. The results demonstrated an increase in strength and ductility of the specimens strengthened with FRP as compared to the control beams.

Almusallam, Al-Salloum, and Alsayed (2001) studied the behavior of unreinforced masonry strengthened with fiber reinforced polymer composite materials. Six masonry walls were retrofit with glass FRP laminates and subjected to out-of-plane and in-plane flexural and shear stresses. The two walls tested in out-of-plane bending were strengthened with one layer of bidirectional GFRP laminate on the tension side. One of the flexural walls was also strengthened with one layer of GFRP on both sides. The out-of-plane flexural capacity was significantly enhanced by the addition of reinforcing materials and the authors viewed this as clear evidence that GFRP laminates are capable of holding the wall together and diminishing the danger of falling debris when a wall has been subjected to damaging blast loads.

Mosallam, Haroun, Almusallam, and Faraig (2001) performed an experimental investigation on the out-of-plane response of reinforced brick walls retrofitted with fiber reinforced polymer composites. Both carbon/epoxy and E-glass/epoxy composite

systems were applied to the tension side of brick wall specimens and the walls were subjected to out-of-plane loading and unloading cycles using a hydrostatic test setup. An analytical model based on a section analysis procedure similar to that used in the analysis of concrete beams was developed to predict wall behavior. It was determined that the experimental results demonstrated the potential of FRP composite retrofit systems as a successful alternative to upgrade the out-of-plane flexural behavior of unreinforced masonry brick walls. Significant increases in the flexural capacity were gained by the addition of reinforcement and the analytical model proved effective in predicting the maximum load of the retrofitted specimens.

Hamilton and Dolan (2001) investigated the flexural capacity of Glass FRP strengthened concrete masonry walls. The GFRP composite was composed of unidirectional E-glass fabric with an epoxy matrix. Their testing program consisted of four "short" wall and two "tall" wall tests conducted on unreinforced concrete masonry that was strengthened with GFRP. The "short" walls were nominally 2 feet long by 6 feet tall and the "tall" walls were nominally 4 feet long by 15 feet 4 inches tall. The thickness of each wall was approximately 8 inches. The short walls each had a single GFRP strip placed in the center of the wall and the tall walls each had 4 strips applied. One tall wall had 2 sets of double-layered strips, while the other tall wall had 4 single-layered strips applied directly to the surface of the wall. The strips were applied so that the fibers were perpendicular to the masonry bed joints. The strengthening systems were designed for the under-reinforced condition in order to avoid having to predict the strength of the over-reinforced cross section and to attempt to force the failure to occur in the FRP composite.

Prior to loading to failure, the specimens were loaded to approximately 25 psf to determine the serviceability behavior at a "working load." Each of the walls was then tested monotonically to failure using an air bag and reaction frame. The walls were set up in an erect position and the supports were designed to simulate a simple-span condition.

The short wall tests demonstrated two modes of failure, including GFRP fracture and a combination of GFRP fracture and delamination. The GFRP fracture occurred at the joint below the midspan, which was the location of the maximum moment. Masonry cracks were found to occur primarily at the mortar joints.

Results of the tall wall tests demonstrated that the lateral capacity of the strengthened walls is equivalent to a similar wall with #5 Grade 60 reinforcing bars spaced at 2 ft along the mid-thickness of the wall. The load capacity was reached for each of the tall walls at approximately 3 inches of deflection.

The tensile capacity of the GFRP strips was determined in other testing and used along with a derived flexural capacity equation to predict the moment capacity of the tested specimens. The capacity equation for the under-reinforced condition was found using equilibrium as

$$M_n = T_{gu}\left(d - \frac{a}{2}\right) \tag{2.1}$$

where M_n= nominal moment capacity in flexural bending, a = depth of the equivalent stress block, and T_{gu} = strap capacity. The prediction was found to be unconservative by 10-20%.

Hamoush, McGinley, Mlakar, Scott, and Murray (2001) investigated the effectiveness of using fiber-reinforced composite overlays to strengthen existing

unreinforced masonry walls to resist out-of-plane static loads. Fifteen walls were tested to failure under a uniformly applied out-of-plane load. Two fiber composite configurations were evaluated during the testing program. The first configuration consisted of a woven fabric with E-glass rovings in the orthogonal direction. The fabric was stabilized with Kevlar yards used as weft in the other direction. Six of the wall specimens were retrofitted with this configuration using two layers of unidirectional bands on the tension side, one in the horizontal direction and one in the vertical direction. The second configuration was formed using a continuous web fabric overlay with Tyfo Hi-Clear epoxy. This configuration was also applied to six wall specimens using two layers of web fibers covering the entire wall area on the tension side. The 15 wall specimens were divided into five groups of three identical walls for testing. The first was a control group and had no external reinforcement. The other four groups were formed by grouping the specimens according to composite configuration and surface preparation technique. Three walls with each composite configuration (total of six) were sand blasted using an air gun and three of each configuration were cleaned manually using a wire brush.

Each of the walls tested was simply supported in a vertical testing frame at the top and bottom using circular pipe supports, and uniform out-of-plane lateral loads were applied using an air-bag wall test apparatus.

Relatively large deformations were recorded in each of the wall specimens during the first increment of pressure. This initial deformation was determined to be a combination of rigid body movement of the walls caused by support seating and flexural deformation due to the beam curvature. Rigid body deflections were obtained for each

specimen and subtracted from the total deflection in order to determine the mid-span deflection.

Shear failure was found to dominate in this testing program. All of the reinforced specimens failed in shear with the exception of one specimen, which failed prematurely in bending. This was possibly due to an imperfection in the block alignment at the mid-span mortar line. It was determined that the shear strength of the masonry walls systems has a major influence on the failure loads experienced by the system. Test results clearly demonstrated that the external reinforcements significantly enhanced the strength and stiffness of the wall specimens. However, the ultimate flexural strength was not achievable unless the premature failure by shear at the support is controlled.

A simplified analytical method was implemented to predict the ultimate flexural strength of the fiber-reinforced masonry wall systems. The method was based on several assumptions, including linear strain distributions through the full depth of the wall, small deformations, no tensile strength in the masonry blocks, and no interfacial slip between the fiber-reinforced composites and the masonry wall. Assumptions were also made for the compressive strength of the masonry and the elastic modulus of the composite systems. Based on these assumptions, the ultimate flexural strength of the composite walls systems was predicted to be reached at a loading of approximately 739.3psf for the web configuration and approximately 509.6psf for the unidirectional band configuration. As mentioned earlier, these loadings were not reached due to premature shear failure.

Tumialan, Galati, and Nanni (2003) performed a field assessment of unreinforced masonry walls strengthened with fiber reinforced polymer laminates by subjecting four full-scale unreinforced masonry walls to out-of-plane loading to failure. Researchers

identified a mechanism of failure not commonly observed in laboratory tests. Walls exhibited arching where crushing at the supports controlled the wall behavior. It was suspected that grouting of tile units at the support regions could have induced a different and preferable failure mode.

An analytical model based on mechanics of the section was presented for determining the transverse load, midheight deflection, and rotations at the supports that the walls were able to resist. Results demonstrated good agreement with experimental results and it is believed that the model could easily be modified to take into account distributed loads acting on strengthened unreinforced masonry walls.

Patoary and Tan (2003) investigated the static out-of-plane behavior of masonry walls strengthened with fiber-reinforced polymer (FRP) composites and proposed a method to estimate the blast resistance of the strengthened walls from the static test data. Four rectangular concrete frames were constructed with 79 x 59 inches openings to house a masonry test specimen. Each of the four walls were strengthened with two layers of a uni-directional glass (MP2G), carbon (MP2C and MP2CI) or bi-directional fiberglass woven roving (MP2WR) fiber fabrics externally bonded to the tension face of the wall. To further increase the wall strength, steel T-section stiffeners were installed on Specimen MP2CI. A uniformly distributed load was applied to the wall specimens using a Kevlar reinforced airbag. At ultimate load, the three specimens without any intermediate stiffener failed explosively by crushing of the bricks. At the same time, debonding of the FRP system occurred at the sides of the walls for the specimens reinforced with glass of carbon FRP sheets and the specimen reinforced with fiberglass

woven roving experienced fiber rupture. The specimen with the T-section stiffener failed gradually by yielding of the stiffener.

A dynamic load factor, defined as the ratio of the maximum dynamic deflection to the deflection that would have resulted from the static application of the peak load or pressure, was used to predict the blast response of the masonry walls. Charts from the US Army's TM5-855-1 were used to determine the blast resistance of the reinforced masonry walls in terms of TNT charge.

It was concluded that the FRP system provided significant improvement in the wall's response to out-of-plane loadings. Failure was caused by debonding and peeling of the fiber fabric at the edges for walls with a high reinforcing index, and by fiber rupture for those with a low reinforcing index.

Tumialan, Galati, and Nanni (2003) researched the flexural behavior of unreinforced masonry (URM) walls strengthened with externally bonded FRP laminates. They also examined the effects of putty filler on the bond strength. The experimental program consisted of 25 masonry walls; twelve built with concrete blocks and 13 with clay bricks. Glass FRP and Aramid FRP laminates were used to strengthen the masonry along the longitudinal axis on the tension side. Putty filler was used on some specimens to fill small surface voids and provide a leveled surface to which the FRP could be adhered. Reinforcing strip widths ranged from 3 – 12 inches.

The strengthened URM walls were subjected to out-of-plane loads and exhibited three failure modes: debonding of the FRP laminate, flexural failure (rupture of the FRP in tension or crushing of the masonry in compression), and shear failure in the masonry near the support.

Test results demonstrated an increase in strength and stiffness of the FRP strengthened walls as compared to the URM specimens. It was observed that, depending on the amount of reinforcement, increments ranging from 5 to 25 times the nominal moment capacity were achieved. The controlling failure mode was determined to be debonding of the FRP laminate.

A model was developed to predict the flexural capacity of simply-supported strengthened walls based on strain compatibility, internal force equilibrium, and the controlling failure mode. The proposed design method provided reasonable estimates of the flexural capacities of masonry walls with externally bonded FRP laminates.

Nanni and Tumialan (2003) evaluated the effectiveness of various FRP composite material systems used to strengthen masonry structures. They also examined different installation techniques. Emphasis was placed on externally bonded laminates, near surface mounted bars, and post-tensioning. Experimental test programs dealing with the out-of-plane and in-plane behavior of strengthened masonry walls were reviewed. After reviewing numerous programs, the authors concluded that depending on the amount of FRP reinforcing, increments ranging from 3 to 14 times the URM flexural capacity were achieved. Test results demonstrated a consistent pattern of initial cracking occurring in the mortar bed joint or at the interface of the mortar and block. As the amount of reinforcing increased, it was observed that the prevalent failure mode transitioned from debonding and flexural failure to shear failure.

Tan and Patoary (2004) investigated the load-deflection response of masonry brick walls strengthened with FRP systems when subjected to transverse loads. A simple analytical model was developed to predict the strength of the walls based on four

potential failure modes, including punching shear through the bricks, crushing of the brick in compression, tensile rupture of the FRP reinforcement, and debonding of the FRP reinforcement at the interface.

To determine the punching shear strength, the FRP strengthened wall was considered analogous to a steel-reinforced concrete slab. An equation was taken from the British Standards Institute BS8110 and modified for use with FRP strengthened masonry walls by considering an equivalent reinforcement ratio and by adjusting the critical punching shear perimeter based on experimental observations. The area of FRP reinforcement was transformed into an equivalent steel area and the ultimate punching shear strength was estimated by

$$P_u = 3.16h(r + 2h)\left(100\frac{E_f}{E_s}\frac{A_f}{bh}\right)^{1/3}\left(\frac{400}{h}\right)^{1/4} \qquad (2.2)$$

for the case of a wall subjected to a concentrated load over a square area with a width r, where E_f = Young's modulus of FRP reinforcement; E_s = Young's modulus of steel; A_f = area of FRP reinforcement; b = width of the wall specimen; and h = thickness of the wall specimen. The critical perimeter was determined to be approximately located at a distance h from the edge of the loaded area.

The moment capacity in the case of flexural compression failure for the strengthened masonry wall was approximated based on strain compatibility as

$$m = 0.67 f_k b(0.75x)\left(\frac{h}{2} - 0.375x\right) + A_f E_f \varepsilon_f \left(\frac{h}{2}\right) \qquad (2.3)$$

where f_k is the characteristic compressive strength and x is the neutral axis depth. Assuming the same stress-strain relation as with compression failure, the moment capacity of the section in the case of flexural rupture failure can be approximated as

$$m = A_f f_{fu}(h - 0.375x) \tag{2.4}$$

where f_{fu} $(= E_f \varepsilon_{fu})$ = ultimate tensile strength and ε_{fu} = ultimate tensile strain of the FRP laminates.

The moment capacity in the case of bond failure was derived based on a previous model developed by Bisby and Green (2000). The model is based on shear lag theory and is only valid in the elastic range. Using essentially the same model, the moment capacity is derived as

$$m = A_f E_f \varepsilon_f \left(h - \frac{x}{3} \right) \tag{2.5}$$

where ε_f is determined based on the calculated limiting force in the FRP laminates that can be applied on the FRP sheet before bond damage occurs. This value is based on a peak shear stress of 8 MPa as suggested by Bisby and Green.

In the case of a square wall with side dimension *L* and subject to a transverse load over a square area of width *r*, the maximum ultimate load supported by the wall can be approximated by

$$P = \frac{8m}{L - 0.5r} \tag{2.6}$$

The value of *m* is substituted from the equation derived for the moment capacity based on the mode of failure observed during testing.

The test specimens were grouped into five series based on the type of FRP reinforcement. One wall was tested with no reinforcement and served as a reference. Three anchorage systems were applied separately on three walls for each type of FRP system to examine the success of each. These systems included bond improvement through grinding and roughening of the wall surface, the use of fiber anchor bolts, and

the use of bars embedded in grooves on the wall surface. Series I – III specimens were tested under a concentrated load, while Series IV and V specimens were tested under a patch load using an air bag. Each wall was laid horizontal with the bonded side facing downwards and simply supported along four sides.

Delamination of the reinforcement occurred in the specimens that did not have an adequate anchorage system. All other specimens failed by punching shear or crushing of the brick in compression except one of the Series V specimens, which failed by fiber rupture.

It was concluded from this series of tests that the load-carrying capacity of masonry walls is significantly increased with the addition of FRP reinforcement, especially when premature failure is prevented through appropriate surface preparation or anchorage system. The FRP bolt anchorage system itself was determined to add stiffness to the systems to which it was applied, and further increased the load-carrying capacity of those walls. It was also concluded that in general, the proposed model predicts the wall strengths with reasonably good accuracy.

Hutchinson, Nicolaisen, and Morrill (2004) conducted an experimental program to investigate the feasibility of retrofitting masonry walls with different polyurethane and polyurethane-fiber combinations. Nine wall sections were tested under combined out-of-plane and axial compression loading to simulate the blast load distribution.

Specimens were loaded in axial compression to a target of approximately 10% of the mortar compressive strength, and then the out-of-plane monotonic load was applied using a four-point load spreader. Each of the tested specimens was coated on the tensile

face with the different polyurethane or polyurethane-fiber combinations. The coatings were applied using a nozzle spray system.

Specimens that were fiber-reinforced consisted of fibers of Type N or Type R that were applied in one or two layers and embedded between the approximately 6.4 mm thick polyurethane coating applications. The Type N fiber is characterized as a stiff, tightly spaced carbon fiber, while the Type R fiber consists of a broader spaced fine-mesh carbon fiber. Test results provided a comparison between the performance of the two types of polyurethanes and fibers, and examined the effect of the thickness of the retrofit. Experimental load-deformation resistance curves indicate that Type I provides superior strength and ductility enhancement. Specimens reinforced with Type I polyurethane were observed to elongate plastically until the loading machine exceeded tensile stroke while Type II reinforced specimens failed in a sudden brittle cross-grain mode. Test results also indicate that Type R fiber provides a greater strength enhancement than Type N for the type and thickness of polyurethane. It was also determined that thicker layers of polyurethane also enhanced the performance of the masonry, but the strength increase was not proportional to the increase in thickness. For example, tripling the thickness of the layer resulted in only a 25% increase in strength. Specimens with thicker layers of polyurethane also experienced some undesirable debonding at the polyurethane-brick interface. Results indicate that even a thin layer of polyurethane can greatly enhance the out-of-plane performance and stability of the masonry wall system. This provides evidence that these retrofits will also enhance impact resistance of brittle masonry structures.

2.2 DYNAMIC TESTING OF CONCRETE RETROFITS

Jerome and Ross (1996) investigated the dynamic response of concrete beams externally reinforced with carbon fiber reinforced polymers subjected to impulsive loads. A series of strengthened laboratory scale beams were tested both statically in three point bending and dynamically using a drop weight impact machine. The beams were externally reinforced on the tension side with one, two, or three ply graphite epoxy panels. In addition to this, some specimens were reinforced on their sides with a three ply CFRP. Midspan displacements and strain measurements were recorded and a high speed framing camera was used to record the beam's displacement-time behavior.

It was concluded that the average static peak bending load was always less than the dynamic peak bending load, even at the lowest drop heights. It was also observed that the dynamic fracture energy was larger than the static fracture energy for the plain concrete control beams, but the opposite was true for the CFRP reinforced beams. This was likely because the addition of CFRP stiffened the beams and therefore enhanced their brittle behavior when loaded dynamically. Beams with three ply CFRP on the bottom and sides had the highest load, displacement, and fracture energy capacities of all beams tested both statically and dynamically, as expected. However, the authors concluded that the addition of just one ply provided tremendous gains as compared to the plain concrete beams.

Crawford, et al (1997) conducted analyses to demonstrate the effectiveness of jacketing columns of existing reinforced concrete buildings with composites to improve their performance in explosive loading events. Two building designs were analyzed in this investigation. One design was primarily for gravity loads and other consisted of

members designed to resist seismic loads. A hybrid model having both continuum and structural elements was used in this study to develop accurate numerical predictions of the structure's blast response. Various charge sizes and standoff distances were evaluated and it was concluded that a jacket can have a substantial beneficial effect on the performance of columns and serve to prevent structural failure of the building. However, it was noted that although failure was prevented, the jackets did not prevent the propagation of high pressures and debris within the building.

Barbero, Davalos, Kiger, and Shore (1997) explored the feasibility of using advanced composite materials (ACM) for retrofitting existing structures against blast pressure loads. Objectives and benefits of reinforcing structures using ACM were examined and current methods for reinforcing and testing reinforced concrete beams with glass and carbon fibers were outlined. It was noted that an ACM reinforced beam often fails by crushing of the concrete in compression. However, shear failure, delamination of the composite material, and tensile failure of the composite material have also been observed. It was concluded that the addition of advanced composite materials can significantly enhance the behavior of reinforced concrete beams by increasing both the strength and energy absorption response of the beam. Based on results of this investigation, it is anticipated that similar positive effects will be observed for ACM reinforced structures subjected to blast pressure loads.

Ross, Purcell, and Jerome (1997) examined the blast response of concrete beams and slabs externally reinforced with fiber reinforced polymers. Concrete beams were internally reinforced with 2 #5 steel reinforcing bars and externally reinforced with a three-ply ($0^{\circ}/90^{\circ}/0^{\circ}$) carbon fiber reinforced polymer laminate cemented to the bottom

and the sides. Slabs were internally reinforced with #5 steel reinforcing bars equally spaced and then retrofitted with a carbon fiber reinforced polymer angle ply laminate (0°/+/-45°/90°). All beams and slabs were simply supported and tested using C4 explosive at a specified standoff distance. Difficulties were encountered in data collection but the dynamic tests indicated that FRP retrofits will stiffen concrete structures and show an increased blast resistance. It was concluded that further tests were needed for CFRP and FRP retrofits subjected to dynamic loads, but results of this analysis were encouraging.

Jerome and Ross (1997) studied the impact resistance of concrete beams externally reinforced with fiber reinforced plastics. Lightweight concrete beams were externally reinforced with variable thickness carbon fiber reinforced strips and tested both statically and dynamically. Static tests were conducted in a load frame and dynamic tests were performed using a drop weight impact machine, specifically a Split Hopkinson Pressure Bar (SHPB). Results from the quasistatic and SHPB direct compression tests indicated that lightweight and normal weight concrete behave nearly identically when loaded quasistatically or dynamically in compression. Tremendous gains in load-carrying capacity were observed in the reinforced beams over plain concrete beams. Increases of 2 to 4 times the load capacity and 11 to 17 times the displacement capacity were easily achieved with the addition of the CFRP. Increases in energy absorption from 30 to 80 times the energy absorption of baseline concrete beams were also achieved. The authors concluded that the addition of external CFRP to the beam significantly stiffened the plain concrete beams, thereby enhancing the beam's brittle behavior when subjected

to impact loads. It was also concluded that failure mechanisms were similar for both static and dynamic loading conditions.

Scott and Mlakar (1998) applied pultruded carbon-fiber reinforced polymer (CFRP) strips to specimens that were designed to simulate typical reinforced concrete bridge girders at a scale of 1:7. The specimens were subjected to both static and dynamic loading.

For the static experiments, the concrete beams were loaded in three point bending. A control beam and a CFRP strengthened beam were both subjected to static loading at a uniform rate of 0.05 inches per minute. The CFRP material did not greatly affect the initial stiffness of the member, but it increased the ultimate flexural capacity of the concrete beams by approximately 40%.

A three point bending setup was selected for the dynamic experiments in order to readily compare the results to those obtained in the static testing. A nitrogen gas-hydraulic loading ram was used to apply a dynamic ramp load. The CFRP material was found to separate from the member during the dynamic testing. A post-test examination demonstrated that separation occurred in the concrete substrate rather than in the adhesive mortar used to bond the strips to the specimens. The experimental results indicated that the maximum dynamic load on the strengthened beam was approximately 130% greater than the static capacity of the control beam, and approximately 60% greater than the strengthened beam's own static capacity.

To better understand the dynamic response of the girder, a single degree of freedom analysis was performed in which the deflection of the midpoint was approximated by its equation of motion. A lumped parameter model was developed from

this analysis. It was found that the calculated deflection, as well as the measured deflection lags the load application due to the inertia of the girder.

Muszynski and Purcell (2003) studied the development, application, and effects of externally applied composite reinforced materials. Concrete structures were strengthened with two types of materials: an autoclave-cured, three-ply, carbon fiber-epoxy laminate, and a knitted biaxial E-glass fabric. The composite systems were tested in two phases. First, strengthened concrete beams were tested in flexure. Field testing was then conducted on reinforced interior walls and support beams of full-scale structures by subjecting them to air-blast loading at short stand-off distances.

To apply the retrofit materials, the walls were first cleaned and voids were filled. Primer was then applied and a thin layer of epoxy was applied to the reinforcing material. The reinforcing material was then pressed against the wall until the epoxy cure time was reached. Once the retrofits were applied, the walls were subjected to full-scale detonations of TNT.

Pressure and impulse data from the tests indicated that the tested structures should have failed catastrophically. However, although the reinforced walls experienced high displacements, they did not fail. The authors concluded that results of this study lend promise to this method of strengthening structures against air blast. They suggest, however, that further dynamic testing is necessary to quantify test results.

2.3 DYNAMIC TESTING OF MASONRY RETROFITS

Ward (2002) researched various methods available to strengthen existing masonry structures and provide resistance to the effects of blast attacks. The author listed six

methods available to reinforce existing masonry, including the following: (1) steel column and plate, (2) steel stud partition, (3) elastomer spray, (4) geotextiles, (5) retrofitted reinforced masonry, and (6) internal concrete skin. Advantages and disadvantages of retrofit systems were listed and the author's evaluation of each method of strengthening was presented.

Johnson, et al (2003) conducted static and dynamic tests to investigate the potential benefits of retrofitting hollow, unreinforced concrete masonry unit (CMU) walls with reinforced and unreinforced elastomeric materials. Eight static and 11 dynamic tests were performed on 1/4 scale CMU walls that were approximately 64-inches wide by 31-inches tall.

Seven different ¼ scale CMU wall retrofits were used in the static and dynamic tests. The 1st two walls were retrofitted with an unreinforced polyurea liner approximately 1/16 inch thick. One of the walls was retrofitted using a spray-on application (R1), and the other using a trowel-on application (R2). The next three wall retrofits consisted of a polyurea lining reinforced with Aramid fibers of varying lengths in an open weave fabric referred to as a scrim. A 100 pound-per-linear-inch (pli) and a 200 pli scrim with fiber orientations of 0/90 degrees and +/- 45 degrees were used in the experiment. The 3rd wall had a spray-on polyurea encompassing a 100 pli scrim applied at a 0/90 degree orientation(R3). The 4th wall was retrofitted with a spray-on polyurea encompassing a 100 pli scrim (R4), and the 5th wall a 200 pli scrim (R5), both applied at a +/- 45 degree fiber orientation. The 6th wall had a spray-on thermoplastic film(R6), and the 7th wall a polyurethane film (R7). One wall was tested with no retrofit and served as the control specimen (C1).

For the static testing, each of the seven walls was individually placed in a pressurized chamber. A neoprene diaphragm was used to administer the hydrostatic load. The test results revealed an increase in ultimate flexural resistance of the retrofitted CMU walls, and that reinforcing the polyurea materials significantly increased the stiffness of the materials as compared to the unreinforced polyureas. The CMU wall response was also clearly affected by the orientation of the reinforcement.

For the dynamic experiments, 20 lbs of Composition C-4 was placed on the ground at distances ranging from 19 feet to 25 feet from the front of the CMU wall. The standoff for each experiment was chosen based on the resistance functions obtained in the static experiments.

The unreinforced polyureas were determined to add some flexural resistance to the CMU wall, but the addition of the fiber scrim reinforcement significantly increased the wall performance. It was concluded that the increase in flexural resistance of the wall was directly related to the strength of the reinforcement and the orientation of the scrim fibers. Both static and dynamic experiments indicated that the spray-on method of application is indeed stronger than the trowel-on method.

Davidson, et al (2004) conducted tests at the Air Force Research Laboratory (AFRL) at Tyndall Air Force Base to determine the effectiveness of sprayed-on polymers to improve the blast resistance of unreinforced masonry walls. Three explosive tests were conducted during the first phase of testing. A highly reinforced reaction frame was constructed to house the 7’4 inch by 12 foot wall panels during testing. Two wall panels were placed in the reaction frame for each of the three tests. Explosive charges were detonated at designed standoff distances to apply a blast load to the wall panels. The

charge sizes and standoff distances were not provided due to the sensitive nature of the research.

The first test consisted of one control wall with no reinforcement and one retrofit wall panel. The polymer coating was applied to the interior face of the retrofit wall. The control wall collapsed after the blast but the retrofit wall remained intact. Since the wall did not reach a capacity limit, the explosive charge was doubled and the standoff distance was reduced by approximately 14% for the second test.

Both the control wall and the retrofit wall were completely destroyed in the second test. The polymer held much of the reinforced wall together, but the wall sheared from its supports due to the extreme energy of the blast. The polymer ripped across the mortar joint at approximately mid-height of the wall and the wall fell on top of itself in two pieces.

Prior to the third test, two additional test cubicles were constructed so that four walls could be tested. Each cubicle was 10 feet by 10 feet and housed one wall panel. One of the walls in the reaction frame had a ¼ inch polymer coating on the interior face that overlapped the roof and floor slabs by 12 inches, while the other wall in the reaction frame was coated with a 1/8 inch thick layer on both the interior and exterior faces with a 12 inch overlap. The walls in the test cubicles were each coated with a 1/8 inch layer of polymer on the interior face only. One of the cubicle wall panels had a 6 inch overlap and one had a 12 inch overlap. The explosive charge used in the third test was the same as the charge used in the second test, but the standoff distance was increased by approximately 30% over the first test.

The results of the explosive testing indicate that the polymer retrofit helped all of the wall panels to remain intact and prevented debris from entering the test structures. Researchers concluded that a sprayed-on polymer retrofit approach to strengthening masonry walls against blast loads is indeed an effective technique.

Fatt, Ouyang, and Dinan (2004) developed an equivalent single degree-of-freedom model that can be used to predict the dynamic response of a polymer retrofitted concrete brick wall subjected to a stand-off explosion. Model development was based on the results of tests conducted at the Tyndall Air Force Research Laboratory. The blast response of a brick wall coated with a layer of polyurea was evaluated and compared to results predicted using the proposed model. The model predictions compared very well with the results obtained using ABAQUS. Authors caution, however, that this model should only be used when the maximum deflection of the wall is expected to be greater than the wall thickness.

Davidson, et al (2005) studied failure mechanisms of polymer reinforced concrete masonry walls subjected to blast loadings. Thirteen spray-on polymers comprised of polyureas, polyurethanes, and a combination of the two were applied to full-scale unreinforced masonry walls. Effectiveness of the retrofit system was defined as the ability of the reinforcement to prevent catastrophic breaching or collapse of the wall that would cause harm to building occupants.

It was observed that a thin elastomeric coating on the interior face of unreinforced masonry walls can be effective at minimizing fragmentation and the potential for collapse of walls subjected to blast loads. It was also determined that the spray-on polymers bonded extremely well to the masonry. Static tests indicated that the bond is stronger

than the tensile strength of the masonry. This resolved the problem of delamination that is often problematic in fiber reinforced polymer retrofit systems.

Finite element results predicted that mortar bonds would fracture at early stages of flexure, resulting in relative displacement between two courses of block. This would cause high shear strains to develop in the polymer coating, emphasizing the importance of shear tearing resistance in the reinforcing material. Overall results indicated that a spray-on polymer reinforcement approach can be effective in enhancing the performance of unreinforced masonry when subjected to out-of-plane blast loads.

CHAPTER III

MATERIAL CHARACTERIZATION

3.1 INTRODUCTION

At the onset of this work, researchers at the U.S. Army Corps of Engineers Engineering Research and Development Center (ERDC) were in need of pertinent mechanical properties for materials being evaluated for use as structural retrofits for masonry walls subjected to air-blasts. Accurate characterization of material properties is also vital in the development of reliable predictive models that will form the basis of future design criteria. A dynamic testing program was underway at ERDC on ¼ scale unreinforced concrete masonry unit (CMU) walls strengthened with various elastomeric retrofits, and accurate material characterization was imperative to better understand the wall response to dynamic loads and to identify those materials that were best suited for use in structural applications. Numerous material systems were received and tested to help identify the most promising hybrid elastomer/fiber combinations for further investigation. The material systems were forwarded from ERDC researchers in two lots; these lots are designated "Stage I" and "Stage II" in the sections to follow.

3.2 CHARACTERIZATION OF ELASTOMERIC MATERIALS

3.2.1 Candidate Material Systems

3.2.1.1 Stage I Materials

During the first stage of dynamic testing by ERDC researchers, polyurea-based elastomeric materials originally designed for use in non-structural applications such as protective truck-bed liners were being examined as potential retrofit materials. Using a

spray-on or trowel-on technique, these materials were being applied to walls alone and with fiber scrim reinforcements. The blast performance of the various strengthened walls was then evaluated. Figure 3.1 shows various coupons harvested from panels of the Stage I materials that were fabricated in the field at the same time that wall retrofits were being constructed for dynamic testing. The materials were labeled based on the composition of the test panels developed for testing.

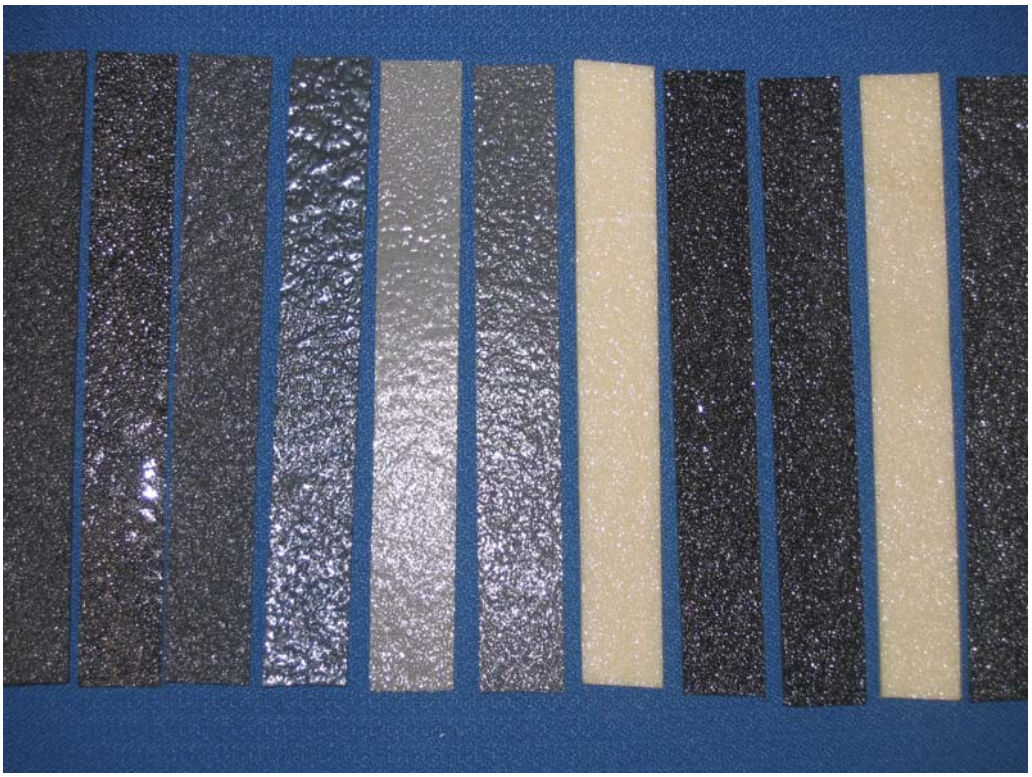

Figure 3.1: Stage I Material Coupons

3.2.1.2 Stage II Materials

Researchers at ERDC then began development of three new material systems that appeared more promising than the Stage I materials. These materials were pre-fabricated and then bonded to the walls, thus simplifying field installation. Figure 3.2 shows the three Stage II materials: an unreinforced elastomer, and two reinforced elastomers with

fiber orientations of 0/90° and +/- 45°. The reinforced films consist of an aramid fiber scrim between two layers of elastomer. Specific details regarding the chemical composition of the Stage II material systems are not available from the U.S. Army at this time due to security restrictions and proprietary agreements with material suppliers. Once the material systems are fully developed and in production, these details are expected to be made available for public release.

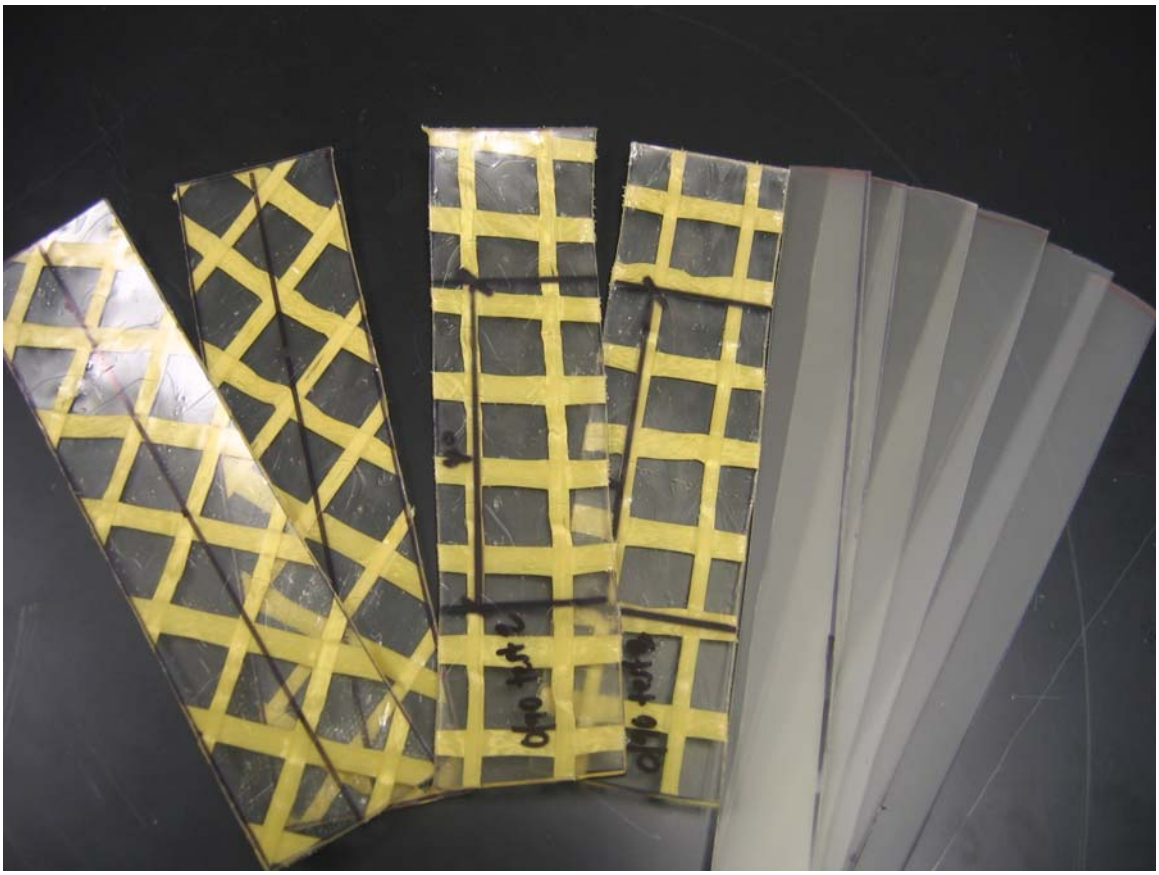

Figure 3.2: Stage II Materials

3.2.2 Tensile Testing of Elastomeric Material Systems

Determining the tensile stress-strain response for the elastomeric materials being used in the current investigation was critical to for two reasons; to identify those material

systems that held the most promise as structural retrofits, and to aid in the development of a reliable predictive behavioral model for the strengthened masonry wall elements. The stress-strain relationships were determined by performing standard direct tension tests on coupons cut from large panels and rolls of material provided by ERDC. Pertinent mechanical properties of the various elastomeric materials were obtained directly from the generated curves. ASTM D412 (tensile test specification for elastomers) and ASTM D3039 (tensile test specification for FRP materials) were referenced in the development of the tensile test procedures used in the current investigation. Coupon gage lengths were originally selected based on the minimum requirements mandated by the specifications. The minimum ASTM gage length was too long, however, to fail the Stage II materials and therefore had to be modified.

3.2.2.1 Stage I Materials

Stage I material tensile tests were performed using both servohydraulic and screw-type test frames as shown in Figures 3.3 and 3.4. Coupons were tested using the standard grips for both machines. Initial tests were performed on the servohydraulic test frame, but travel restrictions made it difficult or impossible to rupture the coupons. The screw-type test frame allowed approximately 3 times more travel, so it was used for the remaining tests for a total of 5 tests per material type. Coupons were cut 8 inches long and 1 inch wide from panels that did not have uniform thickness. This made it challenging to fabricate coupons suitable for testing. Load was applied at a rate of 1 inch per minute and an extensometer was used to measure strain until the specimens reached

3% strain, at which point the extensometer was removed to prevent damage at specimen failure. Results from this series of experiments are presented in Section 3.4.

Figure 3.3: Servohydraulic Test Frame – Stage I Material Testing

Figure 3.4: Screw-Type Test Frame – Stage I Material Testing

3.2.2.2 Stage II Materials

The existing wedge grips used to hold the Stage I materials during tensile testing were too narrow to accommodate the greater coupon width needed to properly measure the stress-strain response of the Stage II materials. In order to evenly distribute the load over the 2-inch-wide coupons, metal T-shapes were employed with C-clamps as shown in Figure 3.5. The stems of the T shapes were then inserted into the wedge grips of the load frame and a tensile load was applied at a rate of 0.75 in/minute.

Figure 3.5: Initial Tensile Testing Setup

After running approximately 2-3 tests on each retrofit material, it was determined that the test method needed modification. As the material deformed, the grips could no longer provide the necessary clamping force and the elastomer repeatedly slipped out of the grips before failure was reached. Due to the excessive deformation experienced during testing, the materials required a gripping mechanism that would continue to tighten as the cross-sectional area was reduced. Figures 3.6 - 9 show the details of the modified testing apparatus.

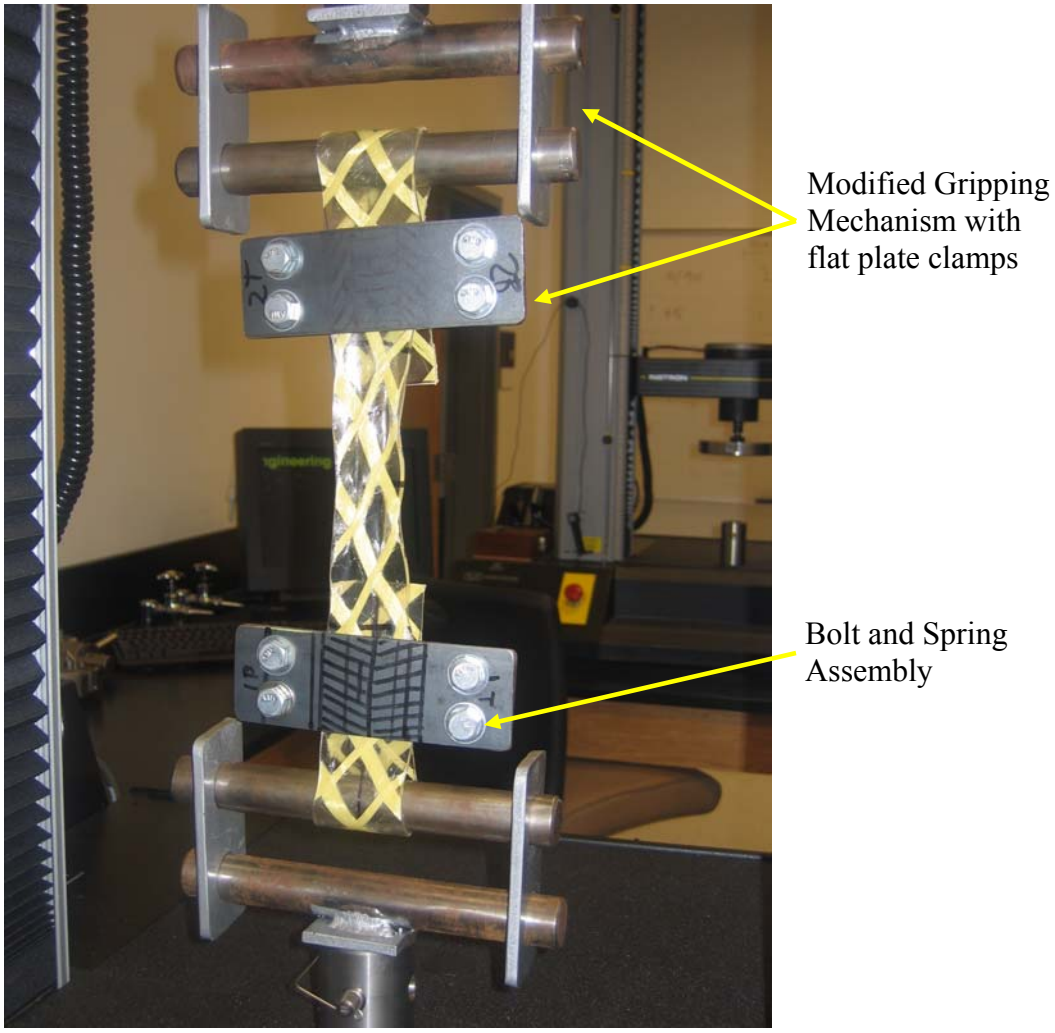

Figure 3.x: Modified Tensile Testing Apparatus

Each end of the elastomer was wrapped around the 1 inch round stock and clamped between two 5¾ inch x 2 inch x ⅛ inch flat steel plates using four ⅜ inch diameter stainless steel bolts and washers as shown in Figure 3.7. Springs were placed between the washers and the steel plates and initially compressed. As the thickness of the elastomer narrowed during testing, the compressed springs forced the metal plates to tighten around the ever-decreasing cross section. Flat 4⅜ inch x 2 inch x ¼ inch steel plates with 1 inch diameter holes were used to connect the round stock supporting the elastomer to another segment of 1 inch round stock that was welded to a base designed to fit directly into the test frame. This connection served as a moment release and helped mitigate bending effects.

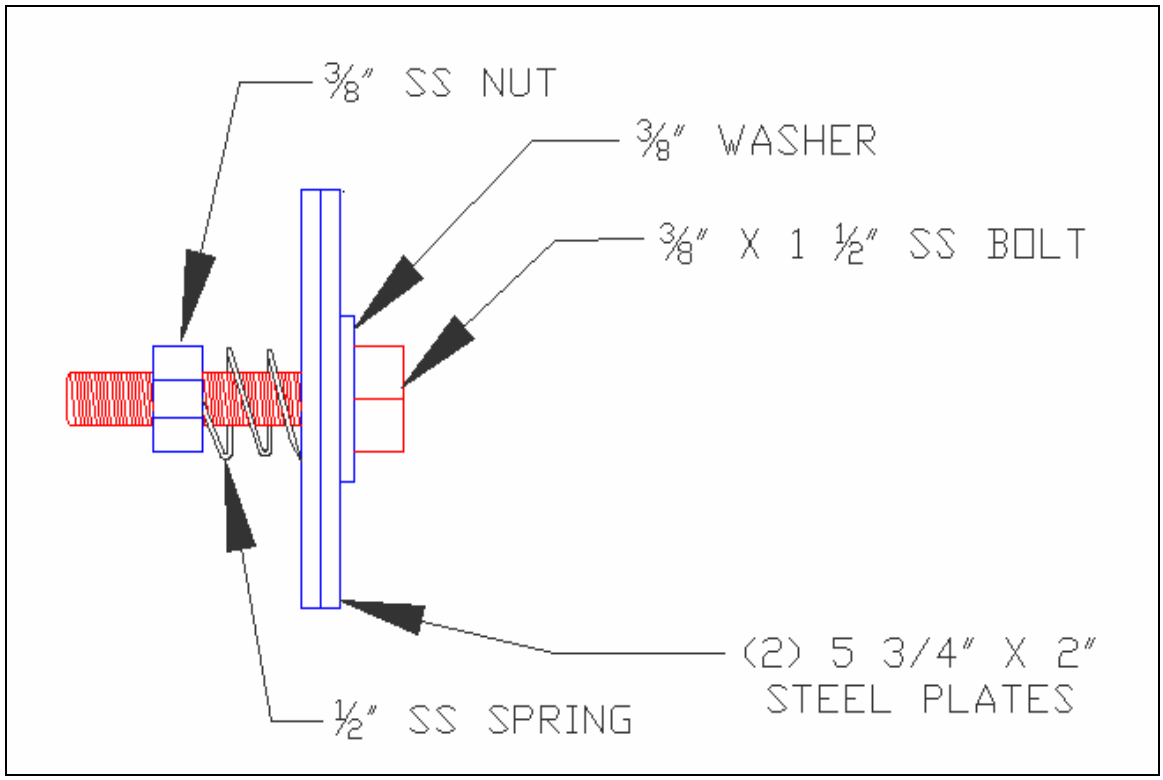

Figure 3.7: Bolt and Spring Assembly

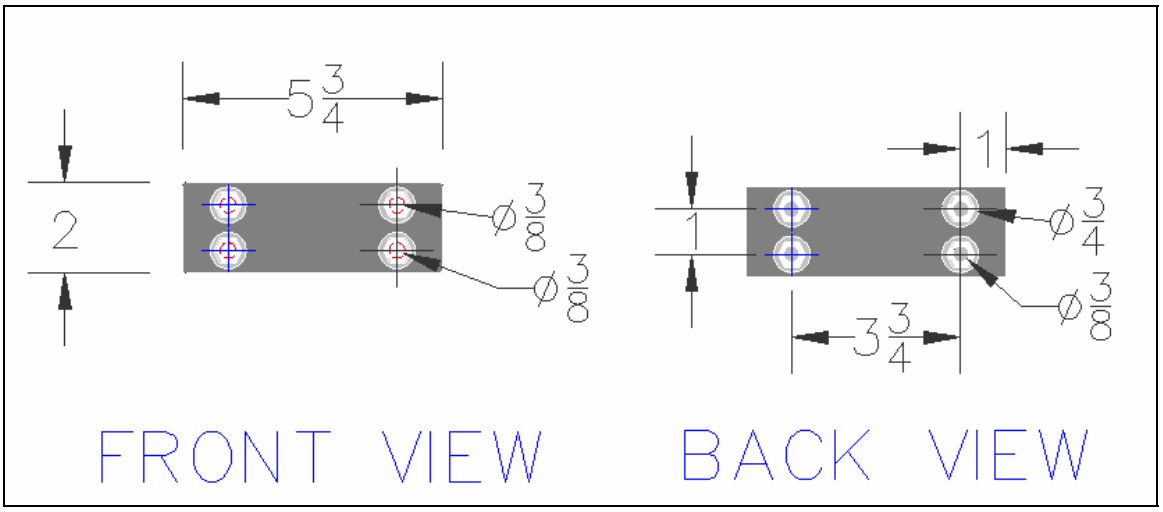

Figure 3.8: Clamp Details

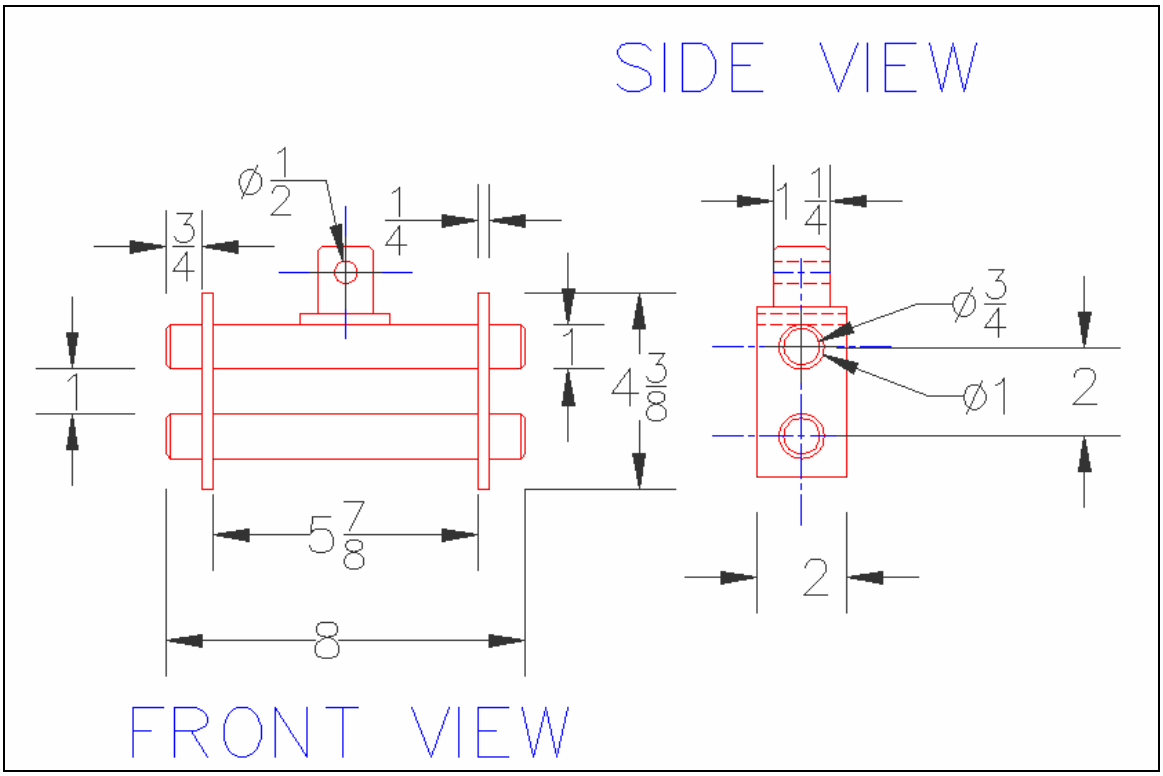

Figure 3.9: Modified Gripping Mechanism

Figure 3.10 shows a test being performed on a 0/90° specimen. The modified testing apparatus remedied the problem of slipping in the grips and was therefore used for the remainder of the tensile testing.

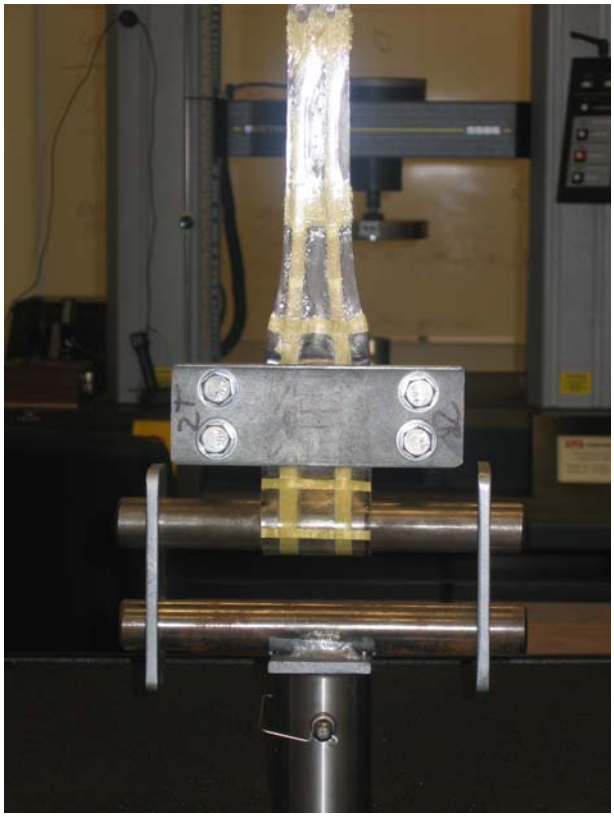

Figure 3.10: Modified Tensile Testing Gripping Mechanism

Figure 3.11 shows a typical tensile test approaching the maximum travel provided by the test frame used in this study. Rupturing the coupons before the frame's travel limit was reached was another problem experienced during material characterization. The original gage length was set at 4 inches, but the gage length had to be shortened in order to rupture the +/- 45° reinforced specimens.

Figure 3.11: Extensive Deformation in 0/90° Specimen

Even after reducing the gage length of the unreinforced elastomer coupons to ½ inch, rupture was not achieved. As such, the test apparatus required further modification. Once a certain level of deformation occurred over the original gage length, deformation spread to the film between the steel plate clamps and wrapped around the round stock as shown in Figure 3.12. To correct this problem, it is suggested that the clamping plates be rigidly connected to the round stock that supports the tensile specimen.

Figure 3.12: Extensive Deformation between the Clamp and the Base in a Typical Tension Test on the Unreinforced Film

The thicknesses of the three Stage II materials are shown in Table 3.1. The width of the unreinforced film coupons was 1 inch, but the reinforced coupons were originally cut 2 inches wide in an attempt to obtain a uniform fiber pattern over the coupon width as illustrated by Figure 3.13.

Table 3.1: Stage II Material Thicknesses

Unreinforced Film	0/90 Film	+/- 45 Film
t_f (in)	t_f (in)	t_f (in)
0.05	0.11	0.11

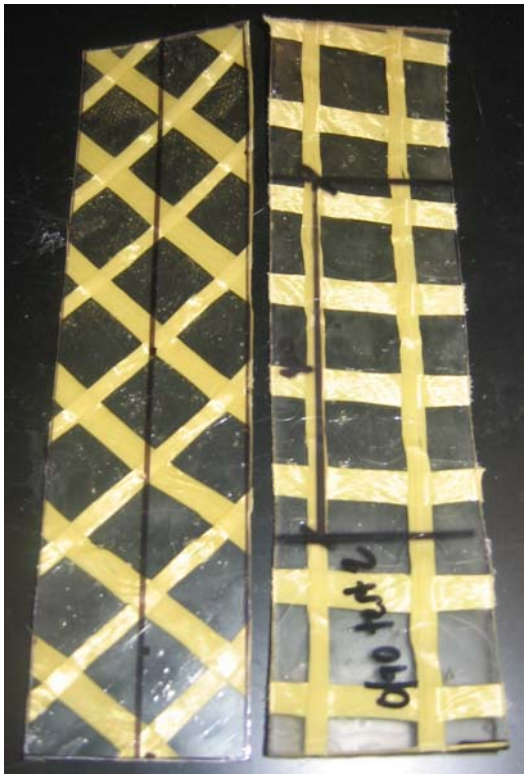

Figure 3.13: Fiber Reinforced Coupons - 2 inch x 8 inch

After running five preliminary tests on each of the reinforced specimens, it became clear that both the width and the gage length of the coupons needed to be modified in order to obtain results that more closely represent the actual tensile capacity of the film (and would be observed during flexural experiments). The fibers were not being engaged in the +/-45° tensile tests because continuous fibers were not gripped in both sets of clamps simultaneously. This was apparent because fibers ruptured during the 0/90° coupons tests, but simply slipped between the layers (Figure 3.14) of elastomer in the +/- 45° tests and rupture of the fibers was never achieved.

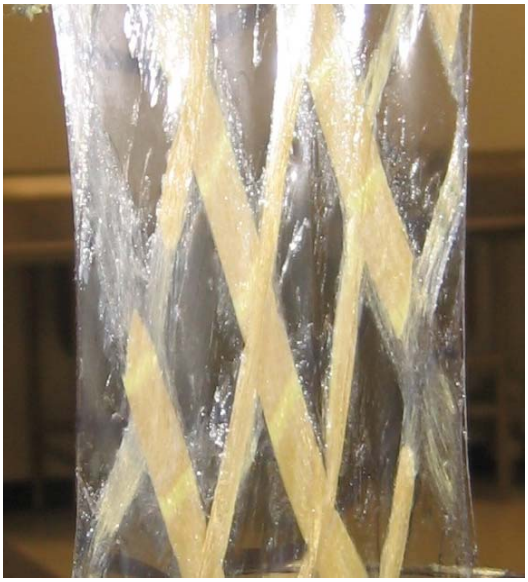

Figure 3.14: Fibers Slipping between Elastomer Layers in +/-45° Coupon

It was predicted that fibers in the sections used as retrofits and tested in flexure would behave differently because of the short span length of the mortar joint and the 7.5 inch width of the section that would allow for more fibers to be engaged. This idea is supported by the photograph of a flexural test specimen shown in Figure 3.15, which clearly shows rupture of the aramid fibers along the mortar joint.

Figure 3.15: +/- 45° Flexural Specimen under Mortar Joint after Testing

As Figure 3.15 demonstrates, approximately 5 fibers in each direction are fully engaged right around the joint. While being loaded, the joint edges of the masonry blocks restrain the fibers and allow them to engage as shown in Figure 3.16. To test this theory in the tensile tests, additional +/-45° coupons with widths of 3.5 and 5.0 inches were cut and tested. Figure 3.17 shows the three coupons widths side by side for comparison.

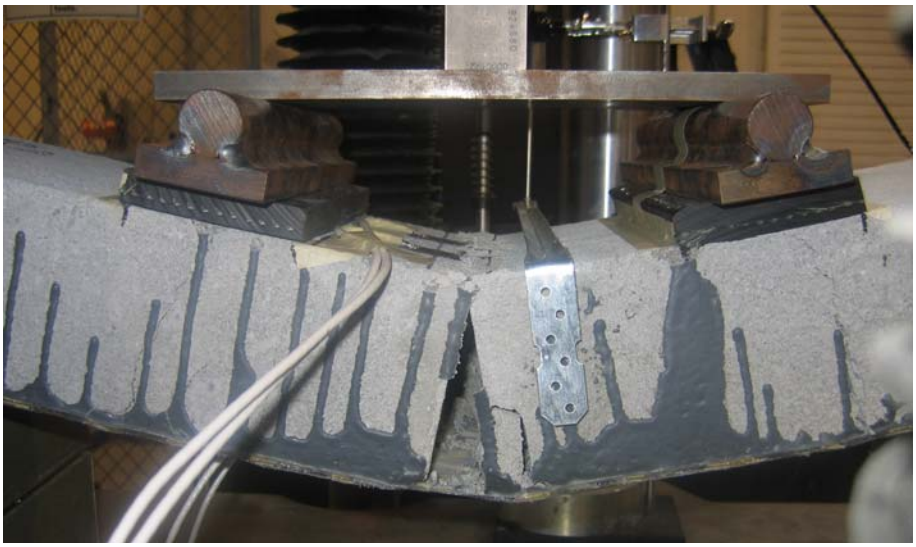

Figure 3.16: Side View of +/- 45° Flexural Test Demonstrating Restraint of Fibers

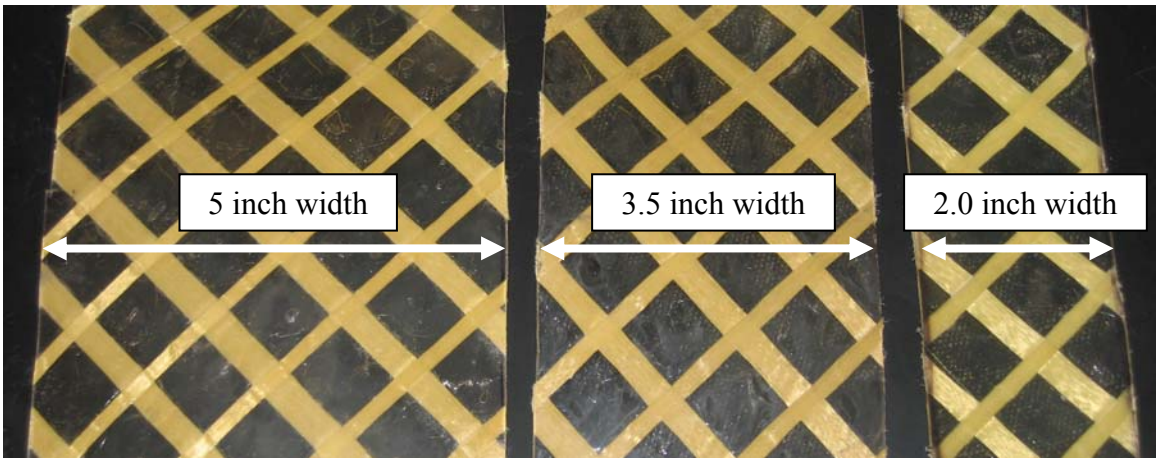

Figure 3.17: Three Coupon Widths used for +/-45° Tensile Tests

In order to test the wider coupons, new clamps had to be designed to accommodate the wider specimens. The clamps were fabricated exactly as the first set of clamps, except the flat plates were 2.25 inches longer, giving them a total length of 8 inches. The new clamps were used to test five 3.5 inch and five 5.0 inch specimens as shown in Figures 3.18 and 3.19. Each of the new specimens were tested with a gage length of 2 inches. Figures 3.18 and 3.19 also demonstrate the number of engaged fibers in each test. For the 3.5 inch specimens, one fiber is engaged whereas for the 5.0 inch specimens, 2 or 3 fibers were gripped on each end. Although increasing the width and decreasing the gage length allowed fibers to be gripped on each end, the new method still did not result in rupture of the fibers for the +/-45° coupons. The fibers slipped before failing, as they did in earlier tests. It appears reasonable to assume that if it were possible to test the coupons in direct tension with 5 fibers engaged and if failure of the fibers was achieved, the ultimate tensile capacity would be higher than that seen in the experiments of the present investigation.

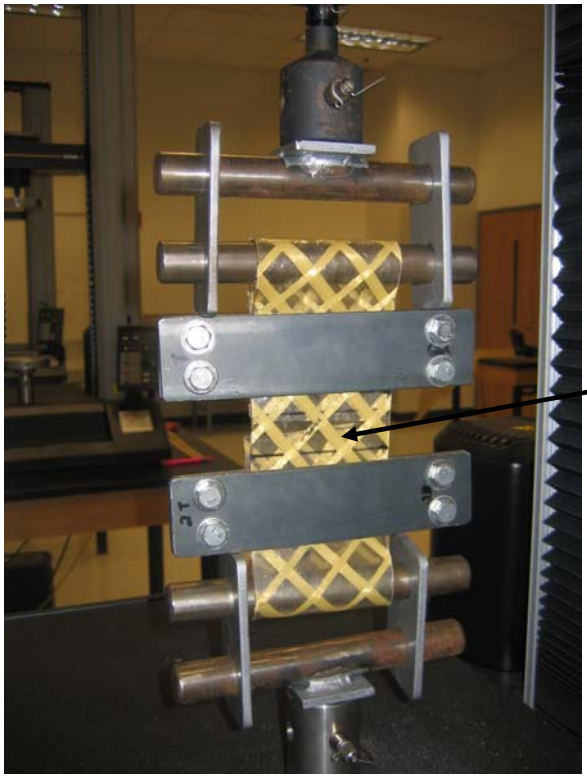

Figure 3.18: Test Setup for +/-45° Coupon 3.5 inches Wide

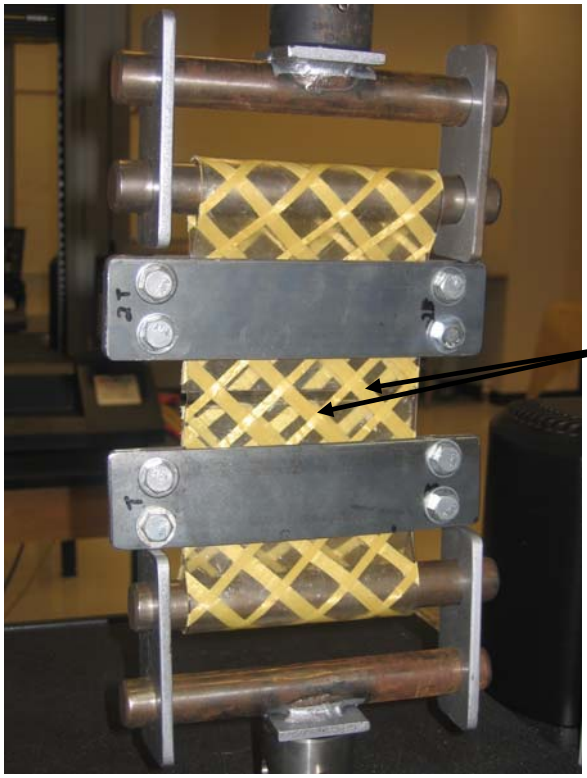

Figure 3.19: Test Setup for +/-45° Coupon 5 inches Wide

The width of the 0/90° test coupons was also altered in an attempt to obtain a more reliable prediction of the ultimate tensile strength. Coupon widths were reduced from 2.0 inches to 1.5 inches and an additional 5 coupons tests were performed. This change was made based on observations during testing that keeping the unengaged fibers and elastomer surrounding the scrim pattern (shown in Figure 3.20) would raise the cross-sectional area but would not contribute to the load carrying capacity of the coupon. Therefore, the calculated ultimate tensile strength would be lower than the actual capacity of the section.

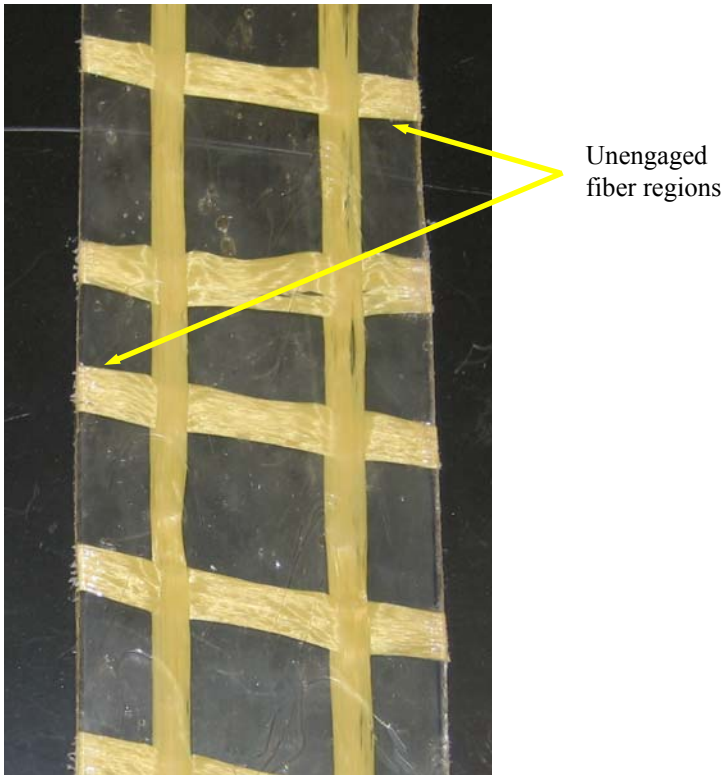

Figure 3.20: Unengaged Portion of 2-inch-wide 0/90° Coupons

3.3 CHARACTERIZATION OF EPOXY AND MASONRY

3.3.1 Tensile Testing of Epoxy Materials

The epoxy used for coupon testing was cured in a Plexiglas mold. The curing surface was not perfectly uniform, causing the thickness of the epoxy coupons to vary from approximately 0.15 to 0.18 inches. Tests were performed in accordance with ASTM D638 except that coupons were rectangular rather than having a reduced width in the coupon gage length. This modification was made because of difficulty fabricating a uniform coupon with the specified shape. Five coupons were cut 6 inches long and 1 inch wide with a 2 inch gage length. They were tested using the wedge grips of the load frame as shown in Figure 3.21, at a rate of 0.25 inches per minute.

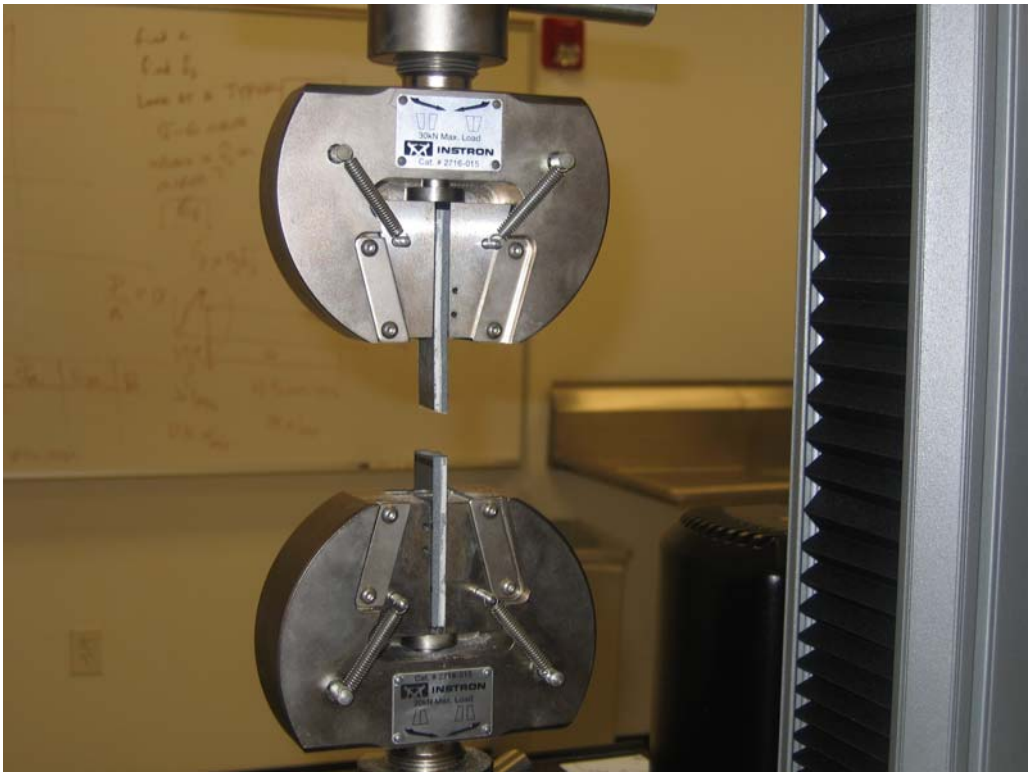

Figure 3.21: Epoxy Specimen after Tensile Rupture

3.3.2 Masonry and Mortar

Determining the material properties of the masonry and mortar used in this investigation was also crucial to understand the response of the strengthened wall elements. Compressive strength and modulus of elasticity were calculated by performing standard compression tests on mortar cylinders and masonry blocks with the same aspect ratios as the larger blocks. Mortar cylinders 3 inches in diameter were cast from the mix used to create the joint in the flexural test specimens. Figures 3.22 and 3.23 show a mortar cylinder and a masonry block, respectively, loaded in servohydraulic test frame. The masonry test specimens were cut from the larger 15.5 in x 7.5 in x 3.5 in blocks obtained from Home Depot. Five masonry and five mortar specimens were loaded in compression at a rate of 0.05 inches per minute until fracture in order to obtain the ultimate compressive strength. Masonry specimens were tested in accordance with ASTM C67 except the required cross-sectional area perpendicular to loading was slightly reduced (to 13.13in^2 from 14.0in^2) in order to maintain the dimensional proportions of the flexural test specimens. ASTM C109 was followed for the testing of the mortar, except cylinders were used because cube molds were not available.

Figure 3.22: Compression Testing of Mortar Cylinder


Figure 3.23: Compression Testing of Masonry Block

3.4 EXPERIMENTAL RESULTS OF MATERIAL CHARACTERIZATION STUDIES

3.4.1 Stage I Elastomers

A total of five specimens were tested for each of the 17 Stage I elastomeric materials. Table 3.2 lists the average modulus of elasticity and ultimate tensile strength for each. Figures 3.24 and 3.25 show typical stress-strain curves for one of the unreinforced and reinforced Stage I elastomers, respectively.

Table 3.2: Mechanical Properties of Stage I Materials

Material	# Coupons Tested	E (ksi)	STD (ksi)	COV (%)	f_{max} (psi)	STD (psi)	COV (%)
DW - 1	5	32.5	4.4	13.7	2056	185	9.0
DW - 1x	5	40.7	5.3	13.0	2579	150	5.8
DW - 8	5	43.4	5.0	11.6	2325	356	15.3
DW - 8x	5	13.4	4.1	30.3	2762	65	2.3
DW - 10	5	33.6	6.5	19.3	1843	138	7.5
SW - 2	5	13.5	1.3	9.4	1244	69	5.6
SW - 5	5	12.5	2.3	18.8	1250	134	10.8
X - 1	5	18.9	3.0	16.1	1437	68	4.7
X - 2	5	17.2	5.0	28.8	1088	70	6.4
X - 3	5	37.8	1.8	4.8	2270	80	3.5
X - 5	5	9.4	1.1	11.2	624	115	18.4
X - 6	5	42.2	6.8	16.0	1876	407	21.7
X - 7	5	18.9	3.5	18.5	1264	101	8.0
X - 8	5	20.7	5.5	26.7	1421	140	9.9
X - 9	5	14.0	2.9	20.5	1224	10	0.8
X - 10	5	22.2	2.2	9.9	1719	41	2.4
X - 11	5	25.1	4.9	19.4	1400	137	9.8

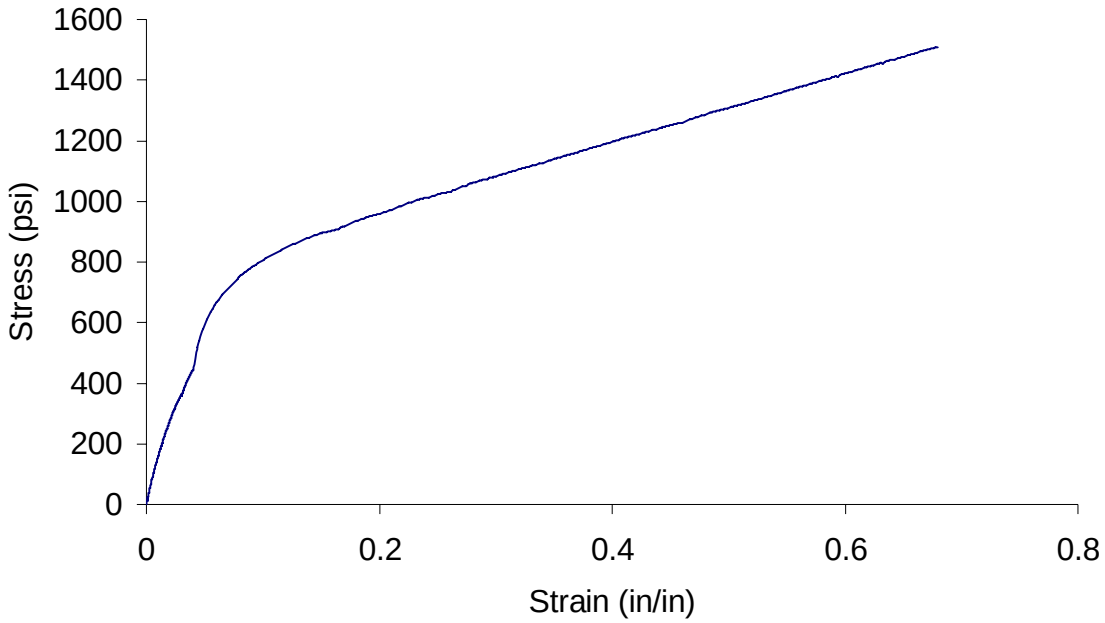

Figure 3.24: Typical Stress vs. Strain for Unreinforced Stage I Elastomer

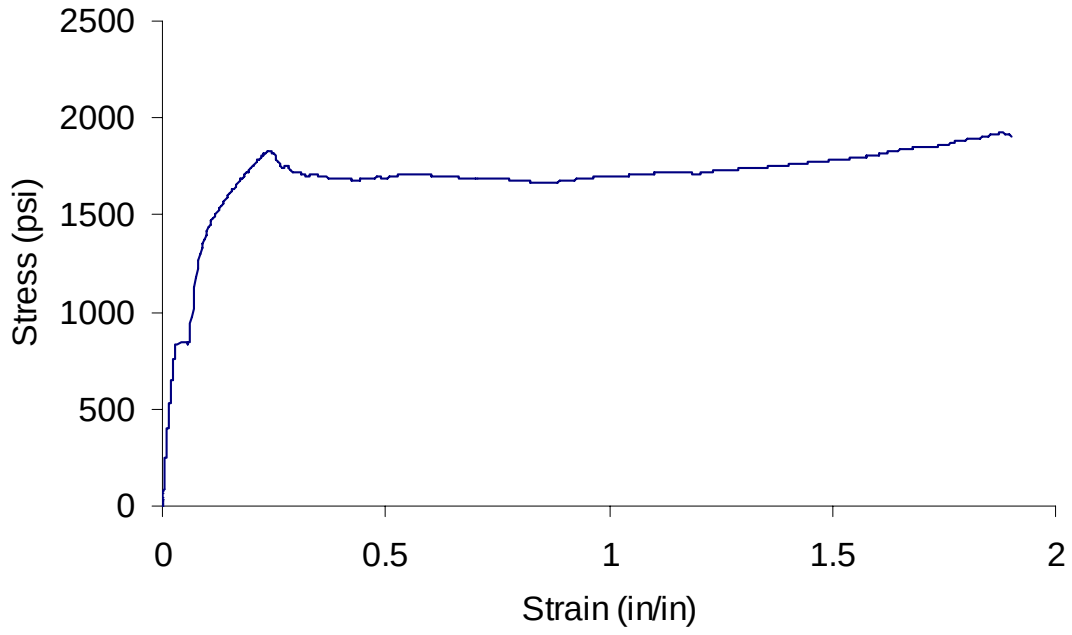

Figure 3.25: Typical Stress vs. Strain for Reinforced Stage I Elastomer

3.4.2 Stage II Elastomers

3.4.2.1 +/- 45° Reinforced Film

Figure 3.26 shows typical stress-strain curves for each of the three +/-45° coupon widths and results are presented in Table 3.3. These results support the theory that engaging the aramid fibers in narrower specimens was problematic. Specimens tested with a 3.5 inch width provided an average increase in tensile strength of approximately 50% and specimens with a 5 inch width increased in tensile capacity by 78% over the 2 inch coupons. The measured stiffness increased in approximately the same proportion.

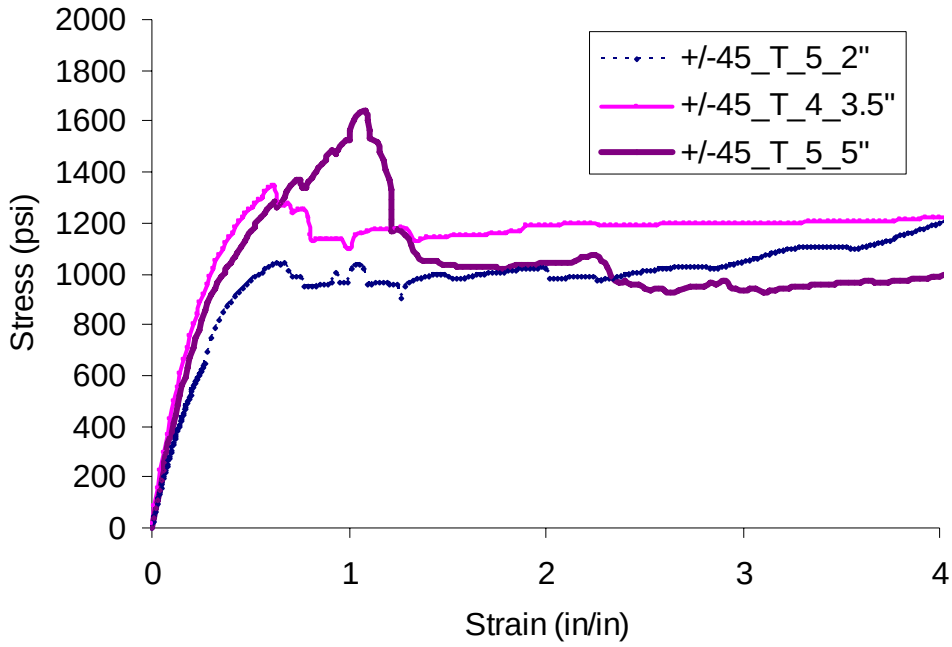

Figure 3.26: Typical Stress-Strain Curves for +/-45° Coupons

Table 3.3: +/- 45° Mechanical Properties by Specimen Width

Specimen ID	w = 2”		w = 3.5”		w = 5”	
	f_f (psi)	E (ksi)	f_f (psi)	E (ksi)	f_f (psi)	E (ksi)
+/-45_T_1	879	2.98	1175	3.80	1548	3.42
+/-45_T_2	853	2.92	1133	3.49	1524	4.30
+/-45_T_3	852	2.79	1247	2.24	1526	3.68
+/-45_T_4	852	2.97	1345	4.25	1548	4.21
+/-45_T_5	1043	3.47	1552	3.91	1643	4.19
Average	896	3.0	1290	3.5	1558	4.0
STD	83.1	0.3	166.9	0.8	49.0	0.4
COV	9.3%	8.6%	12.9%	21.9%	3.1%	9.8%

The plot of Ultimate Tensile Strength vs. Specimen Width shown in Figure 3.27 demonstrates the trend of increasing tensile capacity with increasing specimen width.

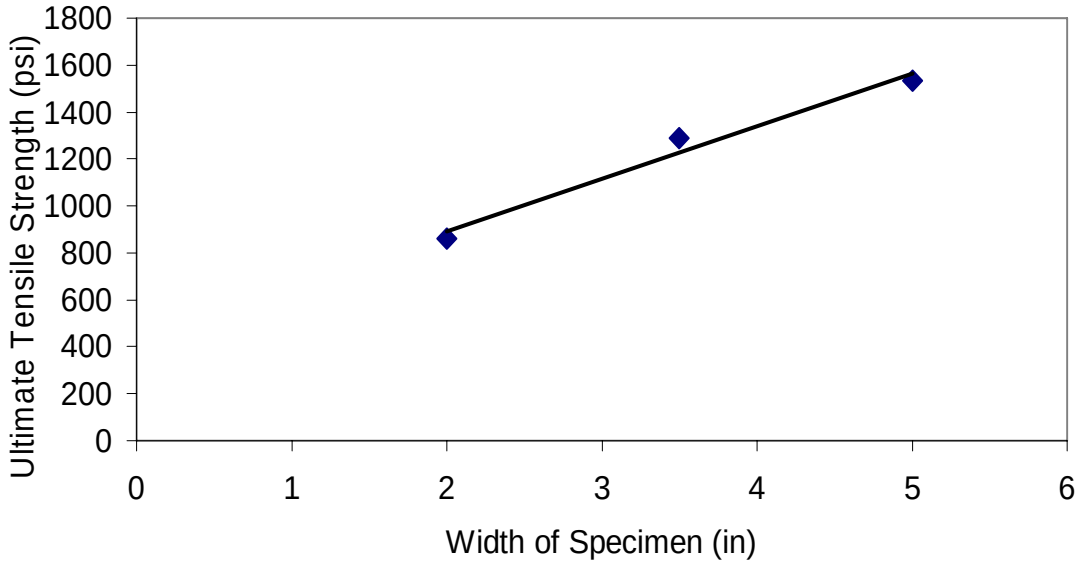

Figure 3.27: Tensile Strength vs. Specimen Width for +/- 45° Coupons

3.4.2.2 0/90° Reinforced Film

A typical stress-strain curve is shown in Figure 3.28 for each of the 0/90° coupon widths and results are listed in Table 3.4. The results for the 1.5-inch-wide 0/90° coupons

demonstrated an increase of approximately 35% in ultimate strength compared with results from the 2-inch-wide coupons.

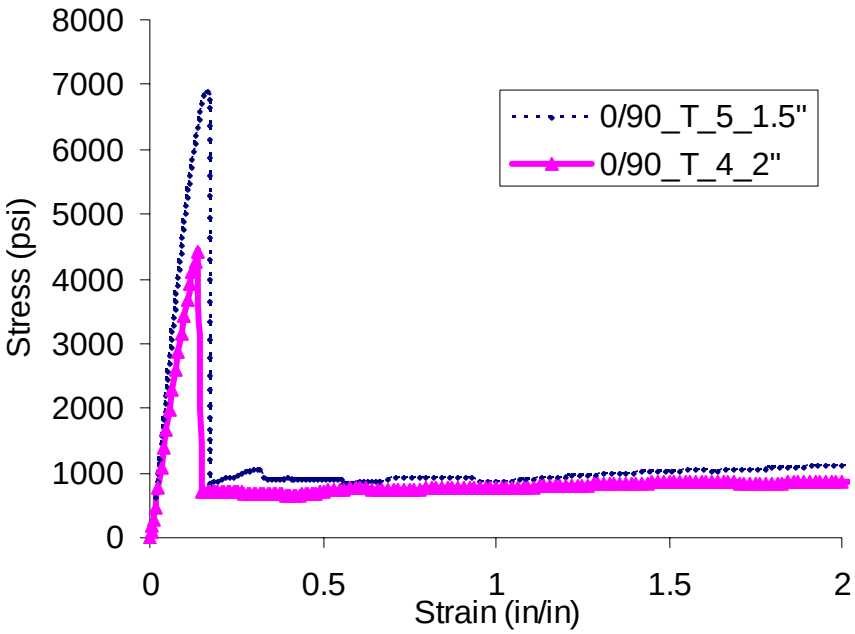

Figure 3.28: Typical Stress-Strain Curves for 0/90° Coupons

Table 3.4: 0/90° Mechanical Properties by Specimen Width

Specimen ID	w = 2”		w = 1.5”	
	f_f (psi)	E (ksi)	f_f (psi)	E (ksi)
0/90_T_1	4673	32.8	5396	30.3
0/90_T_2	4047	32.8	5504	33.5
0/90_T_3	4195	39.2	5330	40.2
0/90_T_4	4405	34.7	5730	38.8
0/90_T_5	4037	41.6	6881	38.7
Average	4271	36.2	5768	36.0
STD	269	4.0	640.3	4.2
COV	6.3%	11.0%	11.1%	11.6%

3.4.2.3 Unreinforced Film

Figure 3.29 shows a typical stress-strain curve for the unreinforced film and results are listed in Table 3.5.

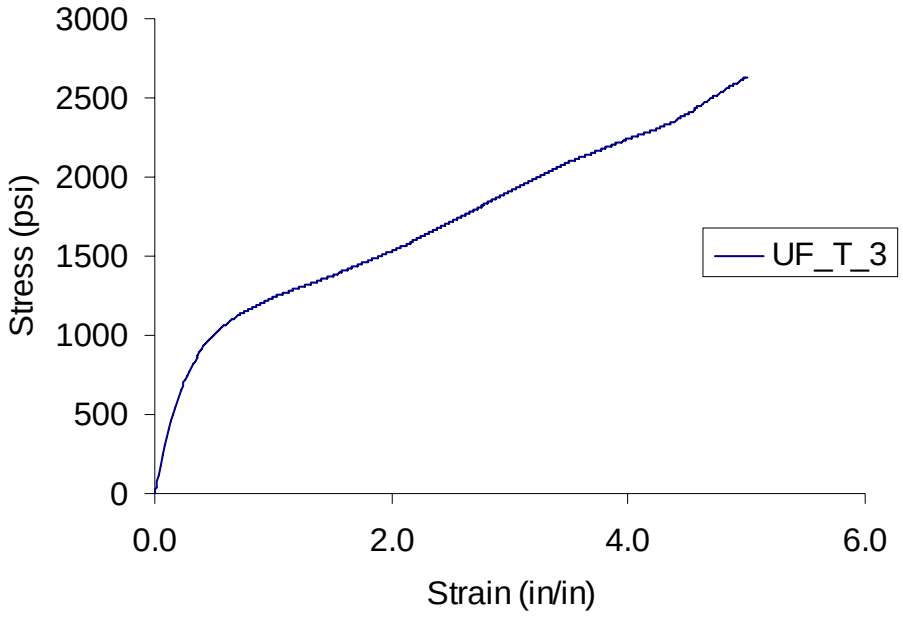

Figure 3.29: Typical Stress-Strain Curve for Unreinforced Film Coupons

Table 3.5: Unreinforced Film Tensile Test Results

Specimen ID	$f_{f=PL}$ psi	E ksi
UF_T_1	876	3.82
UF_T_2	778	3.58
UF_T_3	976	3.65
UF_T_4	854	3.43
UF_T_5	802	3.64
Average	857.2	3.6
STD	77.1	.1
COV	9.0%	3.9%

3.4.3 Epoxy

Table 3.6 lists the strength and modulus values for the epoxy used in this test program and Figure 3.30 shows a typical Stress vs. Strain curve.

Table 3.6: Epoxy Tensile Test Results

Specimen ID	f psi	E ksi
Epoxy_T_1	1664	5.90
Epoxy_T_2	1498	6.82
Epoxy_T_3	1752	6.14
Epoxy_T_4	1761	6.19
Epoxy_T_5	1731	5.76
Average	1681	6.2
STD	109	0.4
COV	6.5%	6.6%

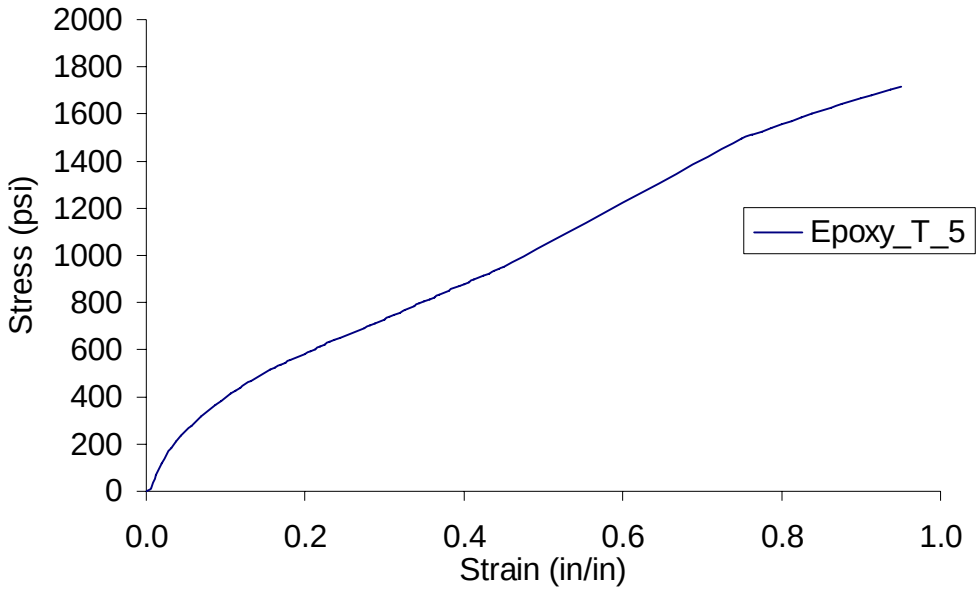

Figure 3.30: Typical Stress-Strain Curve for Epoxy Coupons

3.4.4 Masonry

Figures 3.31 and 3.32 show a typical mortar cylinder and masonry block failure, respectively. Both the mortar and the masonry exhibited similar shear failures.

Figure 3.31: Typical Mortar Cylinder Failure

Figure 3.32: Typical Masonry Block Failure

Average values for compressive strength of the mortar and the masonry are listed in Table 3.7. Since the average compressive strength of the mortar was lower than that of the masonry, the compressive strength of the mortar was used in the development of the predictive model. Failure of the section was assumed to occur when the masonry crushed, and crushing occurred at the mortar joint. Therefore, the compressive strength of the mortar joint governed the failure.

Table 3.7: Compression Test Specimen Details

Test ID	Mortar	Masonry
	f'_m (psi)	f'_m (psi)
C_1	1593	2202
C_2	1457	1873
C_3	1418	1863
C_4	1564	1732
C_5	1346	1922
Average	1476	1942
STD	102	174
COV	6.9%	9.0%

3.5 SYSTEMS SELECTED FOR FLEXURAL TESTS

From this series of tests and input from ERDC researchers, three material systems were chosen for further study. These systems included the unreinforced elastomer film, the +/- 45° reinforced elastomer film, and the 0/90° reinforced elastomer film. These Stage II materials were chosen because as the ERDC dynamic test program continued, it became evident that quality control would be a problem during field installation. A high degree of skill was required to mix and apply the material in a uniform fashion. The uniformity that the Stage II materials provided was highly desirable, and this was the

basis for which they were chosen for further study. Each of these retrofits would be applied to unreinforced masonry for flexural testing with the same epoxy that was characterized during tensile testing.

CHAPTER IV

FLEXURAL EXPERIMENTS

4.1 TEST SPECIMENS

A total of twenty flexural tests were performed in this phase of the experimental investigation. Test specimens were prepared by joining two standard 7.5 inch x 15.5 inch x 3.5 inch masonry blocks utilizing Type S mortar. The mortar joint was fabricated nominally 0.5 inches wide, making the entire length of the test specimens approximately 31.5 inches. The specimens were allowed to cure for 48 hours prior to applying the retrofit materials. While the mortar joint was allowed to cure, the elastomeric retrofit materials were cut from large rolls provided by ERDC researchers. Rectangular sections slightly wider than the two-span masonry specimens were cut off the rolls as shown in Figure 4.1.

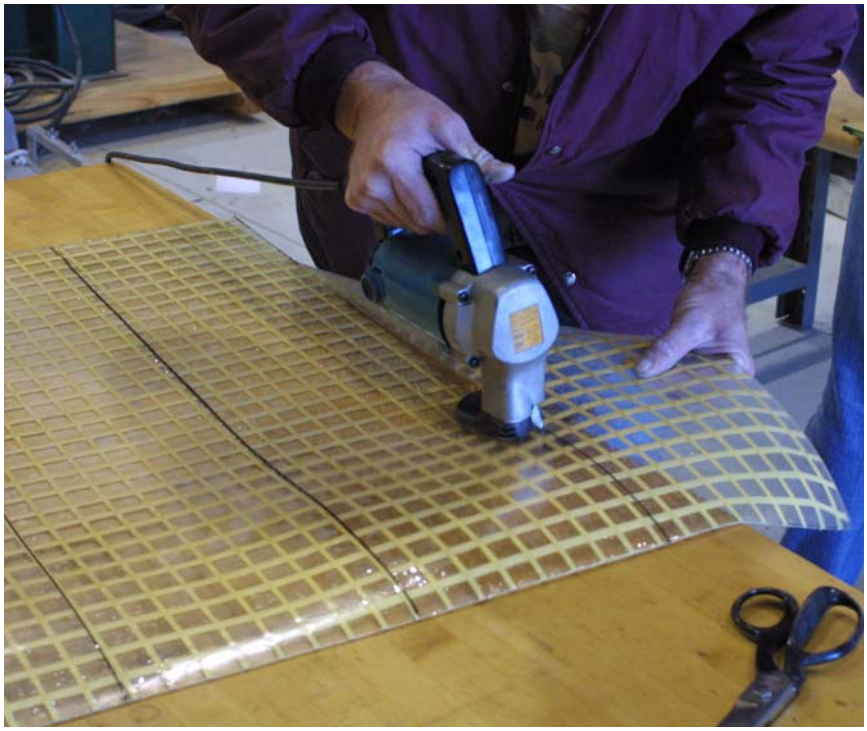

Figure 4.1: Elastomer Retrofit Section Fabrication

This was done to ensure that the retrofit would completely cover the masonry. Before applying the retrofit materials, the masonry elements were cleaned with a wire brush and wiped with alcohol to remove any loose debris or other deleterious materials. The retrofit sections were also cleaned with alcohol, and a primer was applied to aid in adhesion as shown in Figure 4.2.

Figure 4.2: Primer Application to Retrofit Material

A standard two-part epoxy was then mixed and applied directly to the surface of the masonry elements. A grooved trowel was used to smooth the epoxy and ensure an even distribution of material on the masonry. Next, the retrofits were applied using rollers as shown in Figure 4.3 to remove air bubbles and promote a good bond between the masonry and the elastomer. The unreinforced film was applied to 10 specimens, and the +/-45° and 0/90° reinforced films were each applied to 10 specimens. Ten additional

specimens were prepared with epoxy and no additional reinforcement. Table 4.1 lists the dimensions of the flexural test specimens.

Figure 4.3: Retrofit Application Process

Table 4.1: Typical Dimensions of Test Specimens

h (in)	b_m (in)	d_m (in)	b_f (in)	t_{rf} (in)	t_{uf} (in)	t_e (in)
31.5	7.5	3.5	8.0	0.11	0.05	0.16

4.2 EXPERIMENTAL SETUP

A four-point flexural test setup was selected to measure the ultimate flexural capacity of the reinforced masonry sections. This setup was chosen as opposed to a three point bend test in order to avoid loading the specimens directly on the mortar joint and to obtain a constant moment region around the joint. This was desirable because the mortar

joint is the critical failure location. Figure 4.4 shows a schematic illustration of the flexural test setup. Roller supports were arranged so that the span length L between supports was 27 inches and the top support span was 9 inches.

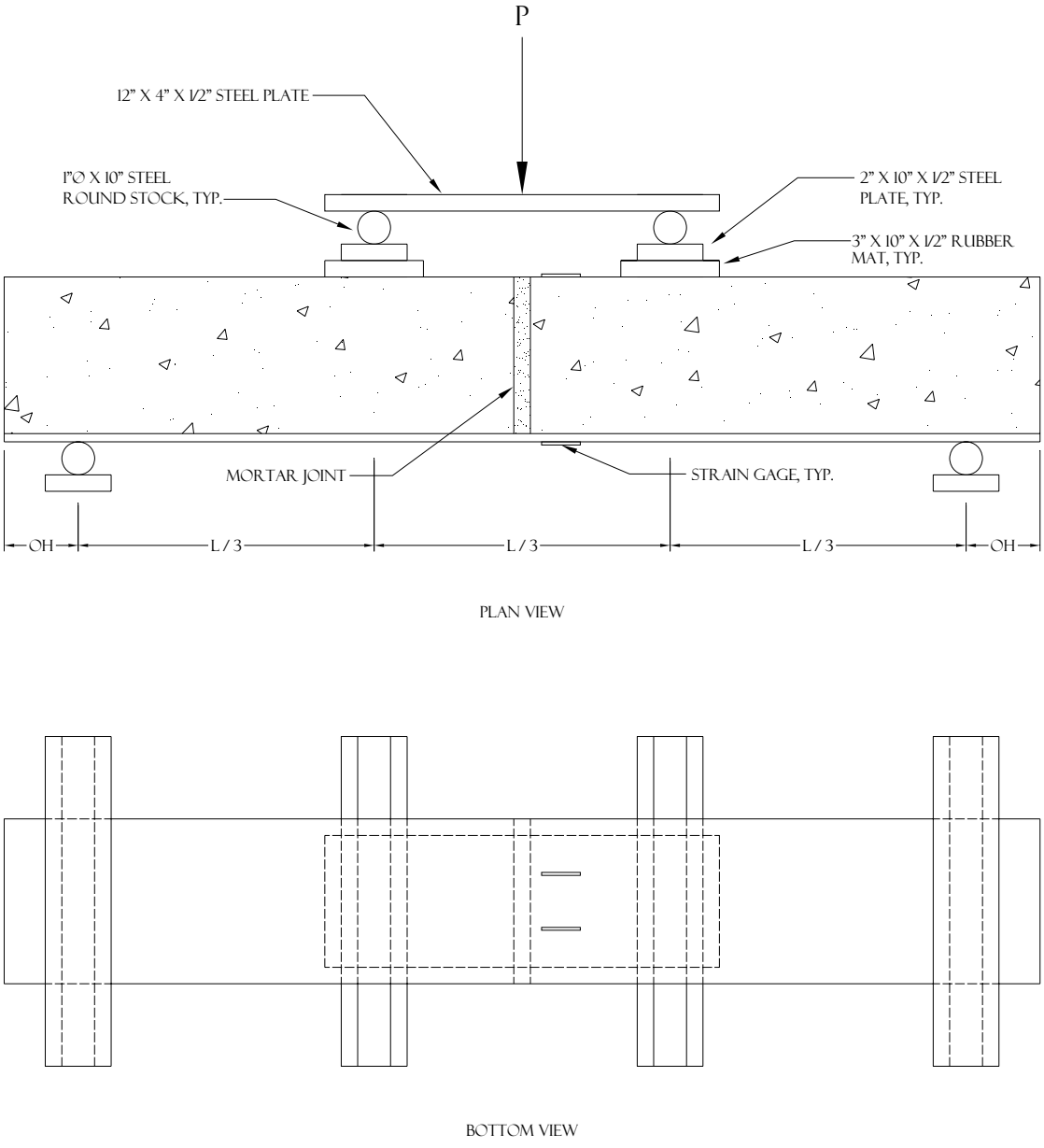

Figure 4.4: Flexural Test Setup

The top rollers were oriented with the flat plate down and seated on 3 inch x 10 inch x ½ inch elastomer mats. This was done to avoid the high contact stresses produced

by the original setup when the rollers were oriented with the round stock down. Even with this change to the original setup, cracks still developed under the top supports during a few tests, as shown in Figure 4.5. This occurred principally when testing the 0/90° reinforced specimens, but also occurred during testing of the +/- 45° retrofits.

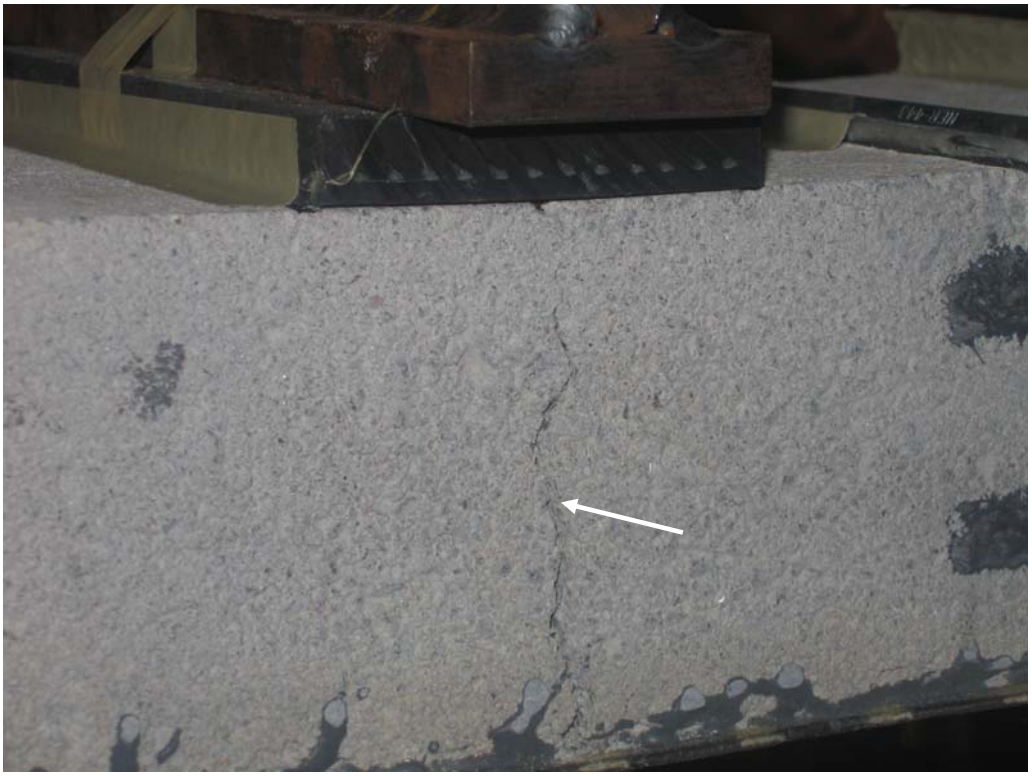

Figure 4.5: Crack under Top Support in a 0/90° Specimen

The flexural test setup was placed in a servohydraulic load frame for load application. Strain gages, a Linear Variable Displacement Transducer (LVDT), and a 5,000 lb capacity load cell were used to collect data during the experiments. Figure 4.6 shows a typical flexural test setup. The LVDT was positioned to record transverse deflections immediately adjacent to the mortar joint at midspan. The load cell was placed between the top compression platen of the load frame and the steel plate that served as a

load distributor. Four-inch square FRP tubes were used to raise the system off the base of the test frame and allow adequate clearance for the specimen to deflect during testing.

Figure 4.6: Typical Test Specimen in Load Frame

Strain gages with a resistance of 350 Ohms and a gage length of 0.75 inches were bonded to the compressive and tensile surfaces of selected test specimens as shown in Figures 4.7 and 4.8. Both tensile and compressive strain gages were centered on a line drawn one inch from the center of the mortar joint. They were not located at the center of the joint to avoid damage due to excessive deformation on the tensile side and crushing of the mortar joint on the compressive side, so that more data could be collected before the gages failed or debonded.

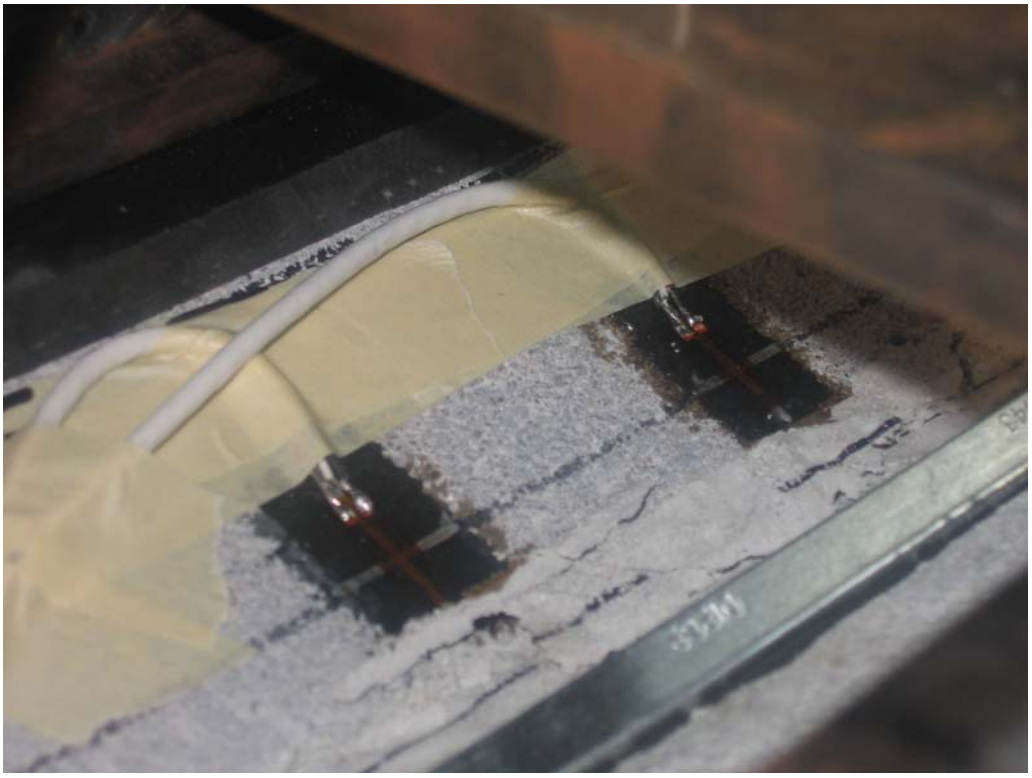

Figure 4.7: Location of Compressive Strain Gages

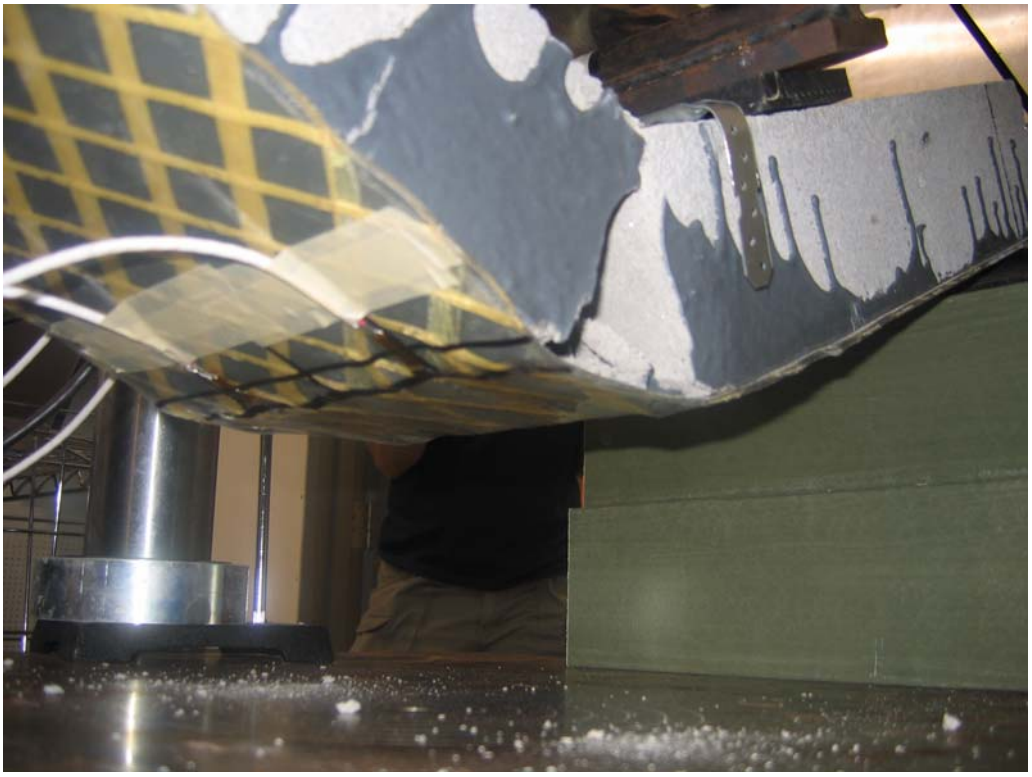

Figure 4.8: Location of Tensile Strain Gages

Compressive strain data was collected for two of the five tests performed for each material system and tensile strain data was collected for three of the five tests. Load and displacement data were collected for every test. The data was collected using a computerized data acquisition system at one second intervals.

4.3 TESTING PROGRAM

For each retrofit material system studied in this investigation, a total of five specimens were tested under the four-point flexural setup described in Section 4.2. An additional control specimen with no reinforcing material was also tested, but the tensile strength of the mortar joint was so low that the specimen failed approximately 5 seconds after loading began; as such, no useful data was obtained. Five specimens were tested with only the epoxy material as reinforcement. This was done to attempt to estimate what percentage of any observed strength increase could be attributed solely to the epoxy bond layer. The remaining 15 test specimens were strengthened with epoxy-bonded elastomer films. One set of specimens was strengthened using the unreinforced elastomeric material. The other test specimens were strengthened with elastomers containing fibers oriented at either +/-45 or 0/90 degrees with the longitudinal direction, as shown in Figure 4.9. Table 4.2 gives the testing matrix utilized in this phase of the experimental investigation.

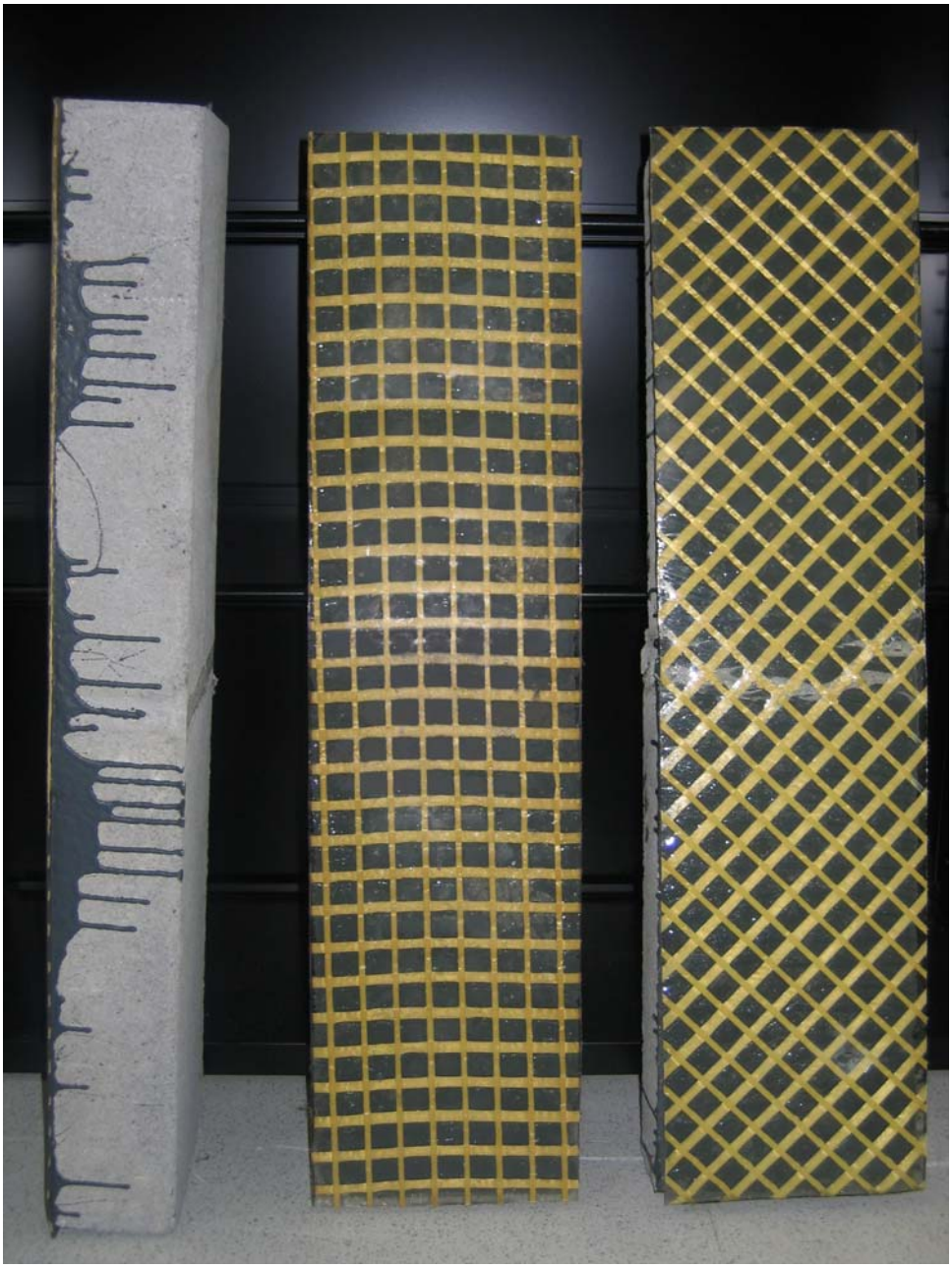

Figure 4.9: Fiber Orientations in Flexural Specimens: Side View, 0/90°, +/-45°

Table 4.2: Test Specimens

Sample #	Sample ID	Reinforcement Scheme	Bond/Application Type
1	SE_TOE_1	Stand alone epoxy	Trowel-on Epoxy
2	SE_TOE_2	Stand alone epoxy	Trowel-on Epoxy
3	SE_TOE_3	Stand alone epoxy	Trowel-on Epoxy
4	SE_TOE_4	Stand alone epoxy	Trowel-on Epoxy
5	SE_TOE_5	Stand alone epoxy	Trowel-on Epoxy
6	UF_TOE_1	Unreinforced film	Trowel-on Epoxy
7	UF_TOE_2	Unreinforced film	Trowel-on Epoxy
8	UF_TOE_3	Unreinforced film	Trowel-on Epoxy
9	UF_TOE_4	Unreinforced film	Trowel-on Epoxy
10	UF_TOE_5	Unreinforced film	Trowel-on Epoxy
11	RF_0/90_TOE_1	0°/90°	Trowel-on Epoxy
12	RF_0/90_TOE_2	0°/90°	Trowel-on Epoxy
13	RF_0/90_TOE_3	0°/90°	Trowel-on Epoxy
14	RF_0/90_TOE_4	0°/90°	Trowel-on Epoxy
15	RF_0/90_TOE_5	0°/90°	Trowel-on Epoxy
16	RF_+/-45_TOE_1	+/- 45°	Trowel-on Epoxy
17	RF_+/-45_TOE_2	+/- 45°	Trowel-on Epoxy
18	RF_+/-45_TOE_3	+/- 45°	Trowel-on Epoxy
19	RF_+/-45_TOE_4	+/- 45°	Trowel-on Epoxy
20	RF_+/-45_TOE_5	+/- 45°	Trowel-on Epoxy

Each specimen was loaded at a rate of 0.25 inches per minute. The specimens with only epoxy reinforcement were loaded until failure by rupture of the epoxy in tension as demonstrated in Figure 4.10. The elastomer reinforced specimens were loaded until crushing of the masonry occurred in the compression zone. Loading was continued after crushing of the masonry for the first test of each elastomer material system in an effort to rupture the films in tension. An additional section of square FRP tube (Figure 4.11) was employed to raise the specimen and allow more transverse deflection, but rupture of the elastomer was not achieved.

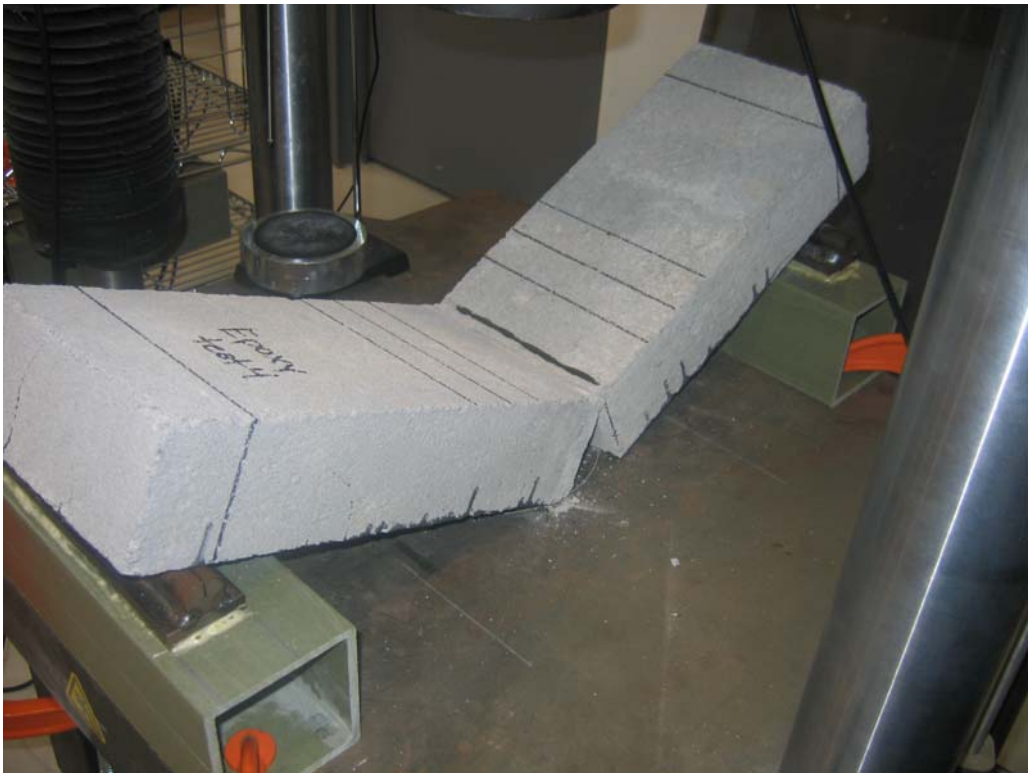

Figure 4.10: Failure of Stand Alone Epoxy Specimen

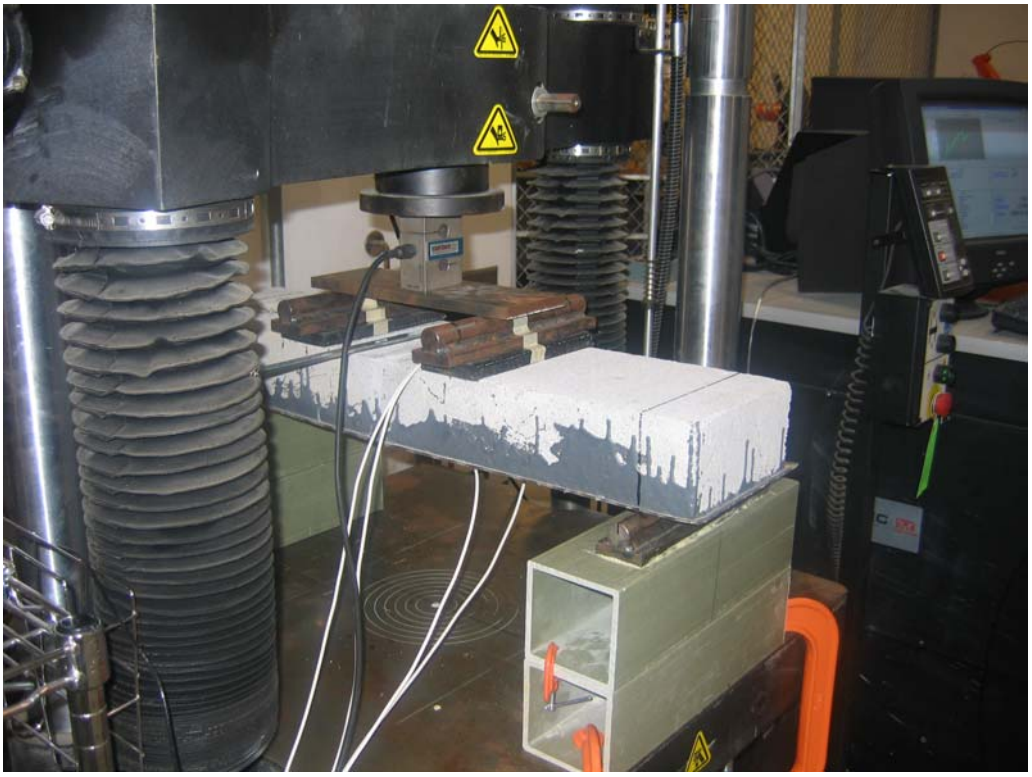
Figure 4.11: Addition to Support Height to Allow Additional Travel

Figure 4.12 demonstrates the extensive deformation in one of the 0/90° specimens that was allowed to continue past crushing of the masonry. The mortar joint completely separated and the load stabilized and stayed constant until the test framed reached its maximum allowable travel. Crushing of the masonry at the top of the compression can also be observed. The specimens reinforced with the other retrofits exhibited similar behavior, as can be seen in Figures 4.13 and 4.14.

Figure 4.12: Extensive Deformation at the Mortar Joint for a 0/90 Test Specimen

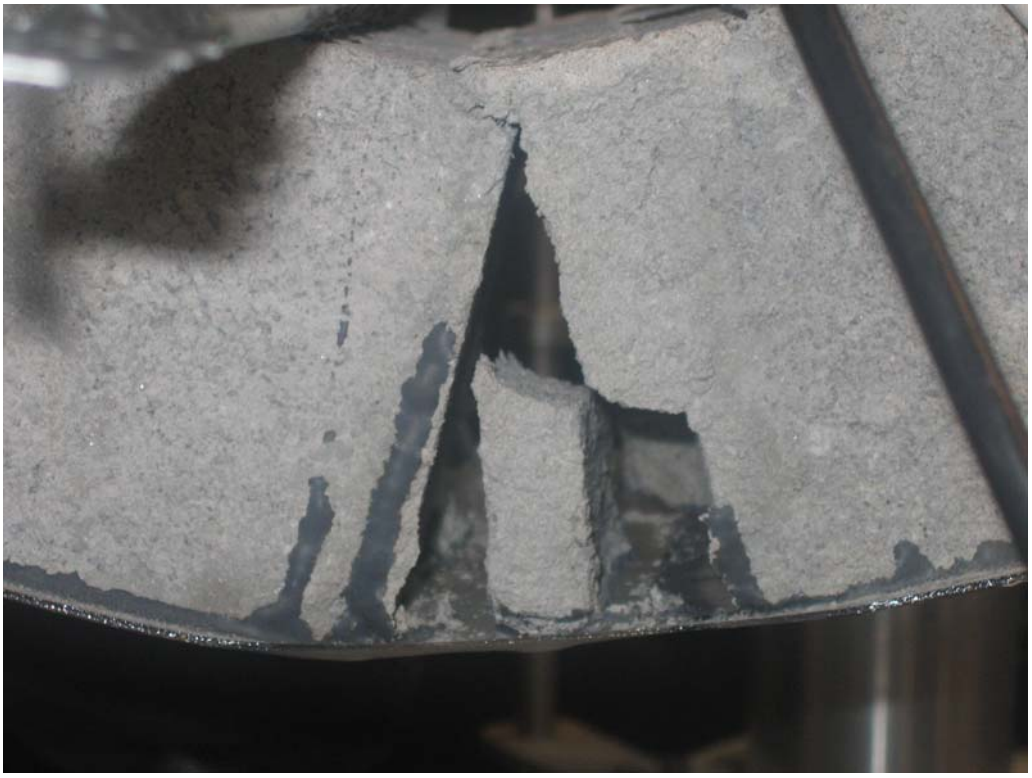

Figure 4.13: Separation of Mortar Joint during Unreinforced Retrofit Test

Figure 4.14: Separation of Mortar Joint during +/- 45° Retrofit Test

For the unreinforced film retrofits, the load gradually decreased from the maximum load before stabilizing. For the reinforced films, however, the load dropped suddenly after reaching a maximum value and remained relatively stable for the remainder of the test.

4.4 TEST RESULTS

4.4.1 Stand Alone Epoxy

Figure 4.15 shows the load versus displacement curves obtained from the four point bend tests performed on the five stand alone epoxy specimens. For each test, the load increased uniformly to a maximum value where cracking occurred at the mortar joint. At this point, the load decreased until failure occurred due to rupture of the epoxy layer.

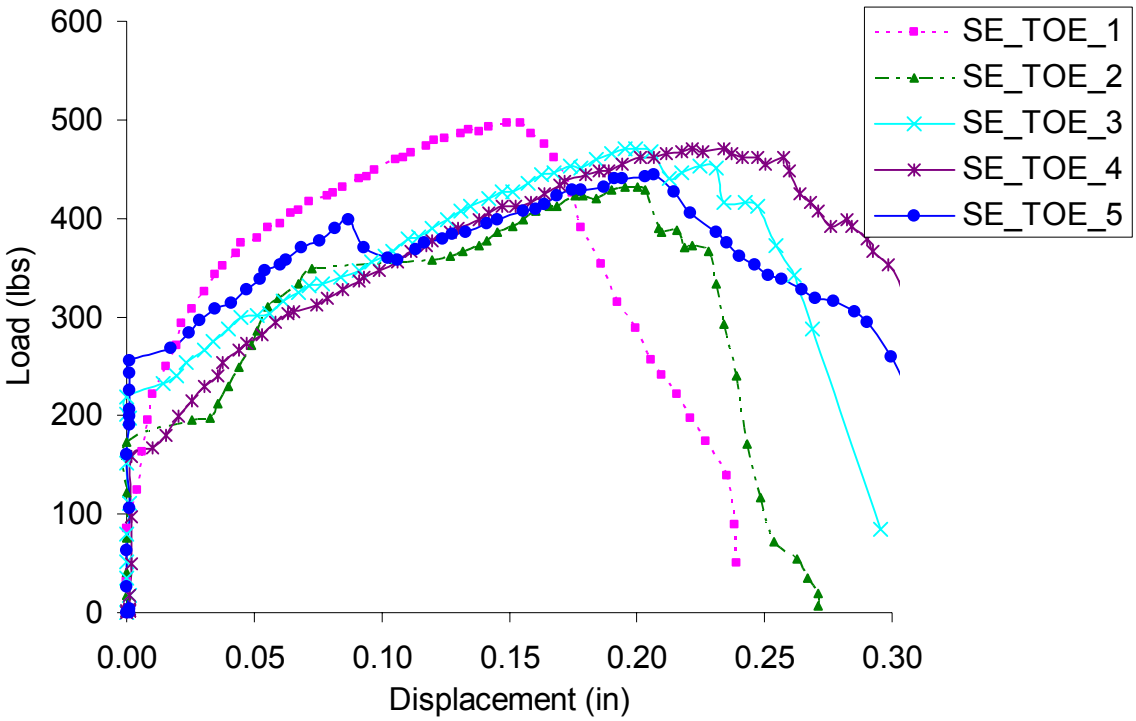

Figure 4.15: Load vs. Displacement Curves for Epoxy Specimens

Load versus tensile strain curves for the three gaged epoxy-only specimens are shown in Figure 4.16. When loading began, the load vs. tensile strain curve followed the same pattern as the load-deflection curve. The load increased rapidly with little increase in strain or in deflection. As loading continued, the strain increased gradually until rupture of the epoxy.

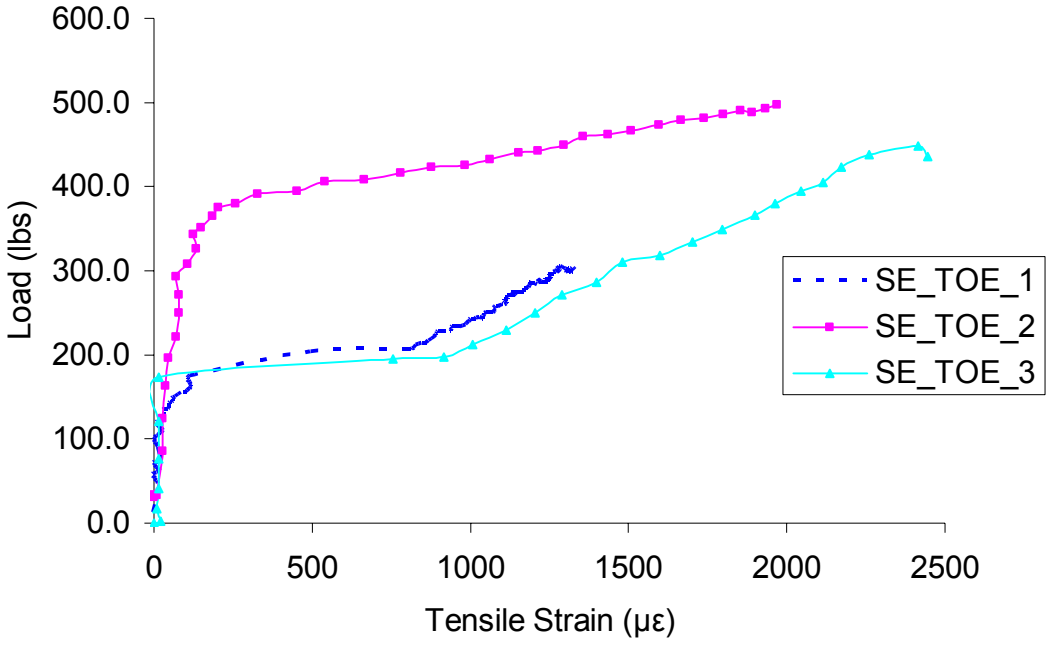

Figure 4.16: Tensile Strain in Epoxy Specimens

Table 4.3 lists the maximum load and resulting moment experienced by the epoxy reinforced masonry specimens. Also listed are the displacements δ and tensile and compressive strain values ε_T and ε_C, respectively, at the maximum load.

Table 4.3: Epoxy Flexural Test Results

Specimen ID	P_{max} (lbs)	M_{max} (lb·in)	δ (in)	ε_T ($\mu\varepsilon$)	ε_C ($\mu\varepsilon$)
SE_TOE_1	497	2237	0.15	1620	174
SE_TOE_2	460	2070	0.10	2022	139
SE_TOE_3	494	2223	0.20	1128	n/a
SE_TOE_4	470	2115	0.22	n/a	n/a
SE_TOE_5	444	1998	0.21	n/a	n/a
Average	473	2129	0.18	1590	157
STD	23	102	0.05	448	25
COV	4.8%	4.8%	27.8%	28.2%	15.8%

*Strain data only available for gaged specimens

4.4.2 Unreinforced Film

Load versus displacement curves for the five unreinforced film retrofits are displayed in Figure 4.17. In all five tests, the load increased steadily until the mortar joint completely separated and crushing of the masonry in compression began to occur. This point was identified as failure of the system and is indicated on the plot.

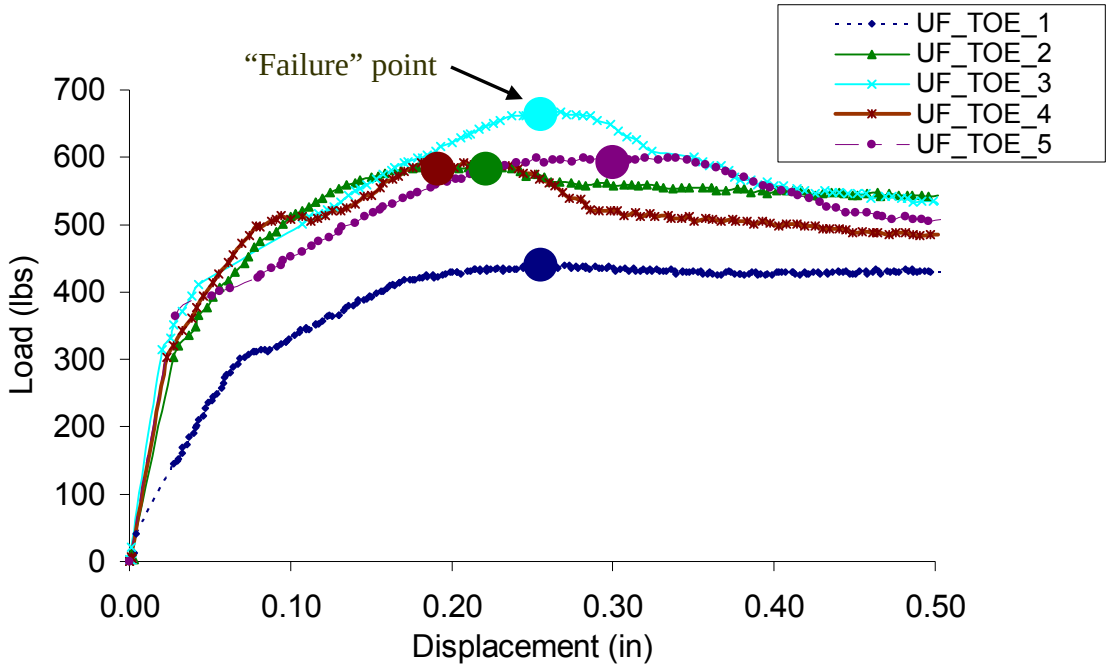

Figure 4.17: Load vs. Displacement Curves for Unreinforced Film Retrofits

Load versus tensile strain curves are shown in Figure 4.18 for the three specimens with gages placed on the unreinforced film. Strain values increased steadily, following the trend of the load-deflection curves until the strain exceeded the capacity of the gages. As such, only the initial portion of the curves are shown. Table 4.4 lists the unreinforced retrofit results.

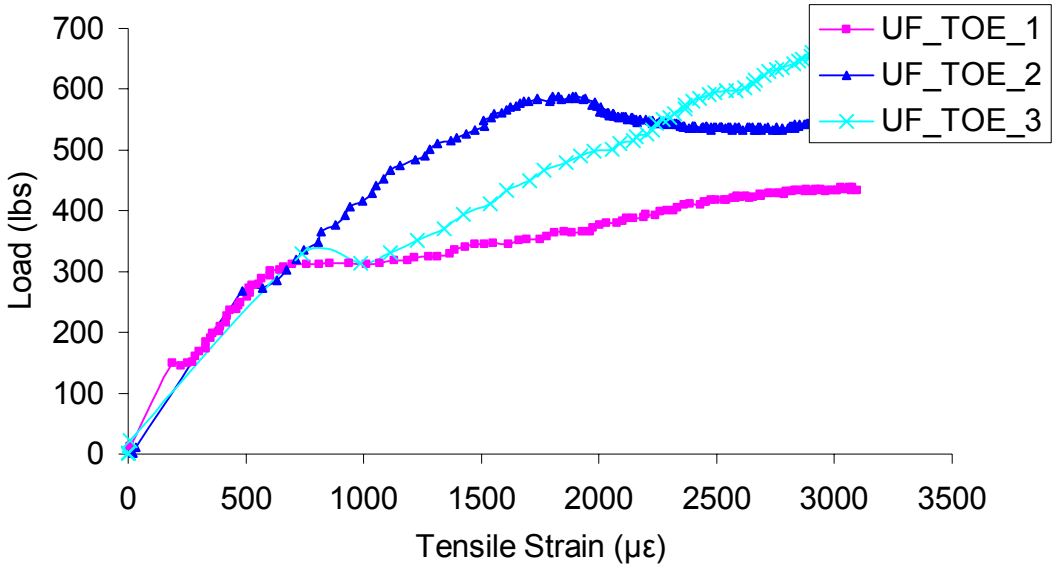

Figure 4.18: Load vs. Tensile Strain for Unreinforced Film Retrofits

Table 4.4: Unreinforced Film Flexural Test Results

Specimen ID	P_{max} (lbs)	M_{max} (lb·in)	δ (in)	ε_T ($\mu\varepsilon$)	ε_C ($\mu\varepsilon$)
UF_TOE_1	440	1980	0.27	4507	115
UF_TOE_2	588	2644	0.23	2523	123
UF_TOE_3	668	3005	0.27	3177	n/a
UF_TOE_4	592	2663	0.19	n/a	n/a
UF_TOE_5	601	2702	0.30	n/a	n/a
Average	578	2599	0.25	3402	119
STD	83	376	0.04	1011	6
COV	14.5%	14.5%	16.9%	29.7%	4.8%

4.4.3 +/-45° Reinforced Film

Load versus displacement and load versus tensile strain data for the +/- 45° retrofits are shown in Figures 4.19 and 4.20, respectively. Spikes in the load-deflection curves indicate the development of cracks under the top supports and at the mortar joint. The peak of each curve (indicated on the plot) is the point where the mortar joint began to fully separate and the loss of load indicates failure of the section by crushing of the masonry in compression. Figure 4.20 shows the initial portions of the load versus tensile strain curves, and Table 4.5 lists the test results. The load-strain curves follow the pattern of the load-deflection curves with spikes indicating cracking. Strain increased until the capacity of the gages was exceeded.

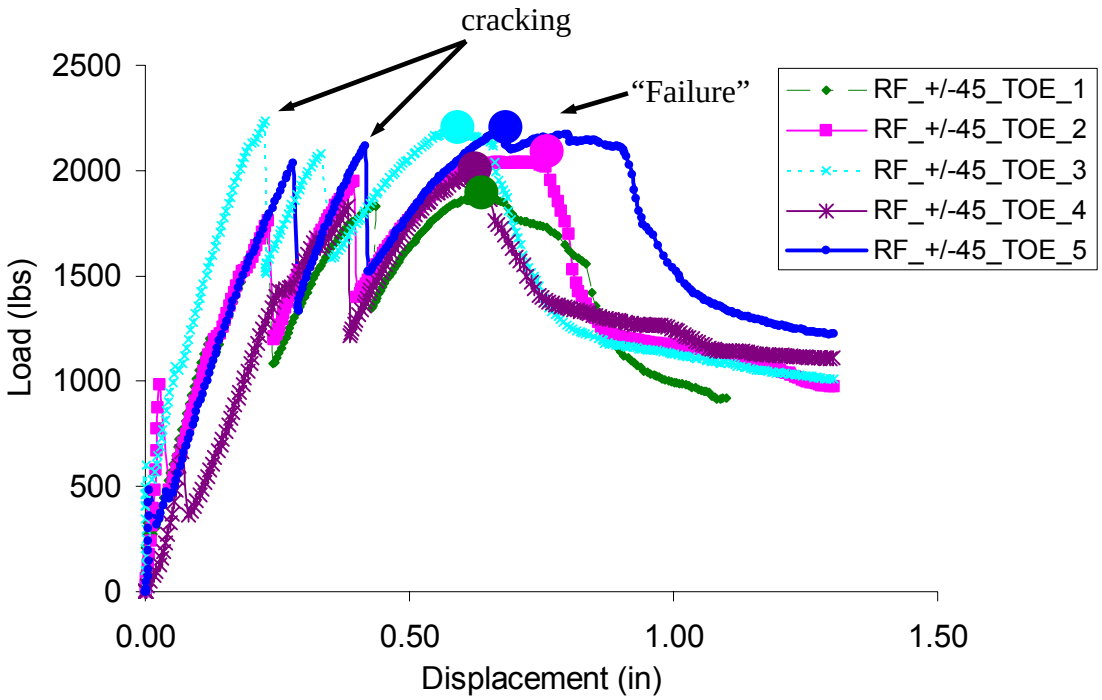

Figure 4.19: Load vs. Displacement Curves for +/- 45° Reinforced Specimens

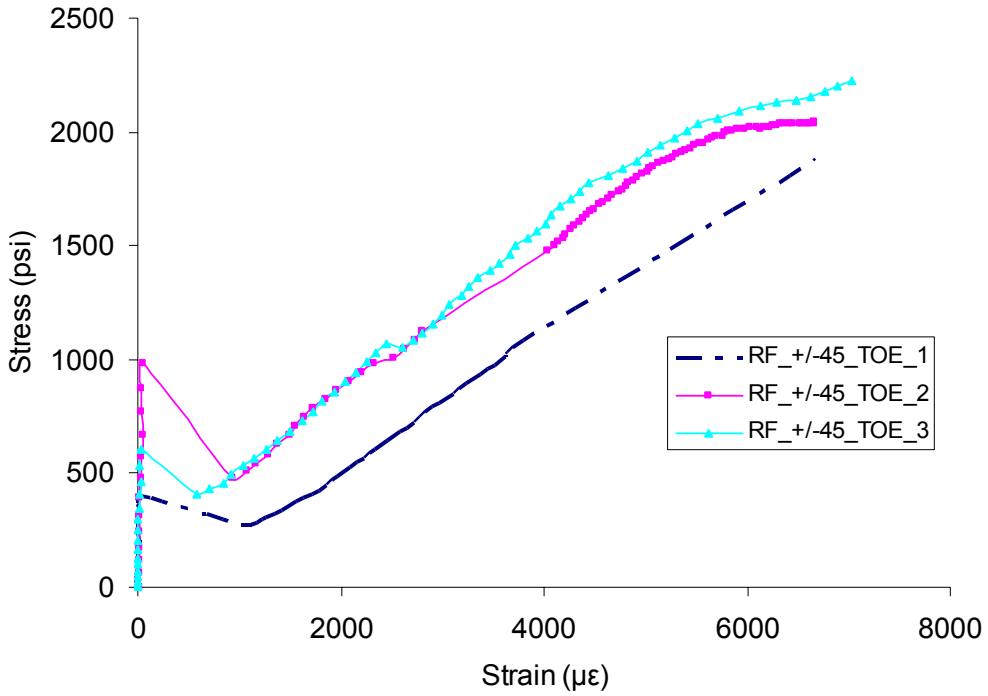

Figure 4.20: Initial Load vs. Tensile Strain for +/- 45° Retrofits

Table 4.5: +/- 45° Flexural Test Results

Specimen ID	P_{max} (lbs)	M_{max} (lb·in)	δ (in)	ε_T ($\mu\varepsilon$)	ε_C ($\mu\varepsilon$)
RF_+/-45_TOE_1	1879	8457	0.64	6672	629
RF_+/-45_TOE_2	2042	9189	0.70	6666	703
RF_+/-45_TOE_3	2237	10067	0.60	7029	n/a
RF_+/-45_TOE_4	1994	8973	0.63	n/a	n/a
RF_+/-45_TOE_5	2192	9862	0.67	n/a	n/a
Average	2069	9310	0.65	6789	666
STD	146	658	0.04	208	52
COV	7.1%	7.1%	5.9%	3.1%	7.9%

4.4.4 0/90° Reinforced Film

Load-displacement and load-strain curves for the 0/90° retrofits are displayed in Figures 4.21 and 4.22, respectively. The load-deformation curves are very similar in shape to those for the +/-45° specimens. Spikes in the curves indicate the development of

cracks in the masonry below the roller top supports and around the mortar joint. Initial cracking occurred at approximately the same load level as in the +/- 45° specimens (approximately 2000lbs) as the curves indicate. The load continues to increase, however, to an average maximum load (indicated on the plot) approximately 60% higher than that of the +/- 45° retrofits; this is likely attributable to the greater stiffness of the 0/90° film. The load-strain curves are also very similar to those obtained from +/-45° tests. They follow the same trend of increasing until cracking occurred causing the load to drop, and then increasing again until the gage capacity was exceeded. The results from the tests on the 0/90° specimens are given in Table 4.6.

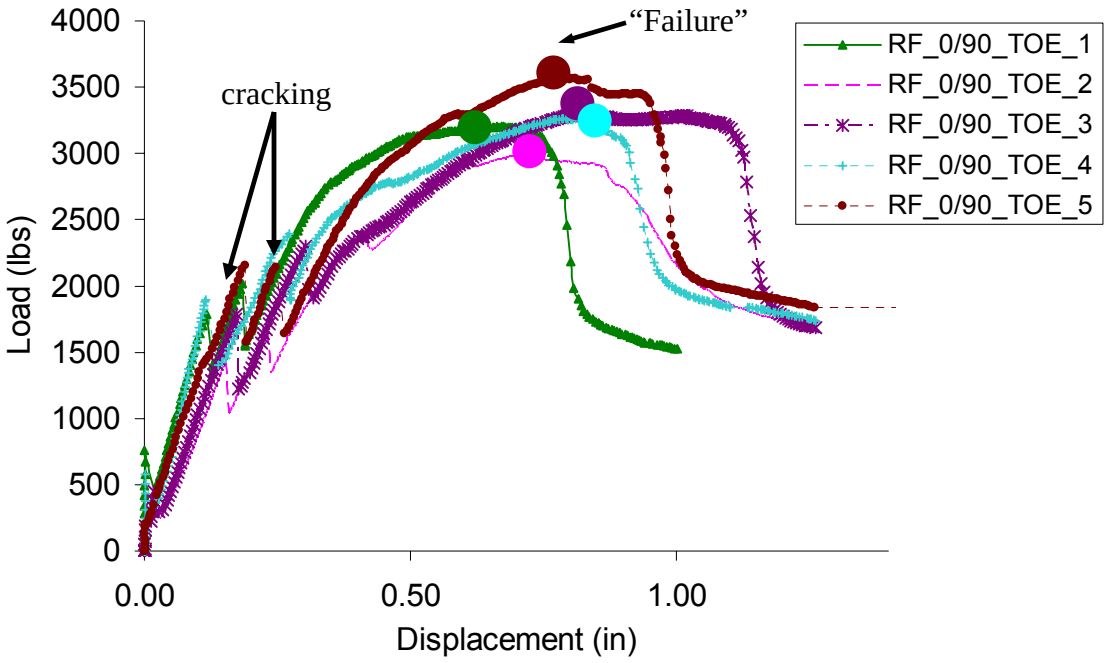

Figure 4.21: Load vs. Displacement Curves for 0/90° Reinforced Specimens

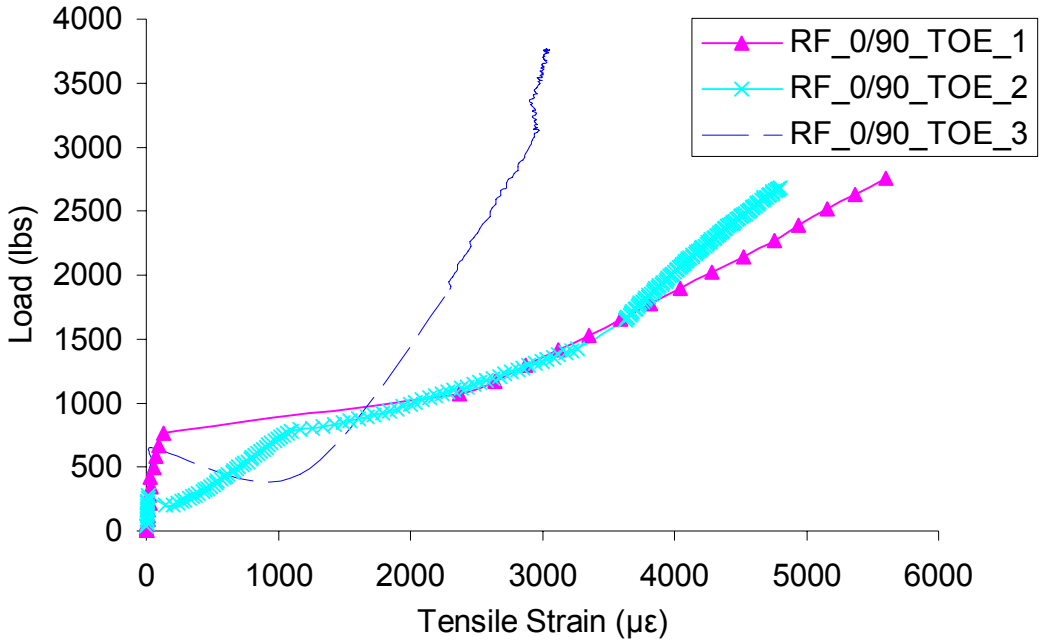

Figure 4.22: Initial Load vs. Tensile Strain for 0/90° Retrofits

Table 4.6: 0/90° Flexural Test Results

Specimen ID	P_{max} (lbs)	M_{max} (lb·in)	δ (in)	ε_T ($\mu\varepsilon$)	ε_C ($\mu\varepsilon$)
RF_0/90_TOE_1	3202	14409	0.66	5355	525
RF_0/90_TOE_2	2987	13442	0.70	5824	463
RF_0/90_TOE_3	3291	14810	0.81	3592	n/a
RF_0/90_TOE_4	3267	14701	0.82	n/a	n/a
RF_0/90_TOE_5	3568	16056	0.79	n/a	n/a
Average	3263	14683	0.76	4924	494
STD	208	938	0.07	1177	44
COV	6.4%	6.4%	9.5%	23.9%	8.9%

Table 4.7 lists the values for M^* for each elastomer retrofit. M* is defined as the moment capacity of the section once the mortar joint has separated, and the masonry has crushed in compression. Also listed are the average displacements at the approximate point where this occurs. A displacement of 0.50 inches was chosen for the unreinforced film as the point where M* would be calculated. This was done because the gradual

slope of the load-displacement curves after the maximum point made it difficult to determine a specific point where the slope decreased suddenly; this point was much easier to discern for the reinforced film specimens.

Table 4.7: M^* Values for Retrofit Materials

Test ID	Unreinforced Retrofits		+/- 45° Retrofits		0/90° Retrofits	
	M^* (lb·in)	δ^* (in)	M^* (lb·in)	δ^* (in)	M^* (lb·in)	δ^* (in)
TOE_1	1931	0.50	4995	0.91	7755	0.85
TOE_2	2439	0.50	5521	0.88	7804	1.20
TOE_3	2409	0.50	5609	0.81	7823	1.22
TOE_4	2185	0.50	6194	0.76	8974	0.99
TOE_5	2273	0.50	6419	1.04	9228	1.04
Average	2247	0.50	5747	0.88	8317	1.06
STD	204	0	567	0.11	722	0.15
COV	9.1%	0%	9.9%	12.2%	8.7%	14.5%

Results of flexural experiments indicated that the 0/90° retrofits possessed the greatest moment capacity of the material systems tested in this investigation. The stand alone epoxy specimens failed by rupture of the epoxy in tension, but rupture of the film reinforcement was not achieved in any of the retrofit specimens. All of the specimens reinforced with elastomer film had the ability to deform excessive amounts without failing in tension. This deformation did not add to the ultimate moment capacity of the static test specimens, but could be useful in dynamic events.

CHAPTER V

DEVELOPMENT OF SEMI-EMPIRICAL MODEL

5.1 INTRODUCTION

Using a typical mechanics model for reinforced masonry, along with the results of the flexural and tensile experiments, a semi-empirical model used to predict the moment capacity of hybrid elastomer/fiber reinforced masonry walls is developed. The U.S. Army plans to use this model in the development of reliable design criteria for masonry walls strengthened against air blast forces with the materials used in this study. This investigation focuses on characterizing the static behavior of these composite systems, which is the first step in understanding the way they will perform in dynamic loading events.

5.2 DEVELOPMENT OF PREDICTIVE MODEL

5.2.1 Mechanics of Film-Reinforced Masonry Sections

Figure 5.1 shows a typical beam used in the flexural experiments and Figure 5.2 shows the strain and stress distributions in the reinforced cross section. The triangular compression distribution was chosen based on the Building Code Requirements for Masonry Structures (ACI 530-99/ASCE 5-99/TMS 402-99).

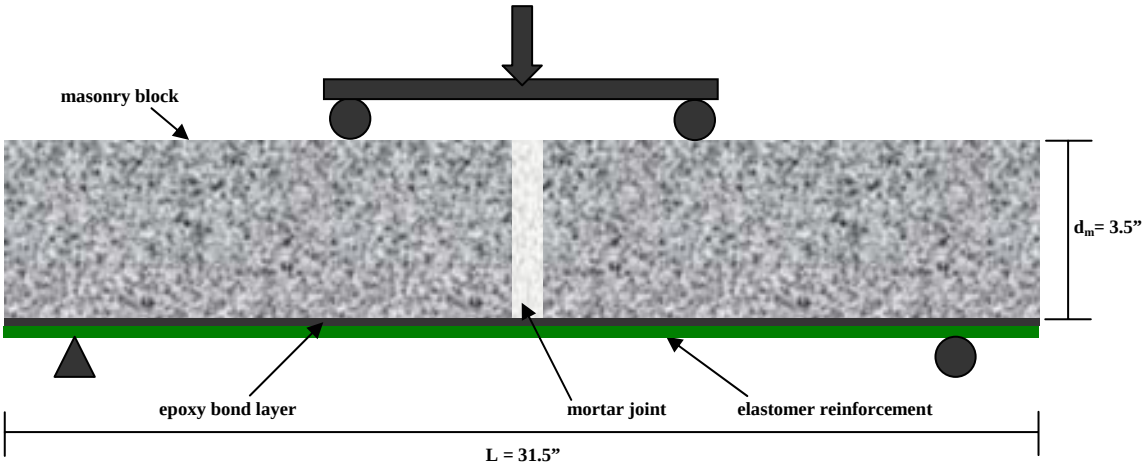

Figure 5.1: Typical Flexural Specimen

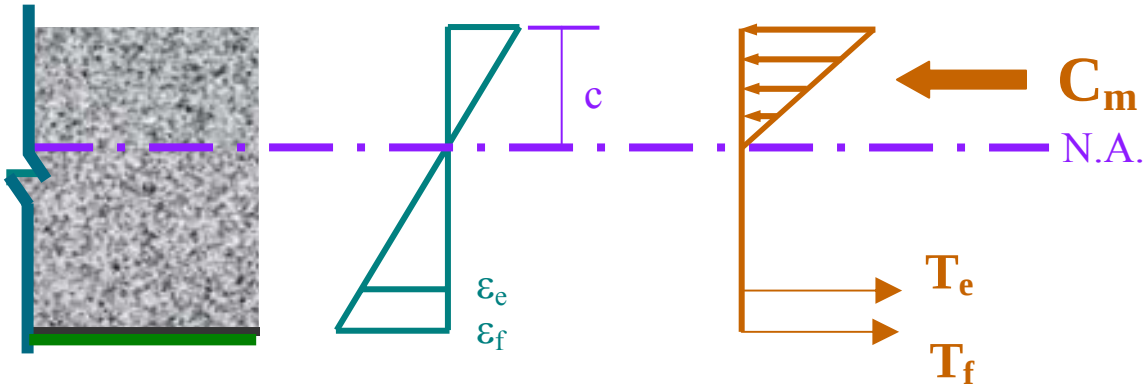

Figure 5.2: Internal Strain and Stress Distribution for Reinforced Masonry

To satisfy equilibrium in the cross section,

$$C_m = T_T = T_e + T_f \tag{5.1}$$

where C_m is the compressive force in the masonry and T_T is the total tensile force. The total tensile force is comprised of an epoxy component, T_e, and a component from the film reinforcement, T_f. The tensile strength of the masonry is neglected based on ACI 530 and therefore does not contribute to T_T. The section is assumed to be controlled by

crushing of the masonry in the compression zone. Thus, the controlling limit state is reached when the maximum compressive strain reaches a limiting value of 0.0025 in/in. It is also assumed that sections perpendicular to the axis of bending that are plane before bending remain plane after bending and the stresses in the concrete and reinforcement can be computed from the strains by using stress-strain curves obtained through material characterization (MacGregor, 2005). Based on the triangular distribution shown in Figure 5.2, the compressive force in the masonry at the limit state may be given as

$$C_m = \frac{1}{2} f_m^{'} b_m c \tag{5.2}$$

where f'_m is the ultimate compressive strength of the mortar determined through compression testing of mortar cylinders as described in Chapter 3, b_m is the width of the masonry, and c is the depth to the neutral axis. The two components of the tensile force can be written as

$$T_T = T_e + T_f = A_e f_e + A_f f_f \tag{5.3}$$

where A_e is the average cross-sectional area of the epoxy bond layer, f_e is the stress in the epoxy layer, A_f is the cross-sectional area of the film reinforcement, and f_f is the stress in the film. The ultimate moment capacity of the section, M_n, can be determined from internal static equilibrium:

$$M_n = \left(T_e + T_f\right)\left(d_m - \frac{c}{3}\right) = C_m\left(d_m - \frac{c}{3}\right) \tag{5.4}$$

where d_m is the depth of the masonry block (ignoring the thickness of the reinforcement).

5.2.2 Determination of Internal Compressive Force

Using the average maximum moment determined from the flexural experiments (see Section 4.4), the depth of the neutral axis, *c*, was calculated by substituting Equation (5.2) into Equation (5.4). Table 5.1 lists the average maximum moment and neutral axis depth for each material system.

Table 5.1: Average Neutral Axis Depth Calculated from Experimental Results

Material System	M_{max} (lb·in)	c (in)
Stand Alone Epoxy	2129	0.11
Unreinforced Film	2599	0.13
+/- 45° Film	9310	0.50
0/90° Film	14683	0.81

After calculating the depth of the neutral axis for each material system, the results were substituted into Equation (5.2) to determine the compressive force C_m at ultimate in the cross section; these results are listed in Table 5.2.

Table 5.2: Average Compressive Force in Strengthened Section at Ultimate

Material System	C_m (lbs)
Stand Alone Epoxy	615
Unreinforced Film	752
+/- 45° Film	2792
0/90° Film	4545

5.2.3 Determination of Tensile Forces in Epoxy and Film Reinforcing Layers

To satisfy static equilibrium (Equation (5.1)), the total compressive force must equal the total tensile force, which the model assumes is comprised of components from the epoxy bond layer and from the retrofit material. In order to estimate the required

stress in the reinforcing film needed to satisfy equilibrium, the tensile contribution of the epoxy must first be determined. The cross-sectional area of the epoxy was estimated based on the depth of the grooves in the trowel used to apply the epoxy layer:

$$A_e = t_e b_m = \frac{d_t}{2} b_m \tag{5.5}$$

where d_t = the depth of the trowel grooves. The strain in the epoxy layer, ε_e, at the maximum load was determined based on the assumption of a linear strain distribution as shown in Figure 5.2 with ε_{mu} = 0.0025 in/in (Tumialan, 2003) using the average neutral axis depth shown in Table 5.1. From similar triangles,

$$\varepsilon_e = \varepsilon_{mu}\left(\frac{d_m - c}{c}\right) \tag{5.6}$$

Table 5.3 lists the average strain in the epoxy layer at the maximum moment for each material system, as well as the cross-sectional areas of the epoxy bond layer and the film reinforcement.

Table 5.3: Average Strain in Epoxy Bond Layer at Ultimate

Material System	A_e (in^2)	A_f (in^2)	ε_e (in/in)
Stand Alone Epoxy	1.17	n/a	0.078
Unreinforced Film	1.17	0.38	0.063
+/- 45° Film	1.17	0.83	0.015
0/90° Film	1.17	0.83	0.008

The stress in the epoxy layer was then estimated from the stress-strain behavior obtained from tensile testing. For each stress-strain curve, the value of ε_e calculated using Equation 5.6 was plotted and the corresponding stress in the epoxy, f_e, was recorded. Figure 5.3 shows a typical stress-strain curve used to determine f_e at ε_e for

each material system. The results indicate that the lower the stiffness of the reinforcing material, the higher the stress in the epoxy; this is expected based on the mechanics of deformable solids. Table 5.4 lists stress values estimated from each curve and the resulting average epoxy stress f_e, which will be used in the model development, along with a comparison to the maximum epoxy tensile strength ($f_{e,max}$ = 1681 psi).

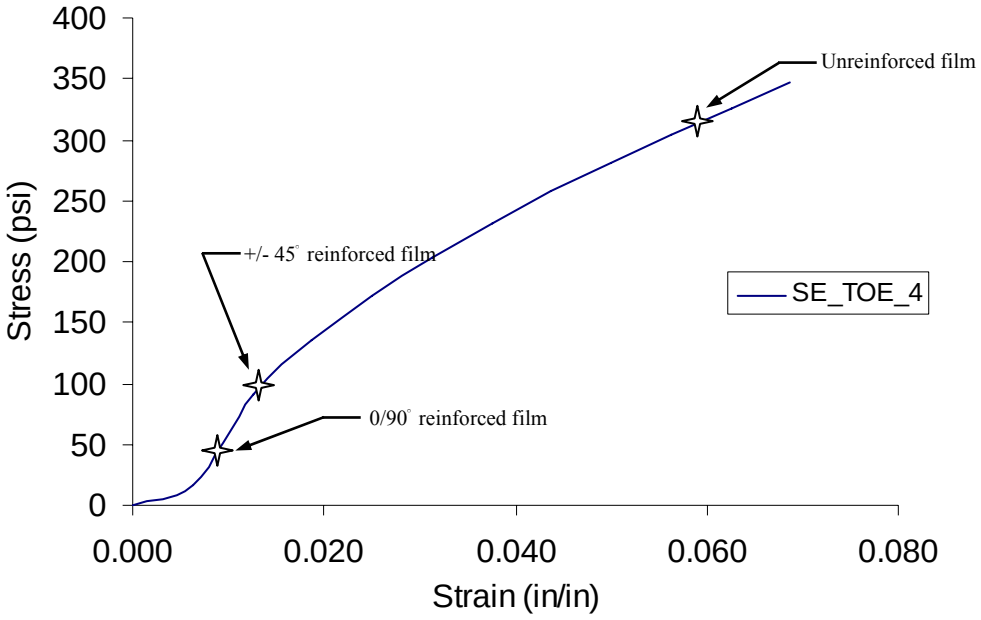

Figure 5.3: Estimation of Stress in the Bond Layer using Stress-Strain Response from Epoxy Tensile Tests

Table 5.4: Estimated Stress in Epoxy Bond Layer for Each Material Strengthening System

Specimen ID	Unreinforced Film $\varepsilon_e = 0.063$	+/- 45° Film $\varepsilon_e = 0.015$	0/90° Film $\varepsilon_e = 0.008$
	f_e (psi)	f_e (psi)	f_e (psi)
SE_TOE_1	304.4	90.3	27.9
SE_TOE_2	349.6	102.4	29.1
SE_TOE_3	316.1	108.2	30.8
SE_TOE_4	325.9	108.9	37.1
SE_TOE_5	297.0	88.0	27.1
AVERAGE	318.6	99.6	30.4
% $f_{e,max}$	19.0	5.9	1.8
STD	20.6	9.9	4.0
COV	6.5%	9.9%	13.2%

Combining Equations 5.1 and 5.3 yields

$$C_m = A_e f_e + A_f f_f \tag{5.7}$$

The average values for C_m, A_e, A_f, and f_e from Tables 5.2 – 5.4 were substituted into Equation 5.7 to determine the stress in the film, f_f. Table 5.5 lists a summary of the calculated values.

Table 5.5: Determination of Tensile Stress in Reinforcing Film Required for Static Equilibrium

Material System	M_{max} (lb·in)	c (in)	$C_m=T_e+T_f$ (lbs)	ε_e (in/in)	$f_{e,avg}$ (psi)	$f_{f,required}$ (psi)
Stand Alone Epoxy	2129	0.11	615	0.078	524	n/a
Unreinforced Film	2599	0.13	752	0.063	319	1010
+/- 45° Film	9310	0.50	2792	0.015	99.6	3243
0/90° Film	14683	0.81	4545	0.008	30.4	5456

The calculated film stress values were then compared to the tensile testing results to determine the effective stress, f_{fe}, which should be used in the predictive model. Table 5.6 lists the tensile strengths for the Stage II materials obtained from the testing program

described in Chapter 3. Results from the 5 inch and 1.5 inch coupon tests were selected for the +/- 45° and 0/90° films, respectively. These values were chosen because it is believed they represent the closest available estimate of the actual tensile behavior of the elastomers when bonded to the masonry, although it is believed that an accurate measurement of the tensile capacity of the +/-45° film was not obtained due to an inability to engage fibers during testing. The tensile strength at the proportional limit of the unreinforced film is reported because obtaining an ultimate tensile strength was not possible with the current test fixture. The proportional limit was determined by plotting the initial portion of the curve up to the last data point before the R^2 value dropped below 0.95. The R^2 value is the square of the correlation coefficient. The correlation coefficient gives a measure of the linear relationship between the x and y values. Values close to 1 indicate excellent linear reliability. It should be noted that tensile strength values averaging 2387 psi were recorded for the unreinforced coupons before the travel limit was reached.

Table 5.6: Strength Values from Coupon Tests

Test ID	Unreinforced	0/90	+/- 45
	$f_{f=PL}$ (psi)	f_f (psi)	f_f (psi)
T_1	876	5396	1548
T_2	778	5504	1524
T_3	976	5330	1526
T_4	854	5730	1548
T_5	802	6881	1643
Average	857.2	5768	1558
STD	77.1	640.3	49.0
COV	9.0%	11.1%	3.1%

The true stress at ultimate for the reinforced films and at the proportional limit for the unreinforced film was estimated by measuring the cross section of tensile test coupons at the moment the curve being generated onscreen reached these points. The original width w_o and thickness t_o of the coupons are listed in Table 5.7, along with the width w_1 and thickness t_1 at either ultimate or at the proportional limit. A ratio of the original cross section to the reduced cross section (shown in Table 5.7) was calculated and multiplied by the stress values in Table 5.6 to determine the true stress values listed in Table 5.8.

Table 5.7: Original and Reduced Cross-Sectional Areas

Material	t_o (in)	w_o (in)	t_1 (in)	w_1 (in)	$\frac{A_o}{A_1}$
Unreinforced Film	0.05	1.0	0.043	0.750	1.55
+/- 45° Film	0.11	3.5	0.088	2.025	2.16
0/90° Film	0.11	2.0	0.095	1.825	1.27

Table 5.8: True Strength Values from Coupon Tests

Test ID	Unreinforced		0/90		+/- 45	
	$f_{f=PL,true}$ (psi)	$f_{f=PL}$ (psi)	$f_{f,\,true}$ (psi)	f_f (psi)	$f_{f,\,true}$ (psi)	f_f (psi)
T_1	1358	876	6847	5396	3344	1548
T_2	1206	778	6984	5504	3293	1524
T_3	1513	976	6763	5330	3297	1526
T_4	1324	854	7271	5730	3344	1548
T_5	1243	802	8731	6881	3550	1643
Average	1329	857	7319	5768	3366	1558
Variation	55.0%		26.9%		116.0%	
STD	120	77.1	813	640.3	106	49.0
COV	9.0%	9.0%	11.1%	11.1%	3.1%	3.1%

The calculated stress values required for static equilibrium are listed in Table 5.9 along with the average proportional limit for the unreinforced film and the average

ultimate tensile strength (engineering and true) for the fiber reinforced films for comparison. Table 5.10 lists the percentages of calculated engineering and true stress values the required stress represents.

Table 5.9: Comparison of Required Stress and Tensile Test Results

Material System	$f_{f,required}$ (psi)	$f_{f,avg}$ (psi)	$f_{f,true}$ (psi)
Stand Alone Epoxy	524*	1681	n/a
Unreinforced Film	1010	857	1329
+/- 45° Film	3243	1558	3366
0/90° Film	5466	5768	7319

*$f_{f,required}=f_e$ for the stand alone epoxy

Table 5.10: Comparison of Required Stress to Engineering and True Strengths

Epoxy		Unreinforced		+/- 45°		0/90°	
f_e = 527 psi		f_f = 1010 psi		f_f = 3243 psi		f_f = 5466 psi	
$\%f_{e,max}$	$\%f_{e,true}$	$\%f_{f,PL}$	$\%f_{f,true}$	$\%f_{f,max}$	$\%f_{f,true}$	$\%f_{f,max}$	$\%f_{f,true}$
31.2	n/a	117.8	76.0	208.2	96.4	94.8	74.7

For the flexural specimens strengthened only with an epoxy layer, the value listed in Table 5.9 is the stress in the epoxy. It will be compared to the average ultimate tensile strength of the epoxy in order to determine the effective stress that should be used in predicting the capacity of the stand-alone epoxy strengthened specimens. The required epoxy stress is 31% of the average ultimate stress for the epoxy determined from the tensile tests (Table 3.6). Figure 5.4 shows the location of the required stress in the epoxy, f_e, (Table 5.9) on a typical epoxy stress-strain curve.

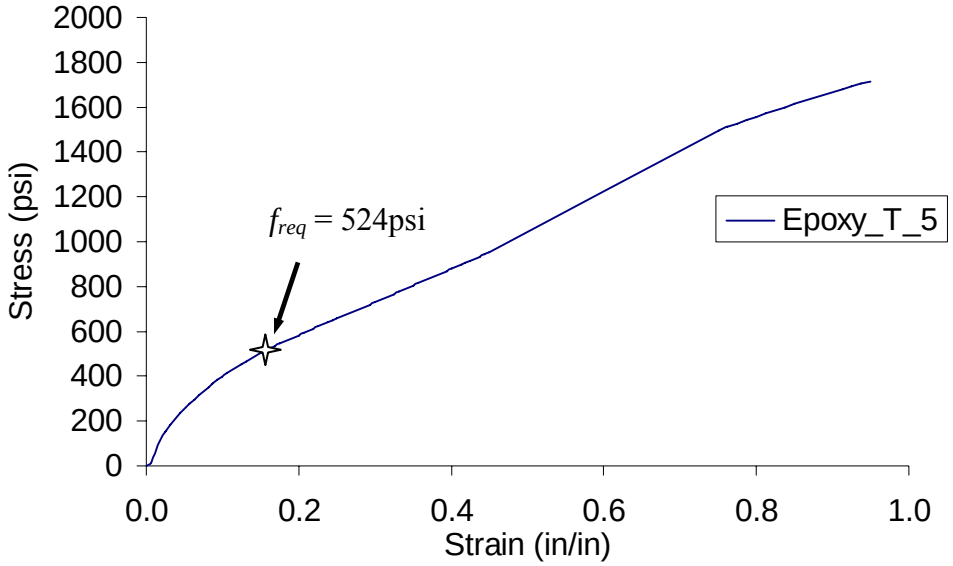

Figure 5.4: Location of f_e on Typical Epoxy Tensile Stress-Strain Curve

For the unreinforced film, the stress required for static equilibrium was approximately 18% higher than the average proportional limit obtained from tensile testing. Figure 5.5 shows a typical stress-strain curve with the location of f_f calculated using Equation 5.7.

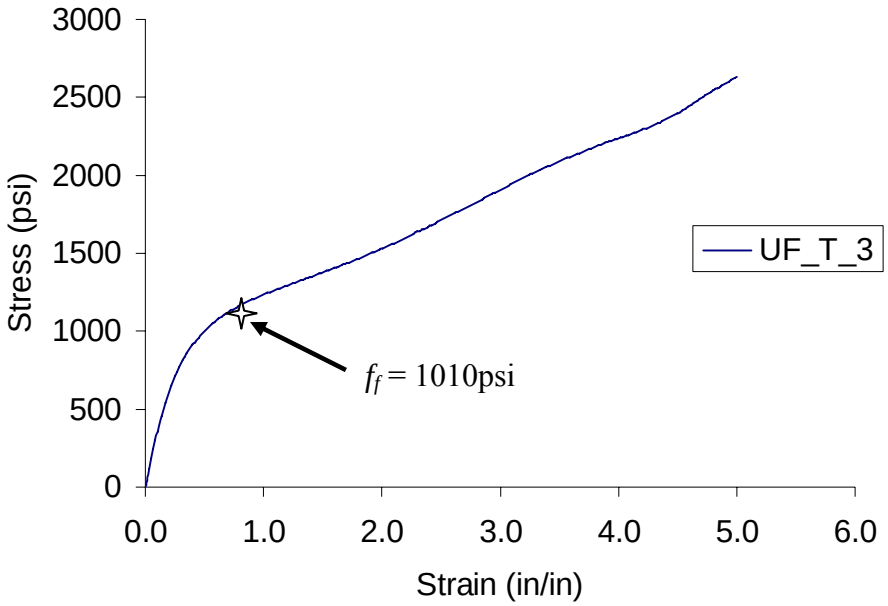

Figure 5.5: Location of f_f on Typical Unreinforced Film Tensile Stress-Strain Curve

As can be seen in Table 5.9, the required stress in the +/- 45° reinforced film is higher than the ultimate tensile strength obtained by material characterization. Figure 5.6 shows the location of the predicted stress, f_f, on a plot with a typical +/-45° stress-strain curve. The required stress value does not fall on the curve. As discussed in Section 3.2, this is attributed to the inability of the tensile test apparatus used in this investigation to engage a sufficient number of fibers in the film. This was demonstrated by material characterization of coupons with varying widths as shown in Figure 3.17. As the width increased, more fibers in the cross section were engaged, and the measured ultimate tensile strength increased. It is expected that a higher tensile capacity would be recorded if it were possible to test a 7.5-inch-wide coupon with a short gage length. This would more closely represent the conditions of the flexural test specimens.

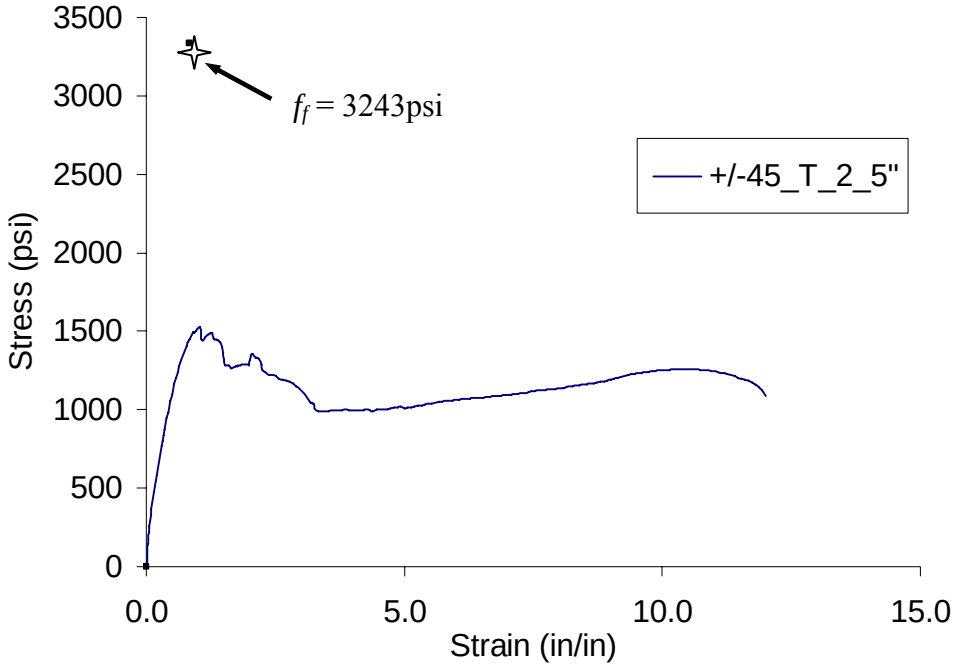

Figure 5.6: Location of f_f on typical +/- 45° Tensile Stress-Strain Curve

Based on experimental observation, it is believed that the +/-45° retrofits, like the 0/90° retrofits, were still in the linear range at the peak load in the flexural tests and that the calculated required stress is more representative of the actual tensile capacity of the film. It is also believed that the tensile capacity is a function of the number of fibers that are engaged during testing. The maximum number of fibers engaged in material characterization was between 2 and 3 in one direction, depending on the way the coupon was aligned in the grips. This is demonstrated in Figures 3.18 and 3.19. As stated earlier, approximately 5 fibers in one direction were engaged around the mortar joint during the flexural tests as shown in Figure 3.15. As such, for this model development, a linear relationship between the fiber area engaged and the resulting maximum stress will be assumed. For the 5 inch coupons, an average of 2.5 fibers were engaged (some tests

engaged 2, others engaged 3). Therefore, the maximum stress in the +/-45° film will be estimated as

$$f_{f,\max} = \left(\frac{5 \ fibers \ engaged}{2.5 \ fibers \ engaged} \right) \cdot f_{\max,5"coupon} = 2 \cdot f_{\max,5"coupon} \qquad (5.8)$$

Therefore, f_{max} for the +/- 45° film will be taken as 3116psi. This will only be assumed for use in the predictive model for this investigation. Obviously, more testing is required to gain a better understanding of the tensile behavior of this film and to obtain more consistent results.

For the 0/90° retrofits, the required film stress is 94.8% of the average maximum tensile strength from the tensile tests performed on 1.5-inch-wide coupons. Figure 5.7 shows the location of f_f on a typical stress-strain curve.

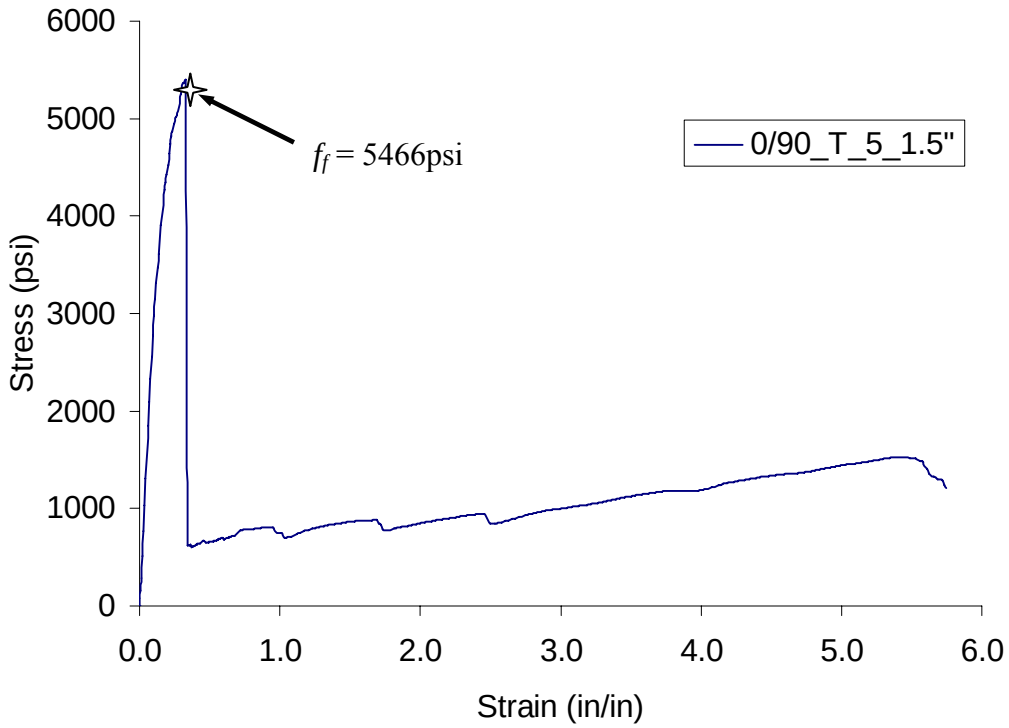

Figure 5.7: Location of f_f on Typical 0/90° Tensile Stress-Strain Curve

A summary of average stresses in the various reinforcing layers for each material system based on the flexural test results is provided in Table 5.11. Note that the average ultimate strength of the +/-45° film has been modified based on Equation 5.8.

Table 5.11: Comparison of Required Stress and Tensile Test Results

Material System	$f_{f,required}$ (psi)	$\%f_{f,avg}$	f_e (psi)	$\%f_{e,max}$
Stand Alone Epoxy	n/a	n/a	524	31.2
Unreinforced Film	1010	118	319	19.0
+/- 45° Film	3243	104	99.6	5.9
0/90° Film	5466	94.8	30.4	1.8

*$\%f_{f,avg} = \%f_{PL}$ for the unreinforced film

5.3 FIRST-PHASE DESIGN CRITERIA

Combining Equations (5.2) - (5.4) leads to the following equation that can be used to estimate the moment capacity of a strengthened masonry section, assuming crushing of the masonry in the compression zone is the controlling limit state:

$$M_n = \left(A_e f_e + A_f f_{fe}\right)\left(d_m - \frac{2\cdot\left(A_e f_e + A_f f_{fe}\right)}{3\cdot\left(f_m' b_m\right)}\right) \tag{5.9}$$

Based on the results of this investigation, a predictive design criteria for unreinforced masonry walls subject to out-of-plane loading is proposed based on Equation 5.9. Conservative values to use for the epoxy stress f_e* and film stress f_{fe} for the various types of film reinforcement are offered in Table 5.12. In the reinforced specimens, the tensile contribution from the epoxy layer is small compared to the contribution from the film and will therefore be neglected in the design equation.

Table 5.12: Proposed Stress Values in Epoxy Layer and Reinforcing Film for Use in Equation 5.9

Material System	f_e^* (psi)	f_{fe} (psi)
Stand Alone Epoxy	$0.30f_{e,max}$	n/a
Unreinforced Film	$0.20f_{e,max}$	f_{PL}
+/- 45° Film	0	$f_{f,max}$
0/90° Film	0	$f_{f,max}$

These values were used with Equation (5.9) to calculate the design moment capacity M_n; the results are given in Table 5.13. A graphical representation of the comparison between the experimentally determined moment capacity M_{max} and the proposed design moment capacity M_n is given in Figure 5.8. A simplified design example using the proposed design guidance is given in Appendix I.

Table 5.13: Theoretical and Experimental Moment Capacities

Material System	Specimen ID	M_n (k·ft)	M_{max} (k·ft)	$M_{max,avg}$ (k·ft)	M_{max}/M_n	Average M_{max}/M_n
Stand Alone Epoxy	SE_TOE_1	0.17	0.19	0.18	1.10	1.04
	SE_TOE_2		0.17		1.02	
	SE_TOE_3		0.19		1.09	
	SE_TOE_4		0.18		1.04	
	SE_TOE_5		0.17		0.98	
Unreinforced Film	UF_TOE_1	0.20	0.17	0.22	0.81	1.06
	UF_TOE_2		0.22		1.08	
	UF_TOE_3		0.25		1.22	
	UF_TOE_4		0.22		1.08	
	UF_TOE_5		0.23		1.10	
+/-45° Reinforced Film	RF_+/-45_TOE_1	0.70	0.70	0.78	1.01	1.11
	RF_+/-45_TOE_2		0.77		1.09	
	RF_+/-45_TOE_3		0.84		1.20	
	RF_+/-45_TOE_4		0.75		1.07	
	RF_+/-45_TOE_5		0.82		1.17	
0/90° Reinforced Film	RF_0/90_TOE_1	1.22	1.20	1.22	0.98	1.00
	RF_0/90_TOE_2		1.12		0.92	
	RF_0/90_TOE_3		1.23		1.01	
	RF_0/90_TOE_4		1.23		1.00	
	RF_0/90_TOE_5		1.34		1.10	

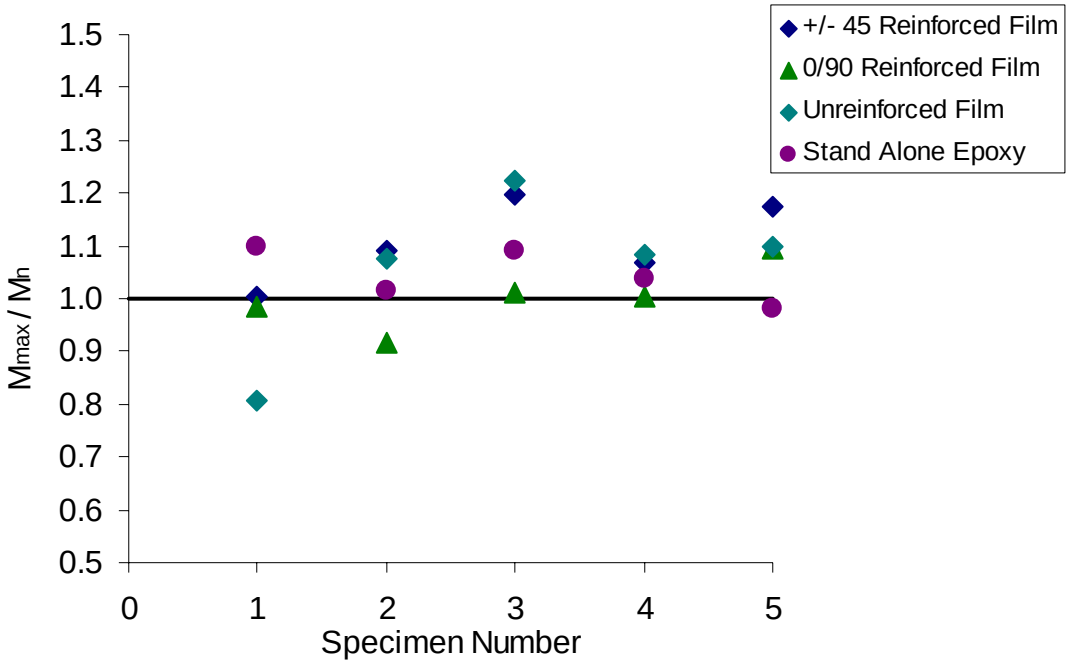

Figure 5.8: Comparison Between Experimental Values and Proposed Design Criteria

The values of M_{max}/M_n less than 1.0 in Table 5.13 denote specimens with an experimentally determined moment capacity lower than the design predictions, which indicates a nonconservative approach. However, this only occurred in four specimens and the variation for these was only greater than 2% in two specimens. While the proposed design guidance is obviously in need of refinement, it appears to provide a reasonable estimate of the moment capacities of the reinforced masonry sections studied in this investigation. The development of rational strength reduction factors for the proposed criteria to ensure consistent conservatism in the design process will be part of future investigations. To illustrate this, Table 5.14 shows the values of M_{max}/M_n that would result from applying a reduction factor $\varphi = 0.6$ (ACI 530, Section 3.1.4) to the design equation predictions; Figure 5.9 shows a graphical representation of results. The inclusion of this reduction factor results in design moments exceeding the experimental

results by 28 – 79% for 19 of the 20 specimens tested. Only one specimen still falls below design predictions by 2%, and it is likely that the mortar joint cracked while the specimen was being loaded into the test frame, causing the experimental maximum moment to much lower than expected.

Table 5.14: Theoretical and Experimental Moment Capacities with Proposed Strength Reduction Factor

Material System	Specimen ID	M_n (k·ft)	M_{max} (k·ft)	$M_{max,avg}$ (k·ft)	M_{max}/M_n	Average M_{max}/M_n
Stand Alone Epoxy	SE_TOE_1	0.10	0.19	0.18	1.82	1.73
	SE_TOE_2		0.17		1.68	
	SE_TOE_3		0.19		1.81	
	SE_TOE_4		0.18		1.72	
	SE_TOE_5		0.17		1.62	
Unreinforced Film	UF_TOE_1	0.17	0.17	0.22	0.98	1.28
	UF_TOE_2		0.22		1.31	
	UF_TOE_3		0.25		1.49	
	UF_TOE_4		0.22		1.32	
	UF_TOE_5		0.23		1.34	
+/-45° Reinforced Film	RF_+/-45_TOE_1	0.43	0.70	0.78	1.63	1.79
	RF_+/-45_TOE_2		0.77		1.77	
	RF_+/-45_TOE_3		0.84		1.94	
	RF_+/-45_TOE_4		0.75		1.73	
	RF_+/-45_TOE_5		0.82		1.90	
0/90° Reinforced Film	RF_0/90_TOE_1	1.22	1.20	1.22	1.55	1.58
	RF_0/90_TOE_2		1.12		1.45	
	RF_0/90_TOE_3		1.23		1.60	
	RF_0/90_TOE_4		1.23		1.59	
	RF_0/90_TOE_5		1.34		1.73	

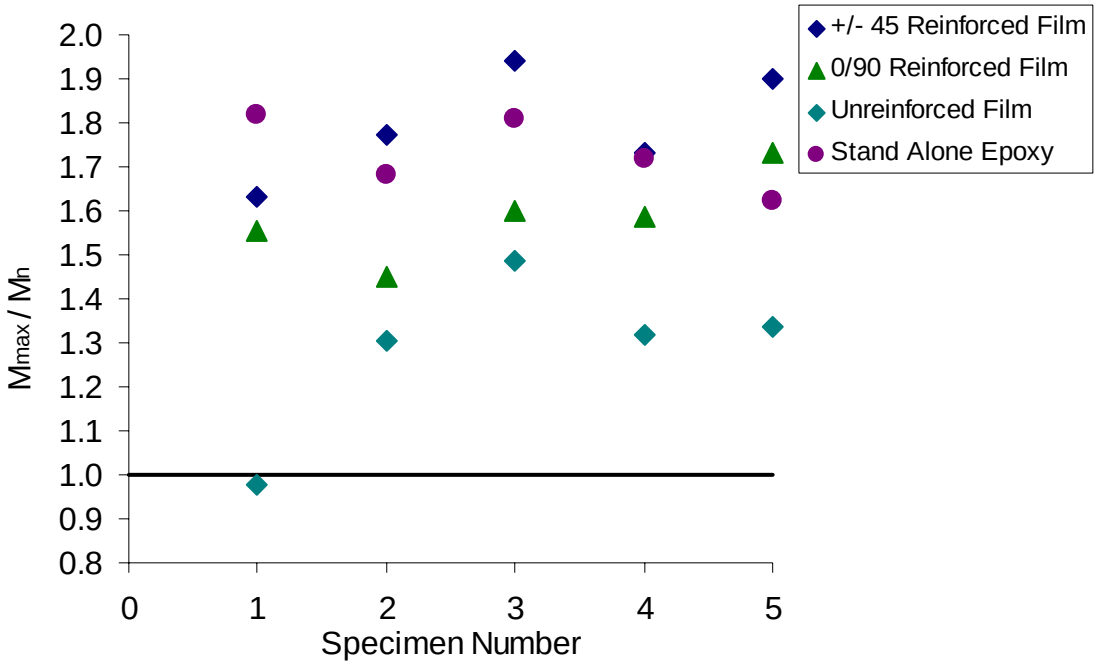

Figure 5.9: Comparison Between Experimental and Design Moments with Proposed Strength Reduction Factor

CHAPTER VI

CONCLUSIONS AND RECOMMENDATIONS

6.1 CONCLUSIONS

Based on the results and observations of this investigation, the following conclusions can be made:

1) Based on tensile testing results and ease of installation, Stage II materials do appear more promising as structural retrofits than Stage I materials. The ultimate tensile strength of Stage II materials was approximately 108% larger than the ultimate tensile strength of comparable Stage I materials. The skill required to properly install Stage I material reinforcement (particularly relative to achieving a uniform thickness) provides further evidence that Stage II materials are collectively the better choice.
2) Due to extensive deformation during tensile testing, standard wedge grips are not sufficient to test these materials. When this was attempted, coupons slipped out of the grips prior to failing. As such, it was determined that pneumatic grips or a modified testing apparatus is required to accurately characterize the elastomeric materials.
3) The failure mechanism of the unreinforced elastomer film in direct tension was not observed due to travel restrictions on the test frame. The 0/90° reinforced film failed by rupture of the fibers oriented at 0° to the longitudinal axis of the coupon followed by slipping of the fibers between the layers of elastomer as it deformed. One layer of film typically ruptured first, and the remaining layer ruptured shortly thereafter. The rupture of both layers of

elastomer completed failure of the system. The +/- 45° reinforced film coupons failed similarly to the 0/90° reinforced film except no rupture occurred in the fibers. The fibers slipped between the two layers of elastomer and the layers deformed until they both ruptured. In order to accurately assess the tensile capacity of the fiber reinforced elastomers, the fibers must be engaged by the load – as was seen in the flexural testing.

4) The shape of the stress-strain curves generated through tensile testing for the unreinforced elastomers investigated in this study were nonlinear in comparison to typical fiber reinforced polymer materials. The curves exhibited linear behavior over the initial portion but rapidly became nonlinear. The addition of fiber reinforcement significantly increased ultimate tensile strength of the materials. The curves also exhibited linear behavior up to a point where rupture of the fibers occurred. The specimens then underwent a rapid loss of load-carrying capacity.
5) In both tensile and flexural testing, excessive deformation in the elastomer films was observed. This deformation was not beneficial in static testing, but the extra energy absorption provided by material's extreme ability to deflect without rupturing could be extremely advantageous.
6) The failure mechanism observed in flexural test specimens was crushing of the masonry in compression. This agrees with the reinforced masonry mechanical model selected for use in the predictive equation developed in this investigation.

7) Both the 0/90° and +/- 45° reinforced films performed more desirably than the unreinforced film in the flexural test program. All three Stage II materials added ductility to the system, but the unreinforced film provided a smaller increase in the flexural capacity of the section.
8) Of the two reinforced Stage II materials, the film with fibers oriented at 0 and 90° seems to be the best choice as a structural retrofit to resist static flexural stresses. It allows a significant amount of deformation (ductile membrane response) but does provide the strength necessary to resist higher loads than the film with fibers oriented at +/- 45°. However, these static test results must be correlated with dynamic test results in order to make an objective assessment on the impact of fiber orientation on the performance of strengthened masonry elements.
9) The predictive model presented in this investigation provides a reasonable estimate of the nominal moment capacity of masonry sections strengthened with the hybrid elastomer/fiber materials examined in this study. Model predictions for each material system varied from the measured experimental results by an average of 6%, with the largest variation of 22% likely attributable to premature failure of that particular specimen during testing.
10) The contribution of the epoxy bond layer to the flexural capacity of the strengthened section should be accounted for when the reinforcing film is extremely pliable, as in the case of the unreinforced material. The addition of reinforcing fibers to the elastomeric material increased the stiffness of the film and thus reduced the contribution of the epoxy layer, so that it may reasonably

be neglected in the development of reliable design criteria for the masonry sections.

6.2 RECOMMENDATIONS FOR FUTURE STUDY

First, it is crucial that additional material characterization of these elastomeric materials be performed to validate test results. Mechanical properties are a vital part of model development and therefore need to be verified. Additional tests should be performed on coupons with varying widths and gage lengths using pneumatic grips or a modified test apparatus similar to what was used in this investigation.

Since the inception of this investigation, U.S. Army researchers developed a further simplified method of field installation. A new "peel and stick" method of application is currently being evaluated in dynamic experiments and needs to be researched in static loading conditions. The new application process consists of a two-sided adhesive film that is first applied to the retrofit material. Then the backing is removed and the film is rolled onto the masonry wall. Researchers are concerned, however, that bond failure is a potential problem with this system of application. Therefore, tests need to be performed to investigate the bond strength and determine experimentally if loss of bond is the controlling mode of failure.

The flexural investigation should be expanded to include uniform loading as opposed to the four point bend test used in this study. This should be done in order to avoid cracking due to contact stresses under the top supports and to better simulate actual loads experienced by the composite system in service, such as blast waves. In addition to

this, the span length, thickness of the epoxy bond layer, and other parameters should be varied to determine the efficacy of the predictive model.

A problem that has been identified in dynamic wall testing performed by ERDC is failure where the retrofit material is anchored at its supports. Further investigation into the bond strength of these materials at anchor points needs to take place.

Reduction factors should be determined for these materials through further experimentation. In the design of externally bonded FRP systems for strengthening concrete structures (ACI 440.2R-02), various reductions such as an environmental reduction factor, C_E and a reduction factor for FRP contribution, ψ, are applied to ensure conservative predictions of ultimate moment capacity. Other reductions are applied based on serviceability and bond efficiency. These factors should be further investigated to determine their applicability to elastomer strengthening systems.

The effects of temperature on these material systems should also be investigated. Large temperature variations could exist between the inner and outer faces of retrofit walls when these material systems are in service and the effect these variations would have on the elastomer's performance should be determined.

APPENDIX A

DESIGN EXAMPLE

PRESSURE ON A STRENGTHENED MASONRY WALL

Determine the maximum out-of-plane static pressure that can be carried by an 8-foot masonry wall. The wall was originally constructed using 3.5 x 7.5 x 15.5 inch masonry blocks, and has recently been retrofitted with a fiber-reinforced elastomeric film that is epoxy bonded to the tension surface, as shown in Figure A.1. Fiber orientation is 0/90° relative to the wall height. The wall is assumed to be simply supported top and bottom. The effects of in-plane axial loads are ignored.

Masonry Strength f'_m =1,900psi

Mortar Strength f'_{mo}=1,500psi

Epoxy tensile strength f_e =1,600psi

Epoxy thickness t_f = 0.13”

Epoxy Cross-sectional Area $A_e = t_f \cdot b_m = 0.975$ in^2

Film tensile strength f_f =5,800psi

Film thickness t_f = 0.11”

Film Cross-sectional Area $A_f = t_f \cdot b_m = 0.825$ in^2

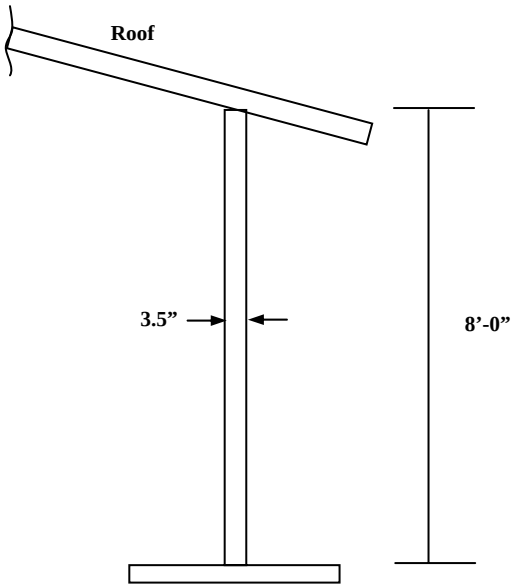

Figure A.1: Retrofitted Masonry Wall

If a strip of the wall is isolated around a mortar joint, the system can be idealized as shown in Figure A.2.

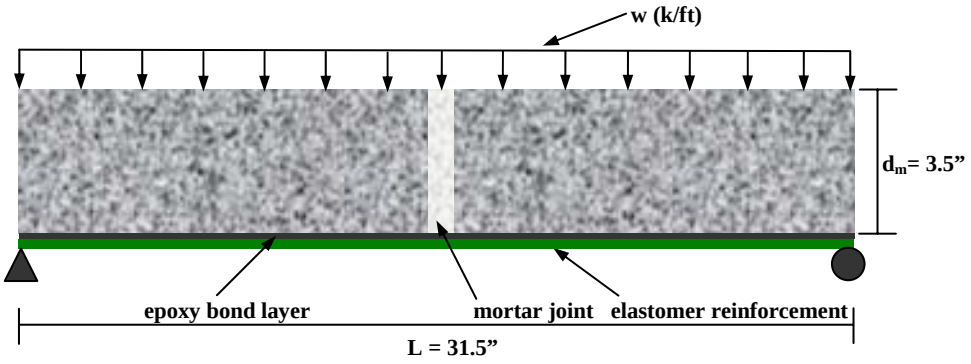

Figure A.2: Critical Section

First, the moment capacity M_n of the section should be determined using the design equation proposed for unreinforced masonry strengthened with an elastomer film,

$$M_n = \left(A_e f_e + A_f f_{fe}\right)\left(d_m - \frac{\left(A_e f_e + A_f f_{fe}\right)}{f_m' b_m}\right) \tag{A.1}$$

Given values are substituted into Equation A.1 to determine the nominal moment capacity. For the 0/90° reinforced film, the tensile contribution of the epoxy is neglected and the effective stress in the film $f_{fe} = f_{max}$. The compressive strength of the mortar will be used because crushing of the mortar will control failure.

$$M_n = \left(0 + 0.825in^2 \cdot 5800\,psi\right)\left(3.5in - \frac{\left(0 + 0.825in^2 \cdot 5800\,psi\right)}{1{,}500\,psi \cdot 7.5in}\right)$$

$$M_n = 14{,}712\ lb \cdot in$$

For a uniformly loaded, simply supported beam, the moment is

$$M_n = M_{\max} = \frac{w \cdot \ell^2}{8} \tag{A.2}$$

Solving for *w* and substituting values yields

$$w = \frac{8 \cdot M_n}{\ell^2} = \frac{8 \cdot 14{,}721 lb \cdot in}{\left(31.5in\right)^2} = 118.6\ {}^{lbs}\!/_{in}$$

$$w = 1.42\ {}^{k}\!/_{ft}$$

The maximum out-of-plane static pressure ρ that can be placed on the wall can be determined using

$$\rho = \frac{w}{b_m} = \frac{1.42\ {}^{k}\!/_{ft}}{\left(7.5in \cdot \left(\frac{1\,ft}{12in}\right)\right)}$$

$$\rho = 2.28\ {}^{k}\!/_{ft^2}$$

APPENDIX B

STAGE II MATERIAL TESTING RESULTS

Epoxy Tensile Test Plots

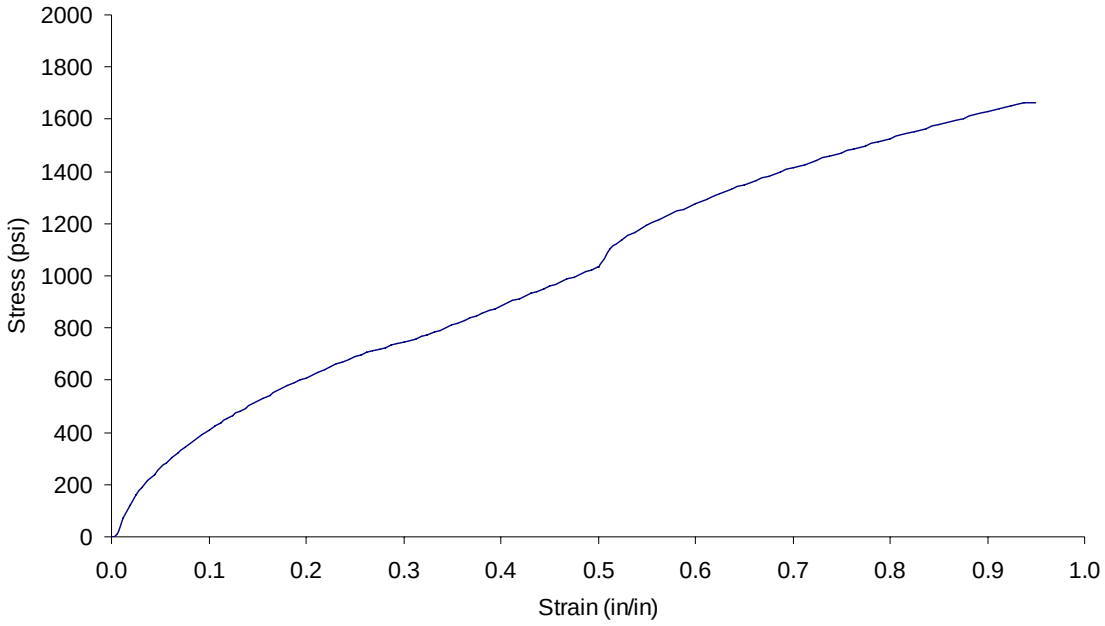

Figure A.1: Epoxy_T_1 Stress vs. Strain

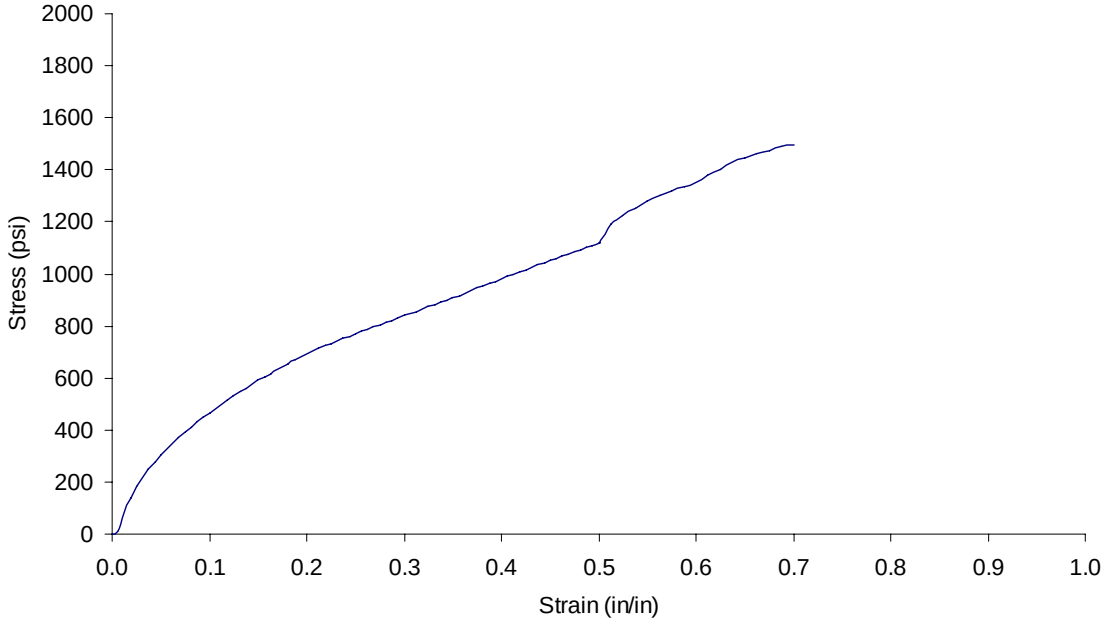

Figure A.2: Epoxy_T_2 Stress vs. Strain

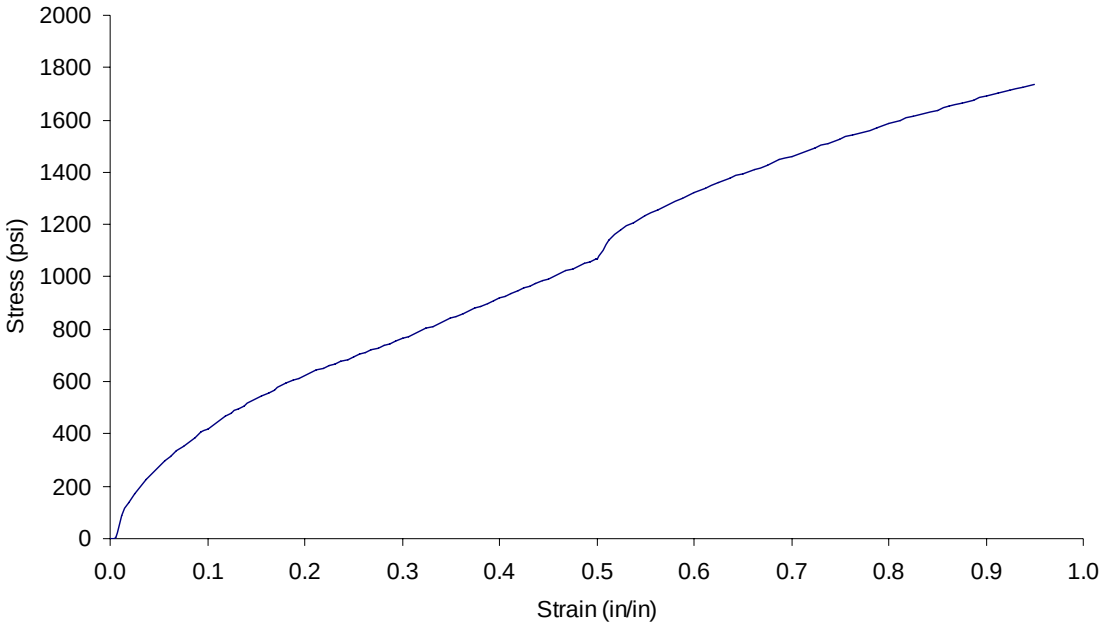

Figure A.3: Epoxy_T_3 Stress vs. Strain

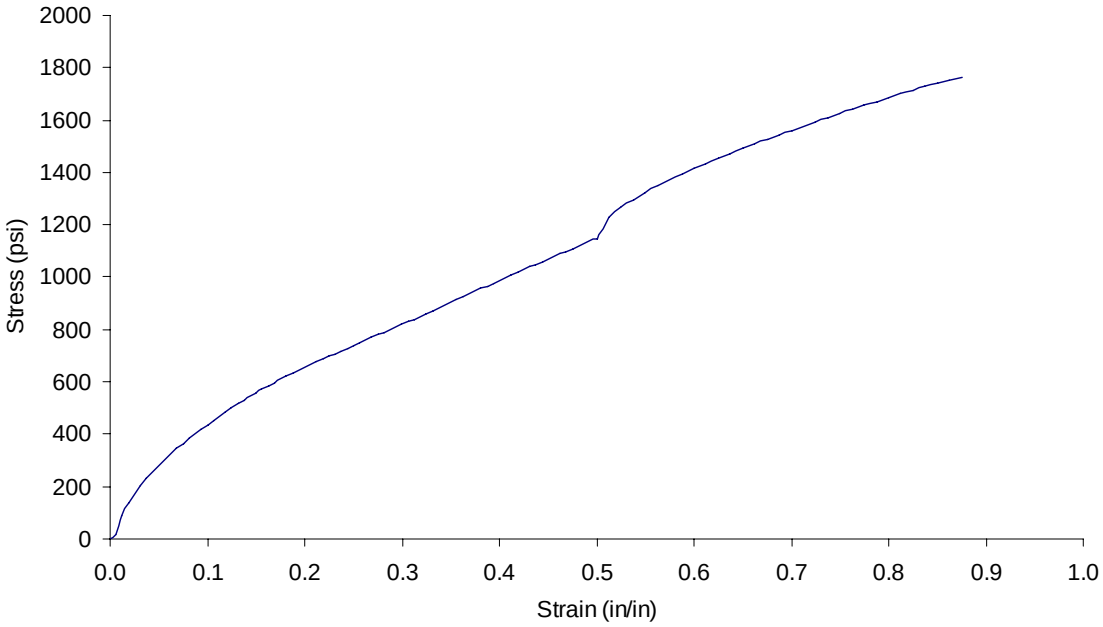

Figure A.4: Epoxy_T_4 Stress vs. Strain

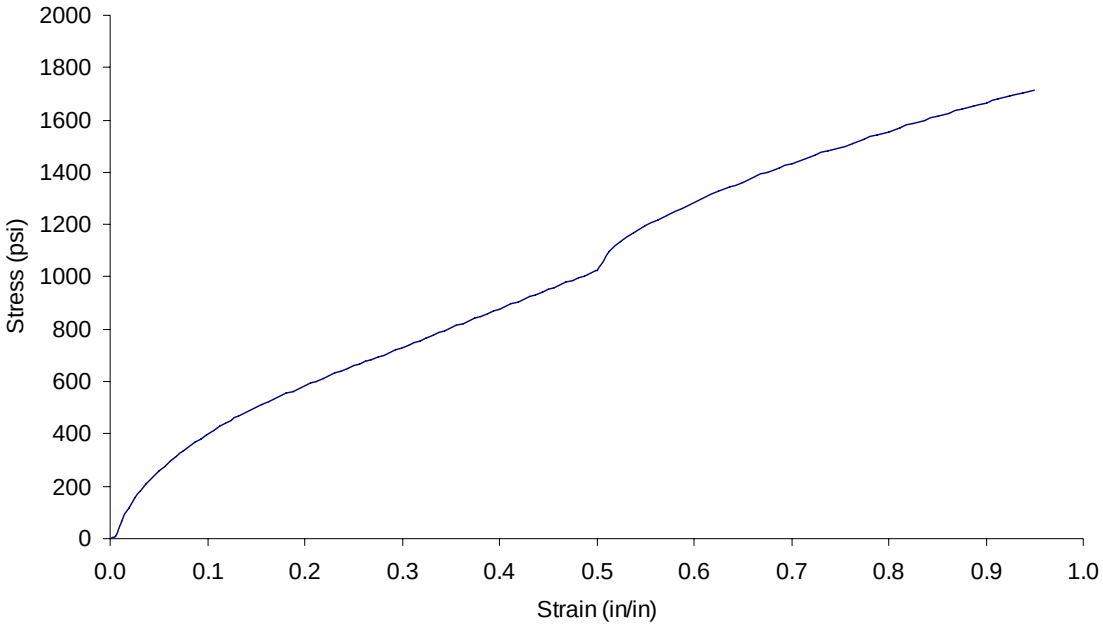

Figure A.5: Epoxy_T_5 Stress vs. Strain

Unreinforced Film Tensile Test Plots

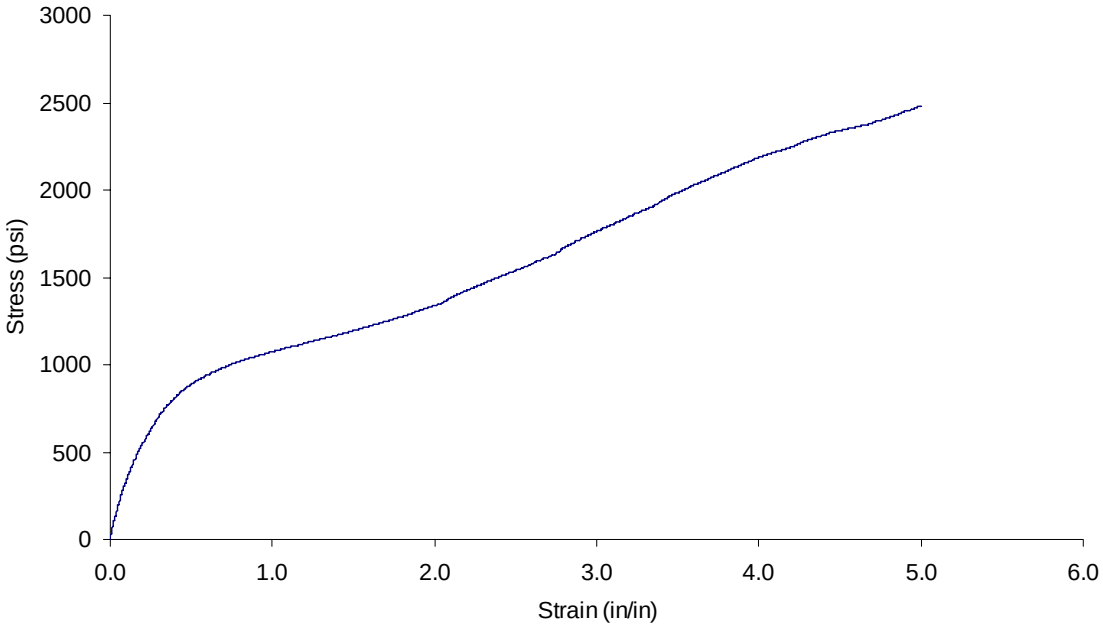

Figure A.6: UF_T_1 Stress vs. Strain

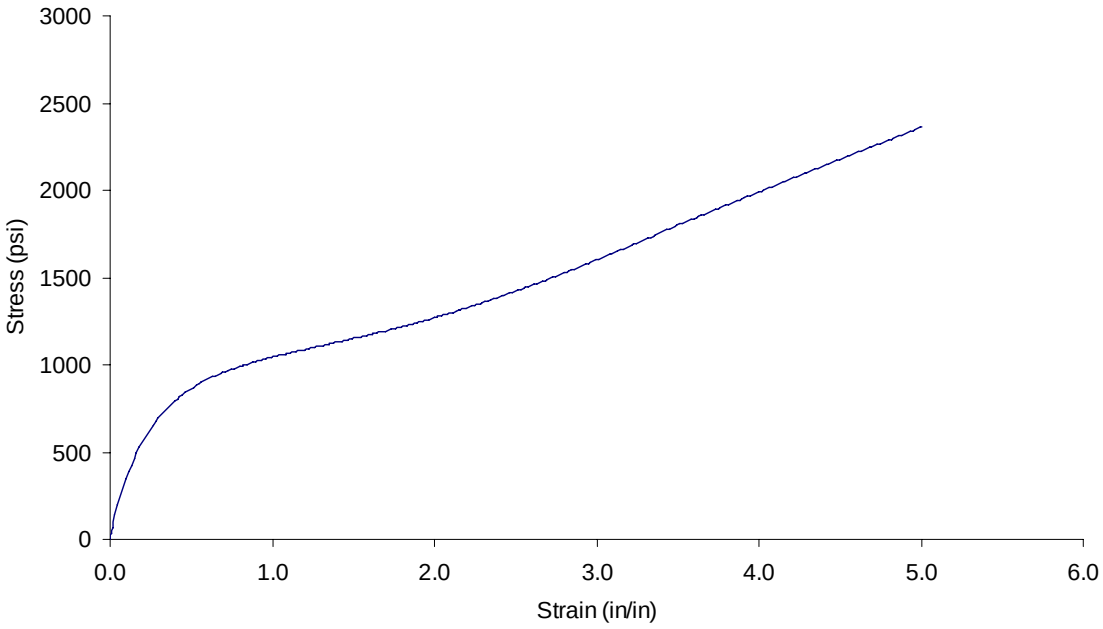

Figure A.7: UF_T_2 Stress vs. Strain

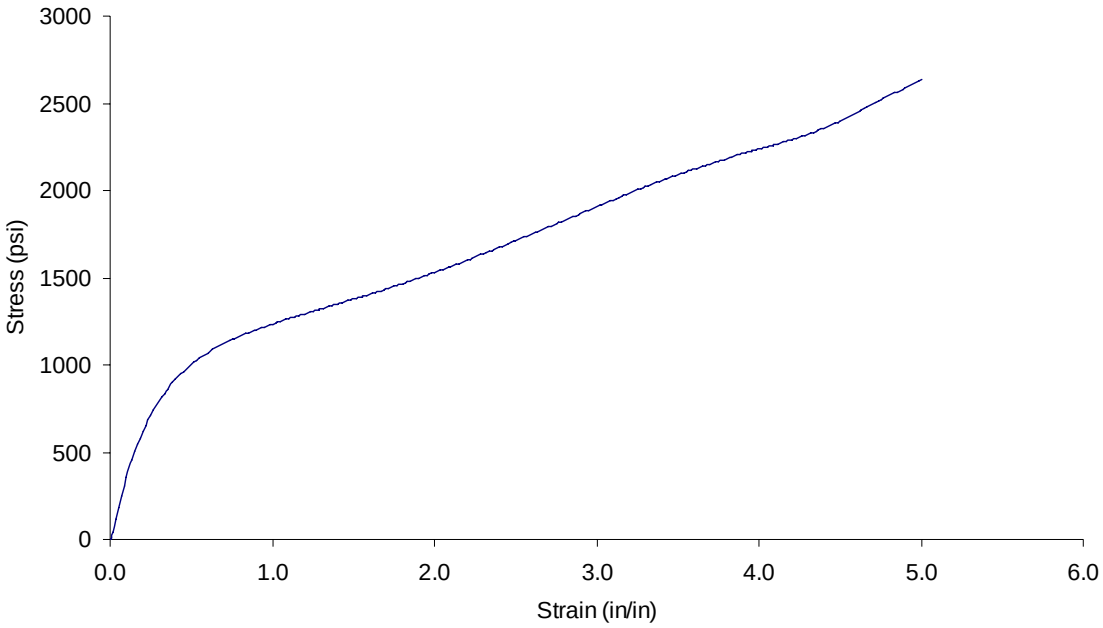

Figure A.8: UF_T_3 Stress vs. Strain

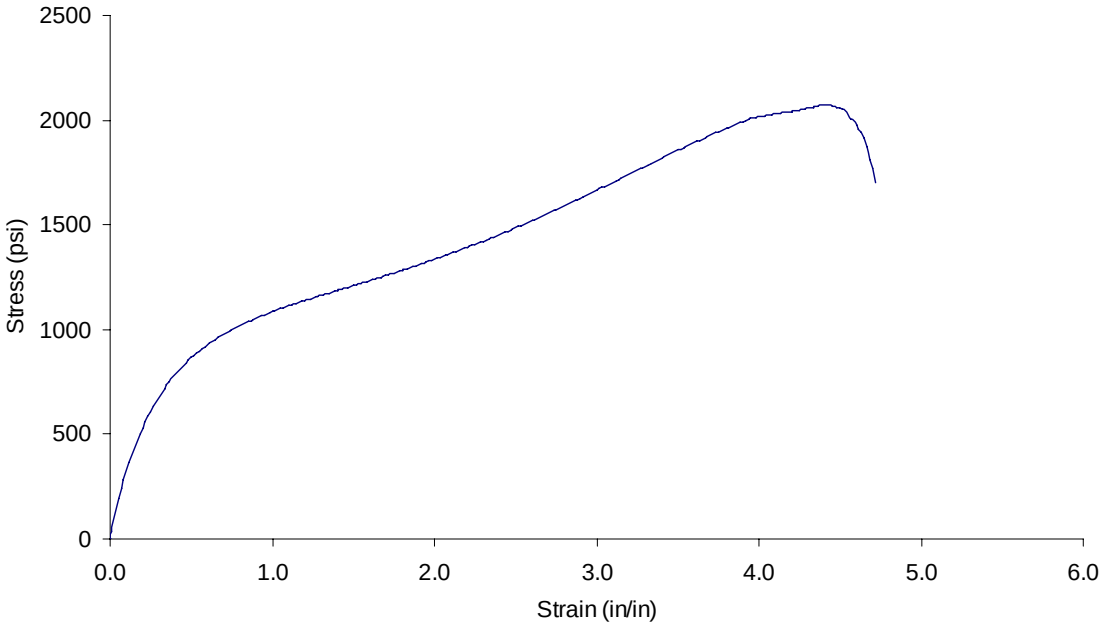

Figure A.9: UF_T_4 Stress vs. Strain

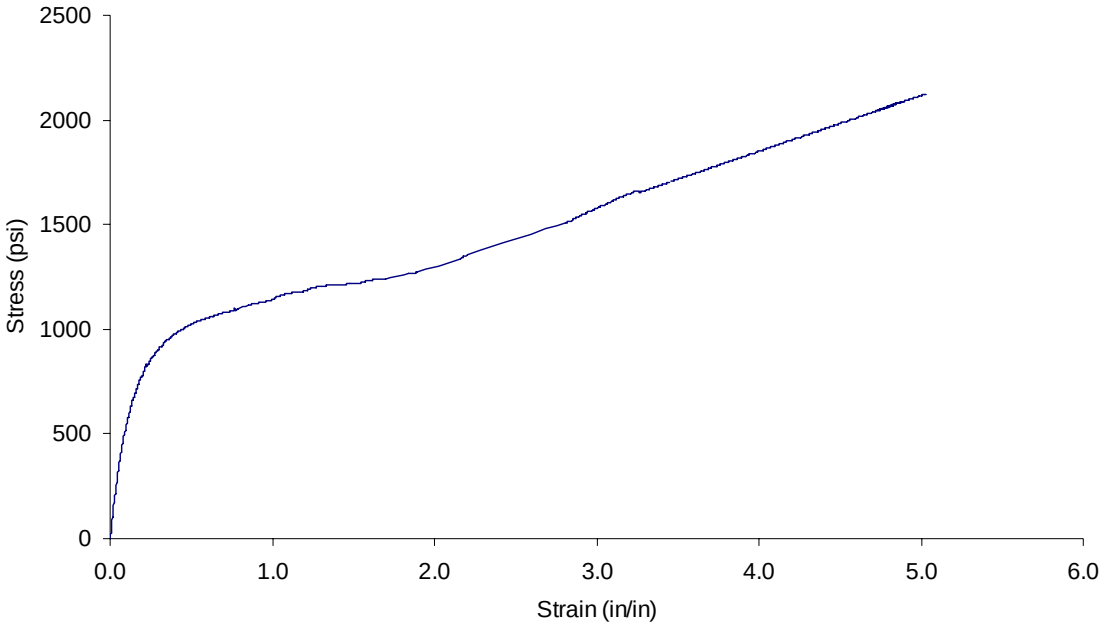

Figure A.10: UF_T_5 Stress vs. Strain

+/- 45° Reinforced Film Tensile Test Plots

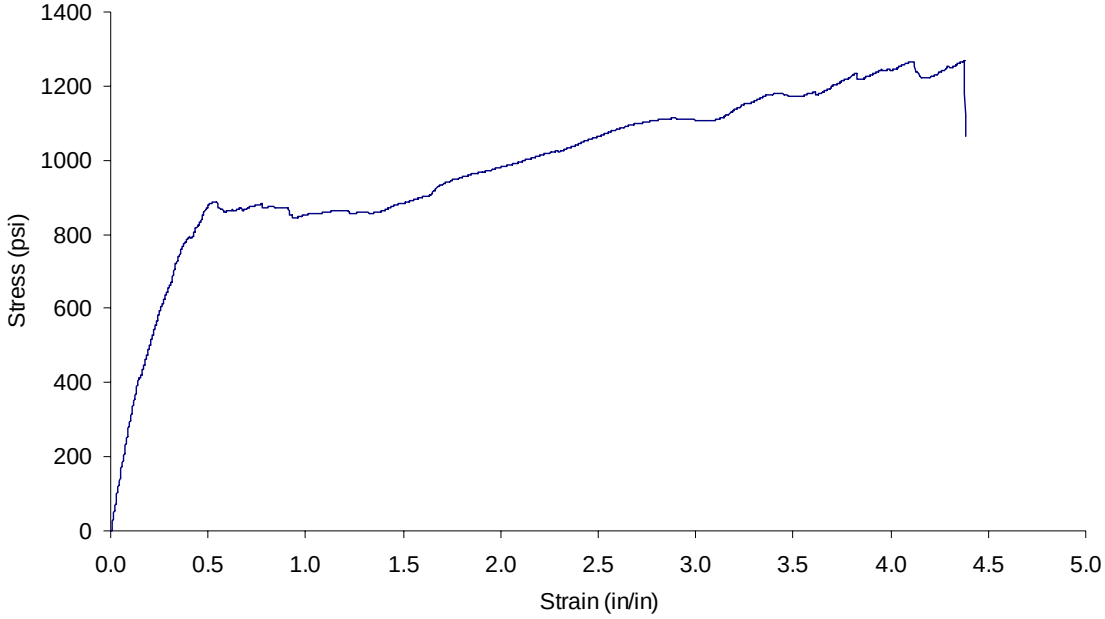

Figure A.11: +/-45°_T_1_2" Stress vs. Strain

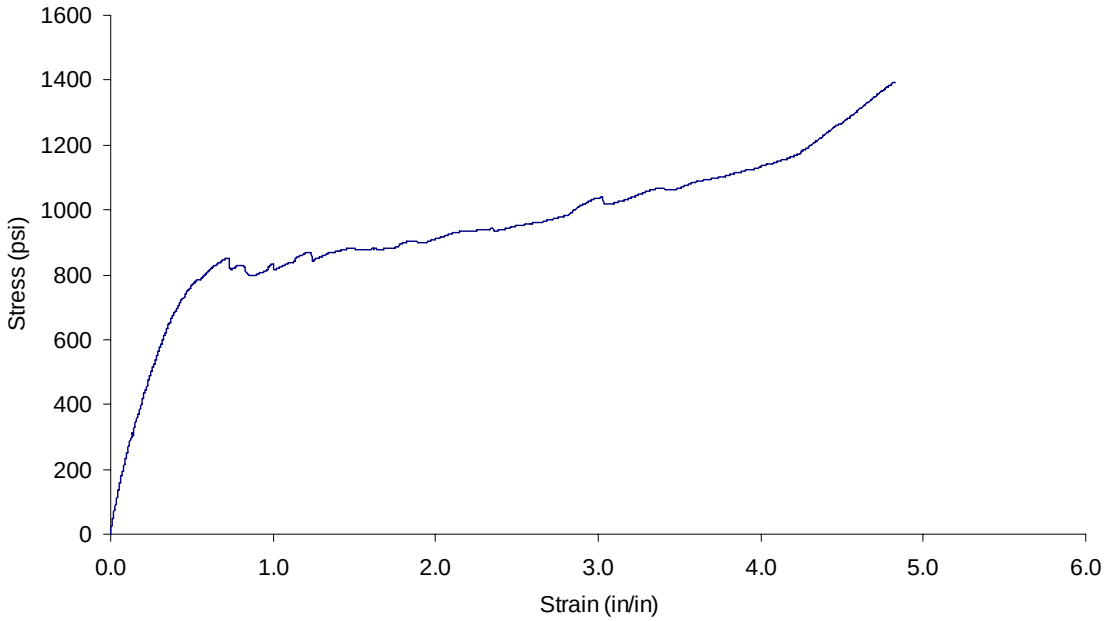

Figure A.12: +/-45°_T_2_2" Stress vs. Strain

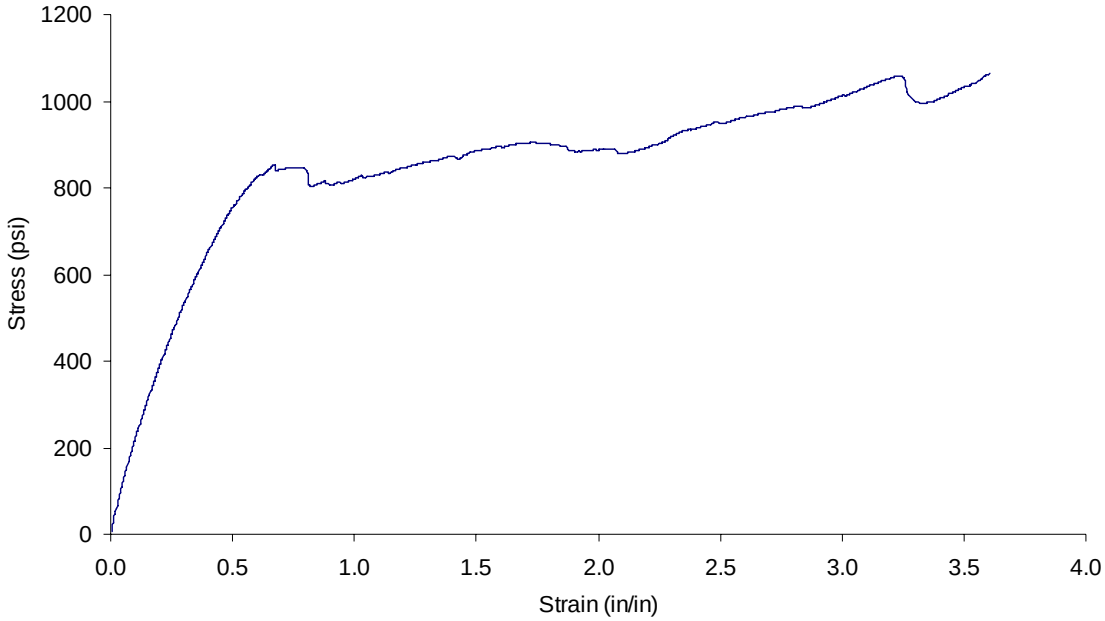

Figure A.13: +/-45° _T_3_2" Stress vs. Strain

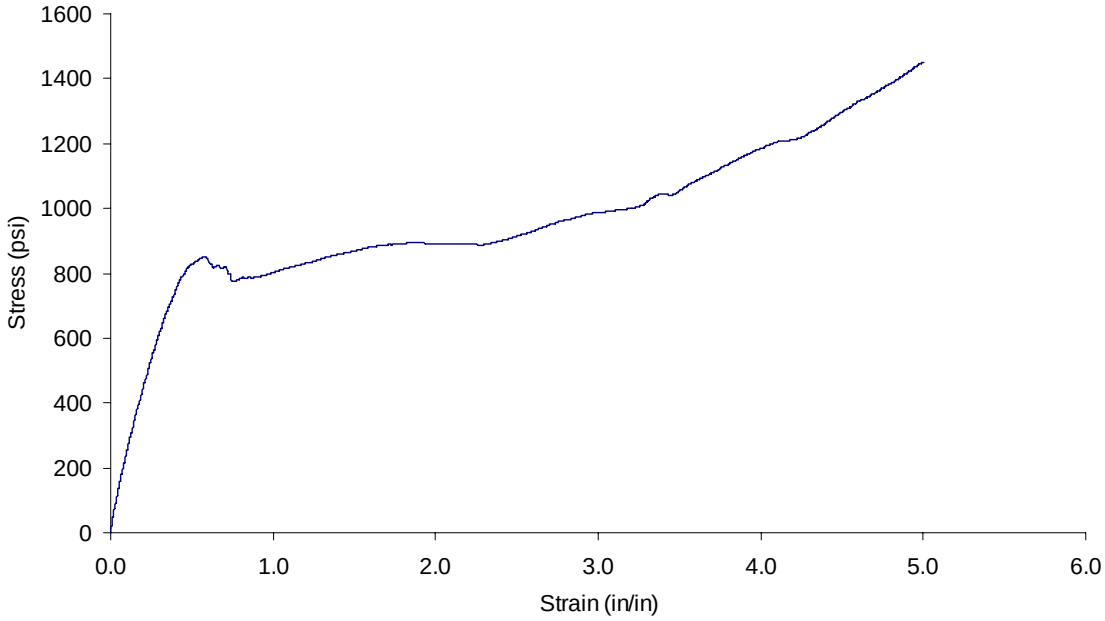

Figure A.14: +/-45° _T_4_2" Stress vs. Strain

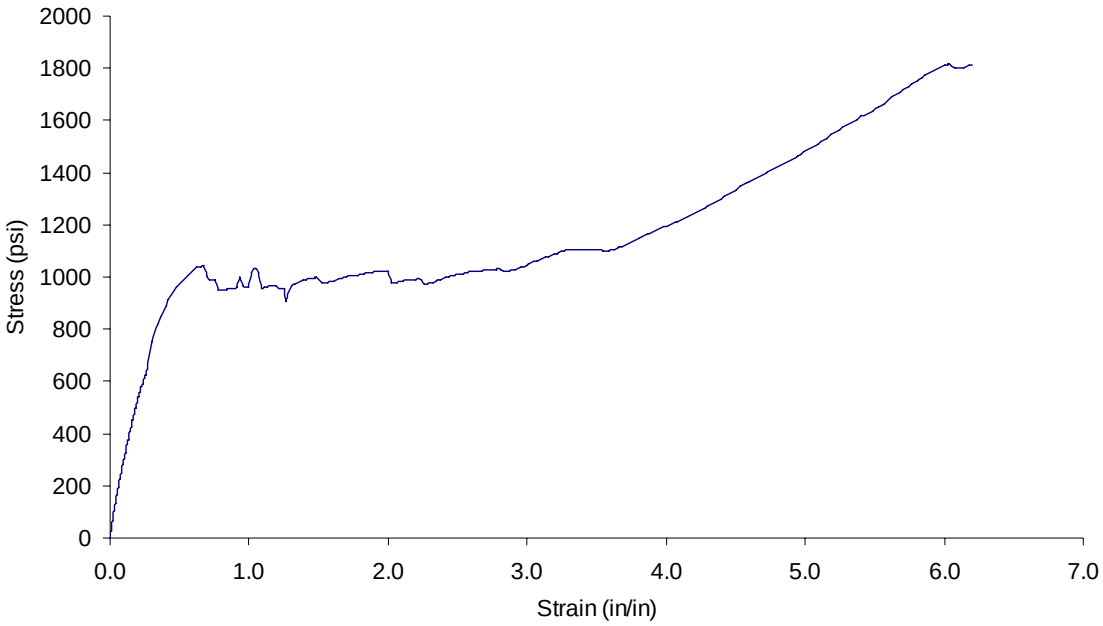

Figure A.15: +/-45° _T_5_2" Stress vs. Strain

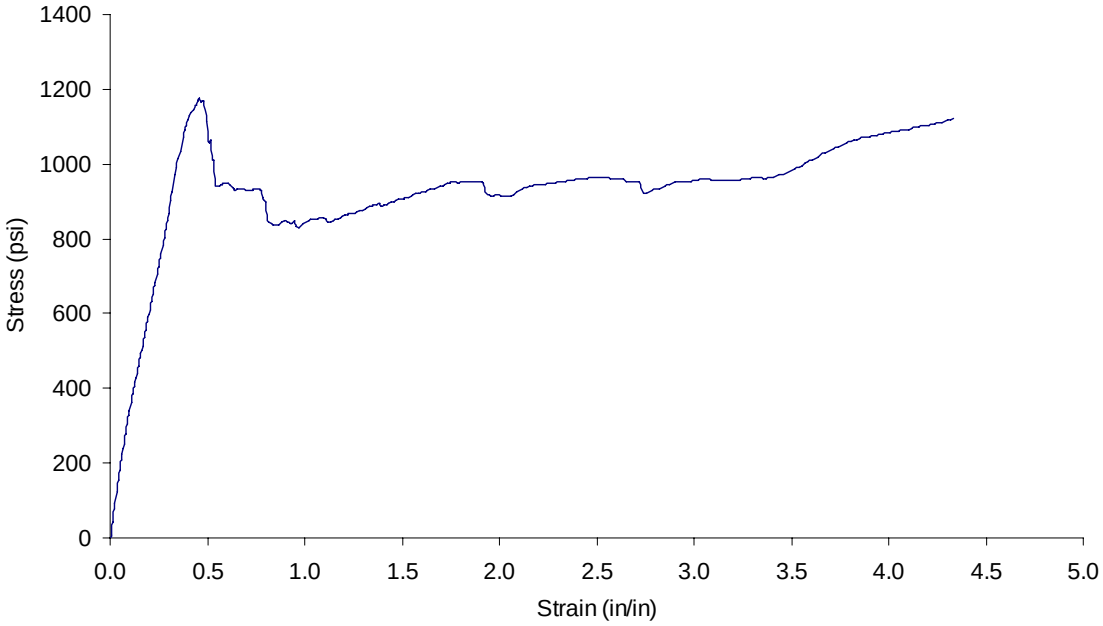

Figure A.16: +/-45° _T_1_3.5" Stress vs. Strain

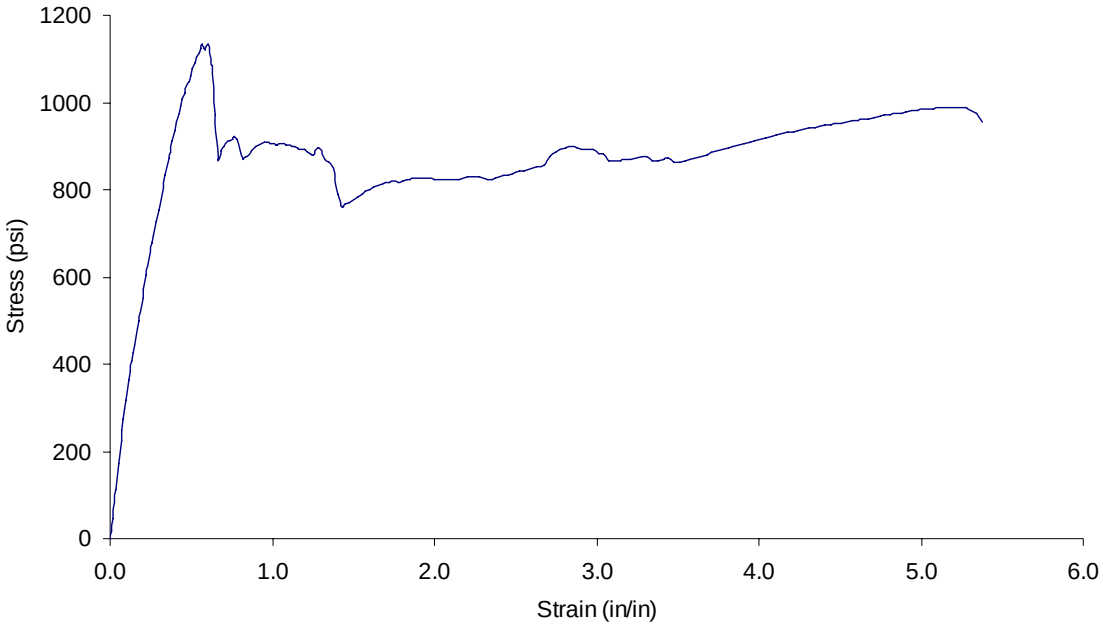

Figure A.17: +/-45° _T_2_3.5" Stress vs. Strain

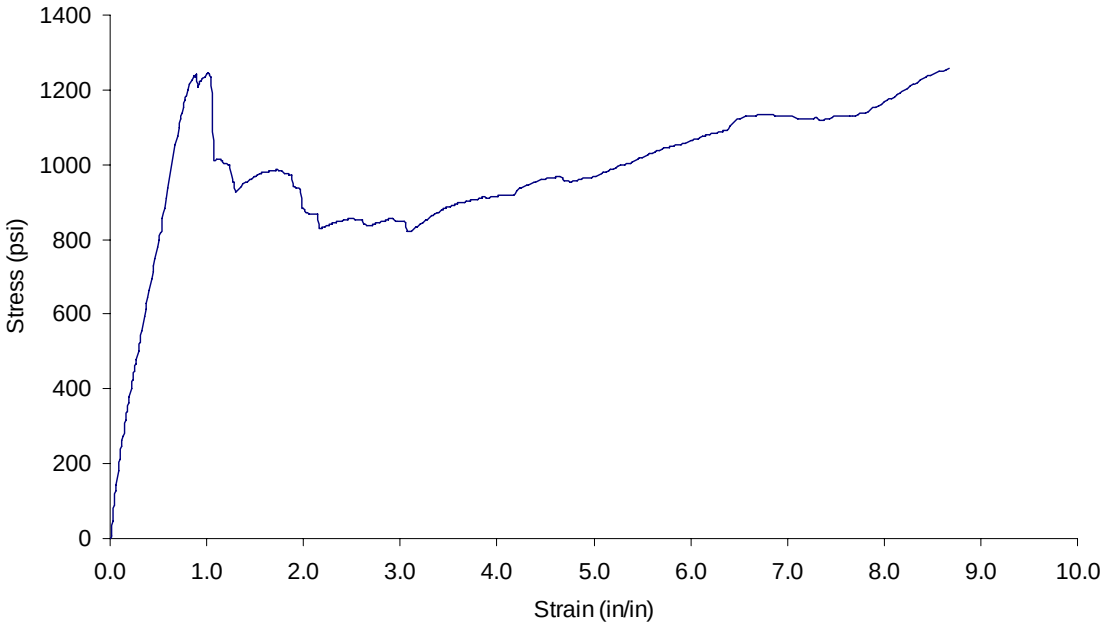

Figure A.18: +/-45° _T_3_3.5" Stress vs. Strain

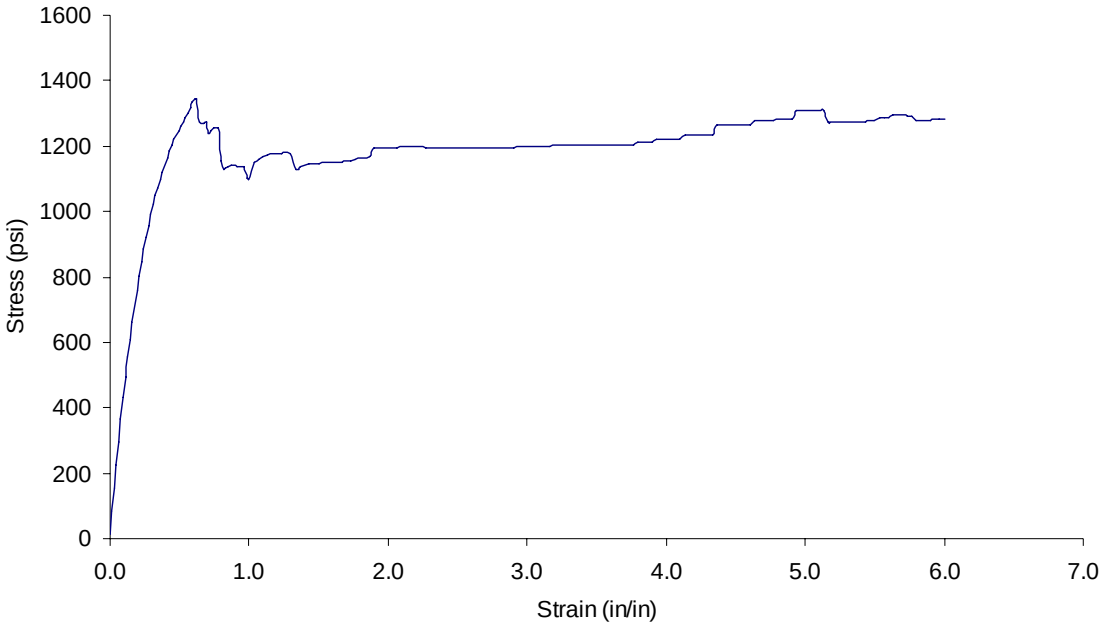

Figure A.19: +/-45° _T_4_3.5" Stress vs. Strain

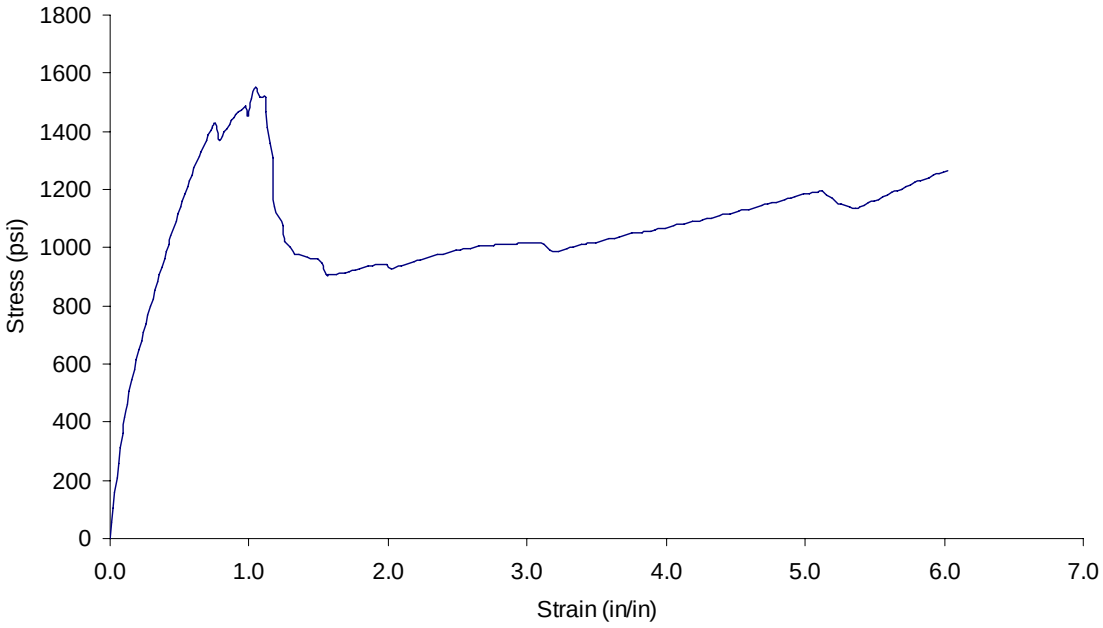

Figure A.20: +/-45° _T_5_3.5" Stress vs. Strain

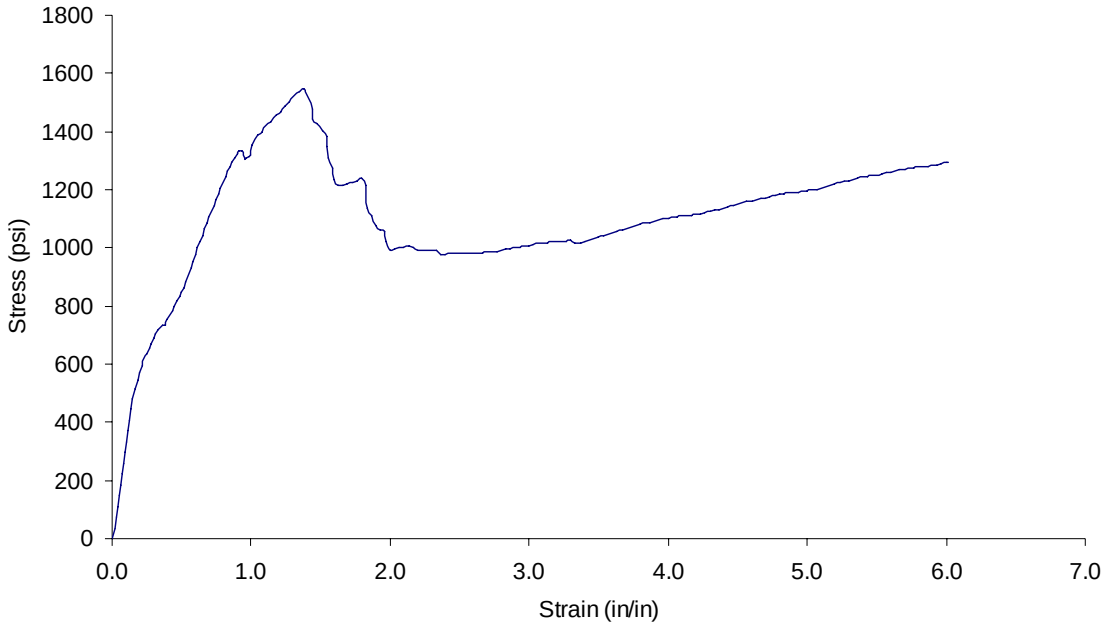

Figure A.21: +/-45° _T_1_5" Stress vs. Strain

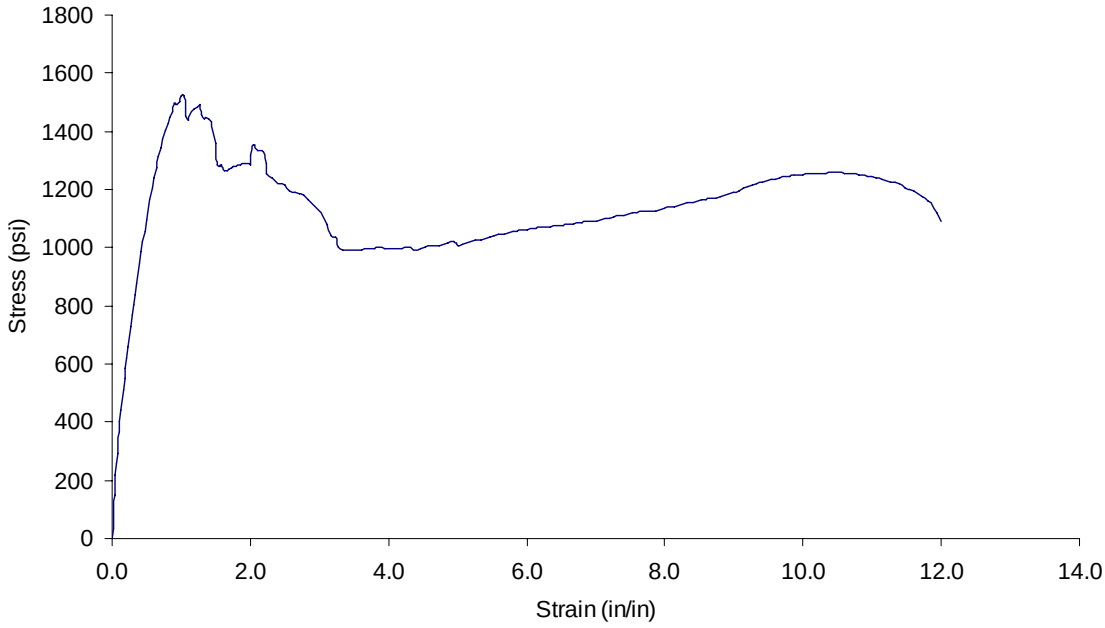

Figure A.22: +/-45° _T_2_5" Stress vs. Strain

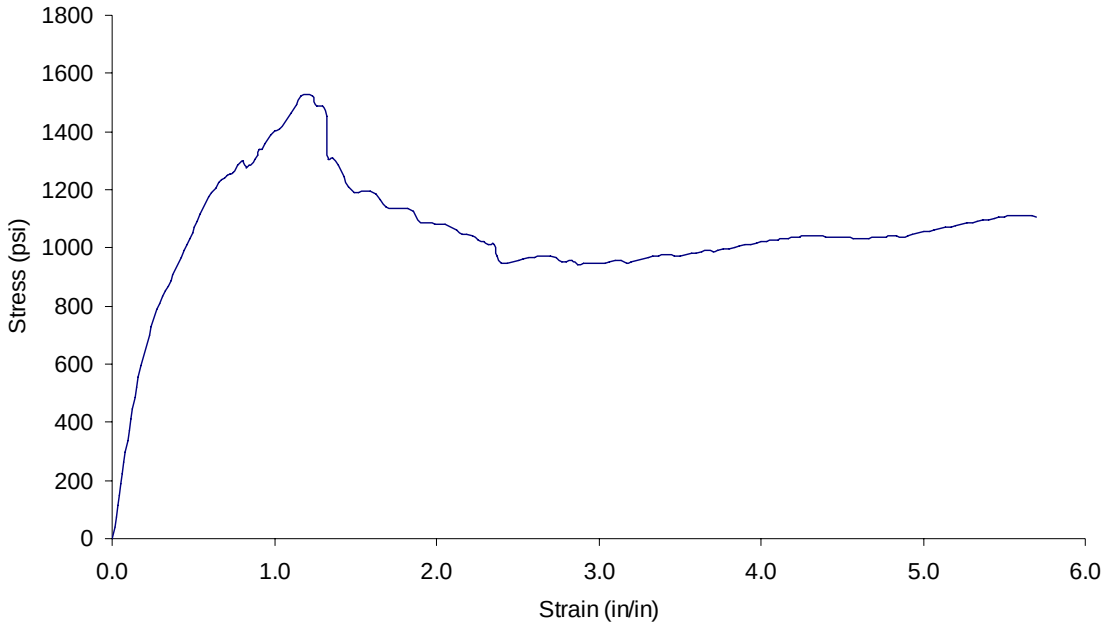

Figure A.23: +/-45° _T_3_5" Stress vs. Strain

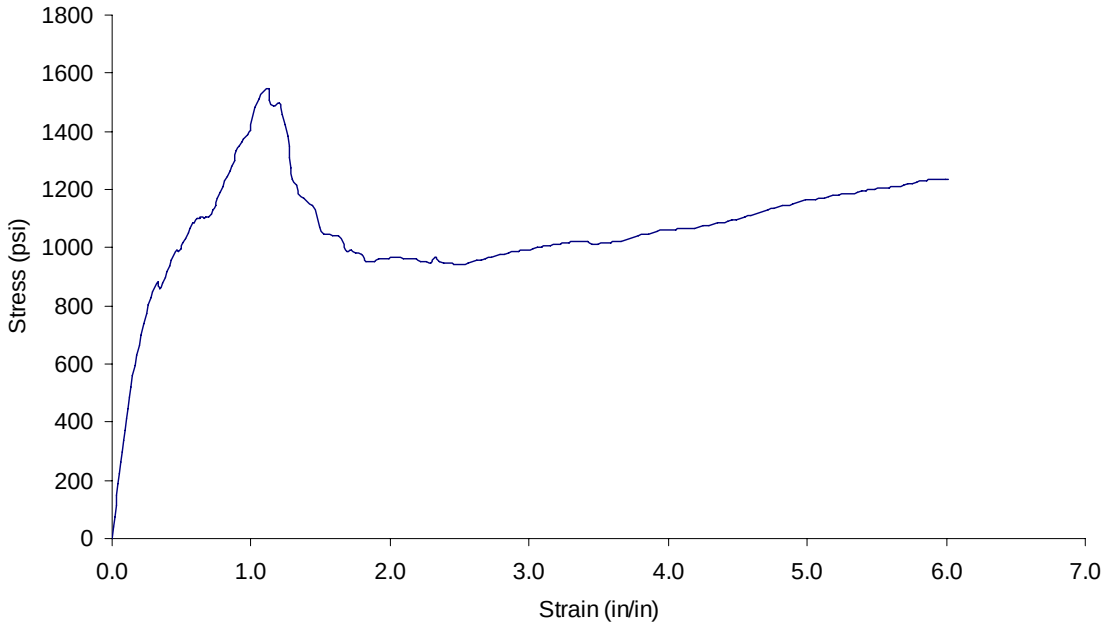

Figure A.24: +/-45° _T_4_5" Stress vs. Strain

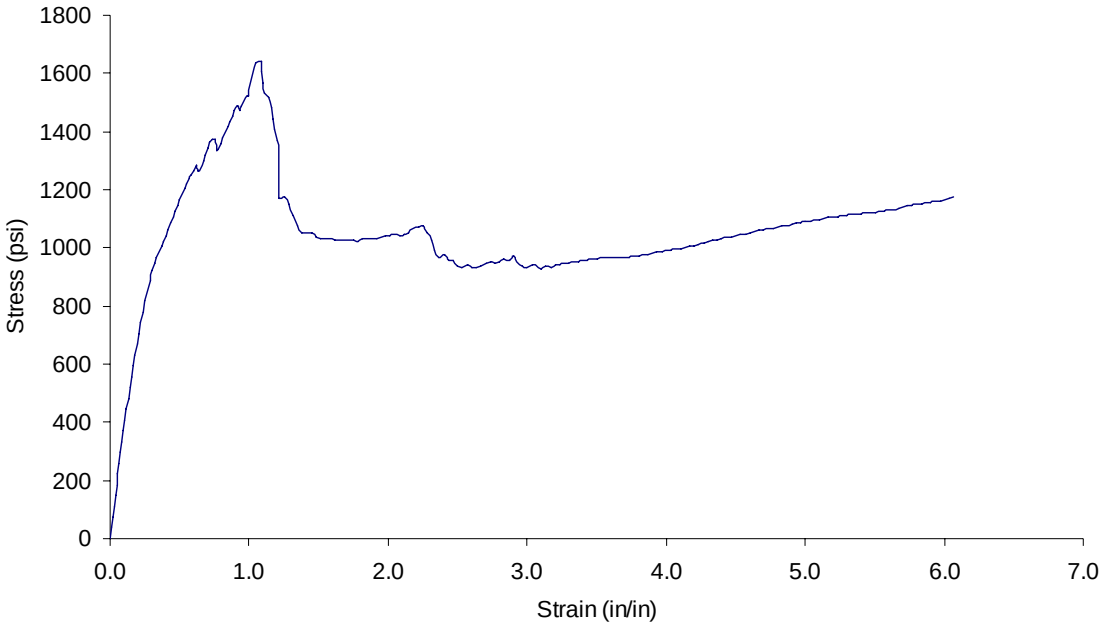

Figure A.25: +/-45° _T_5_5" Stress vs. Strain

0/90° Reinforced Film Tensile Test Plots

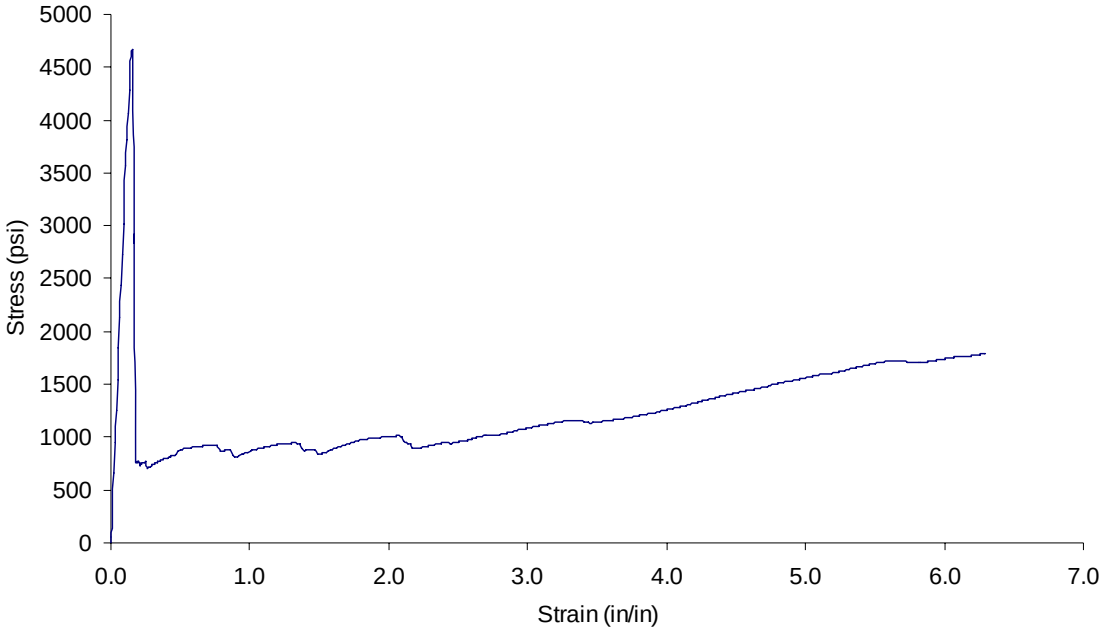

Figure A.26: 0/90°_T_1_2" Stress vs. Strain

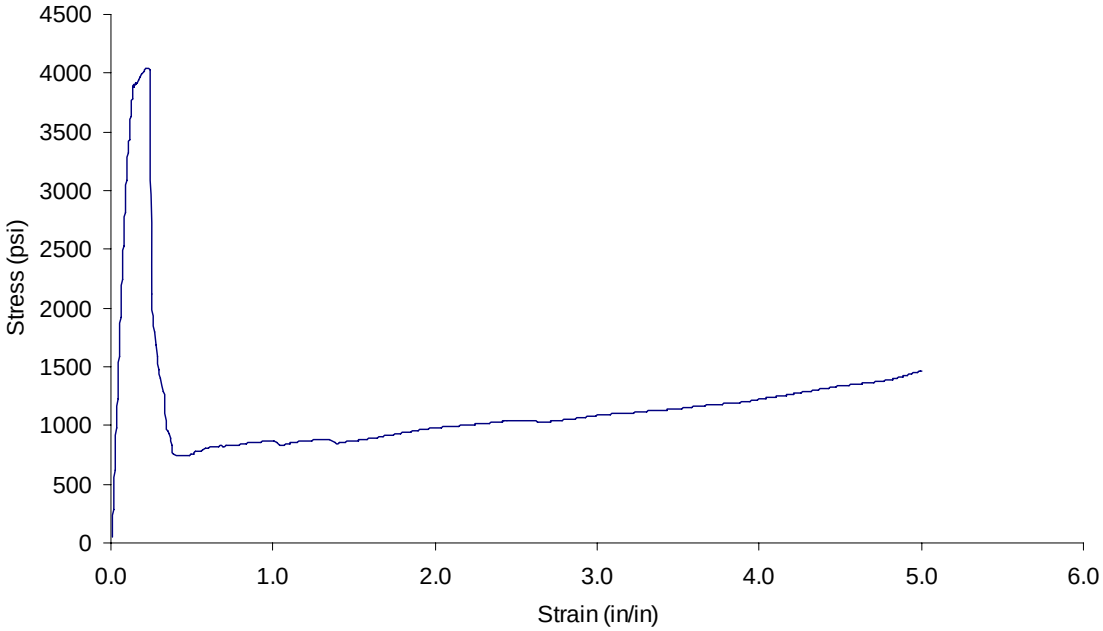

Figure A.27: 0/90°_T_2_2" Stress vs. Strain

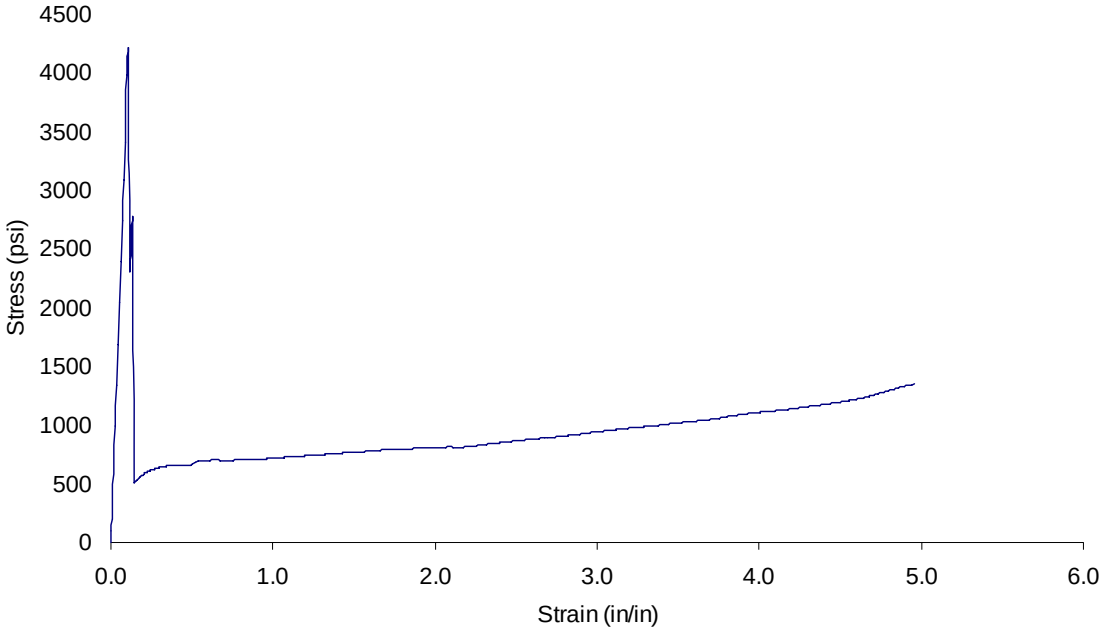

Figure A.28: 0/90° _T_3_2" Stress vs. Strain

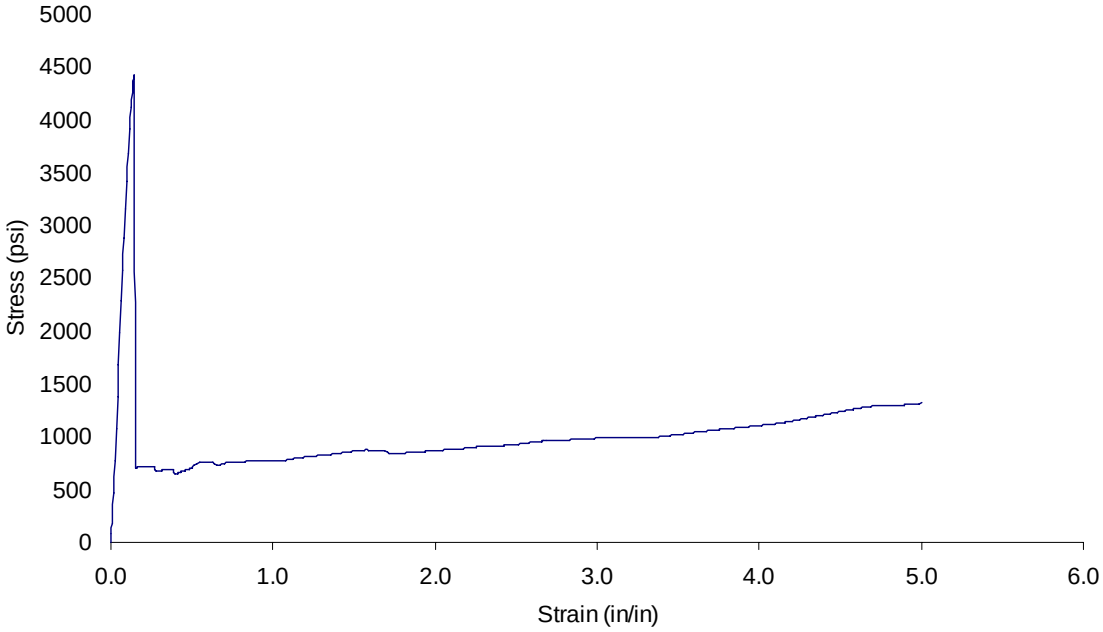

Figure A.29: 0/90° _T_4_2" Stress vs. Strain

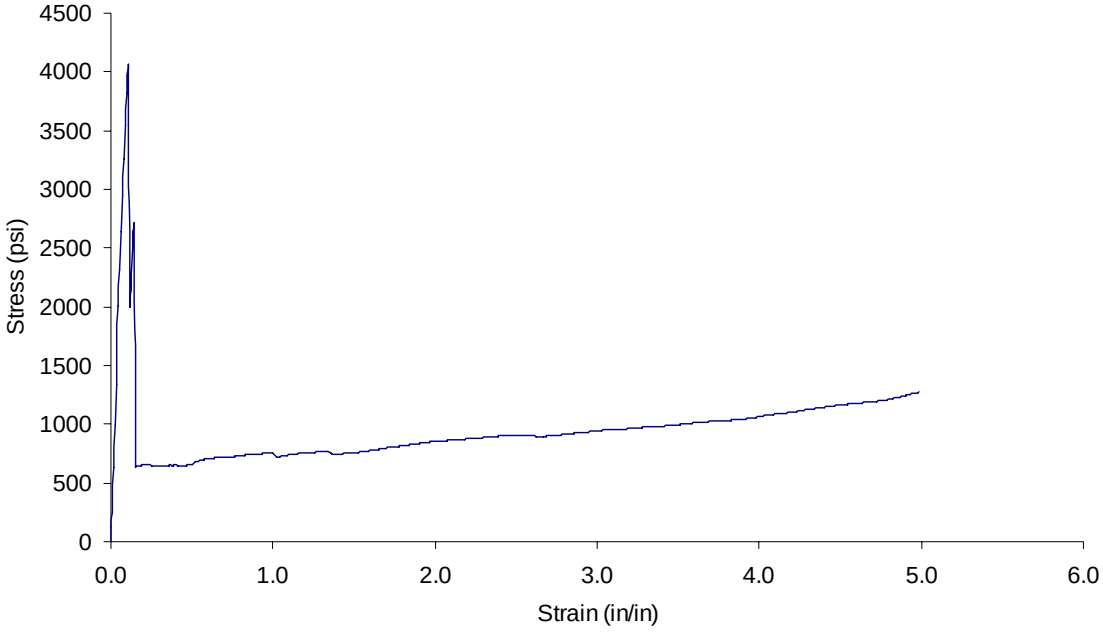

Figure A.30: 0/90° _T_5_2" Stress vs. Strain

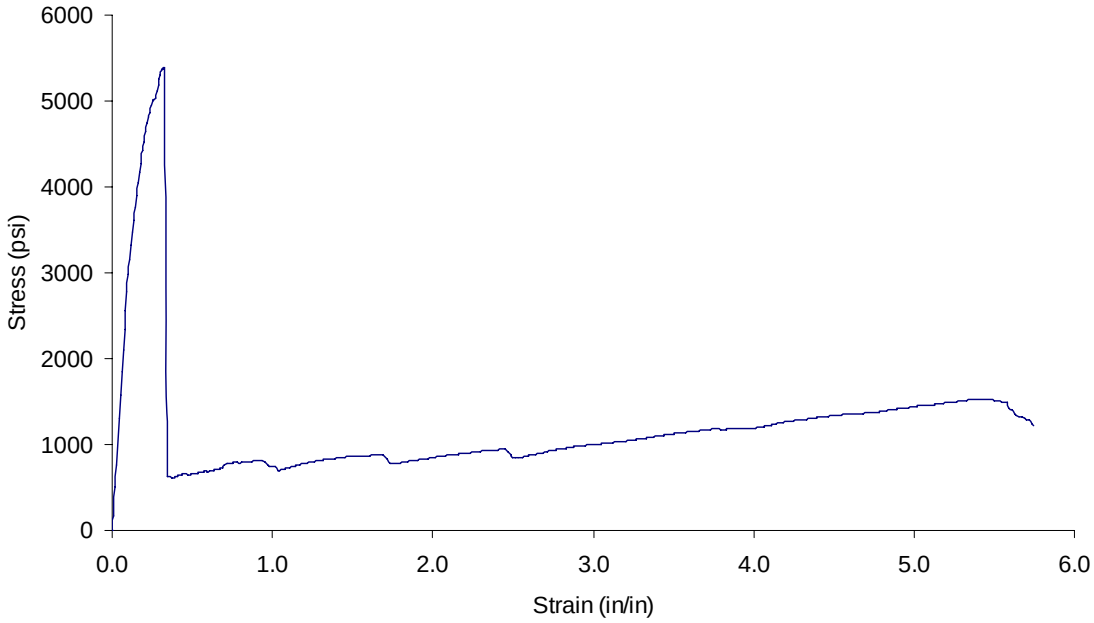

Figure A.31: 0/90° _T_1_1.5" Stress vs. Strain

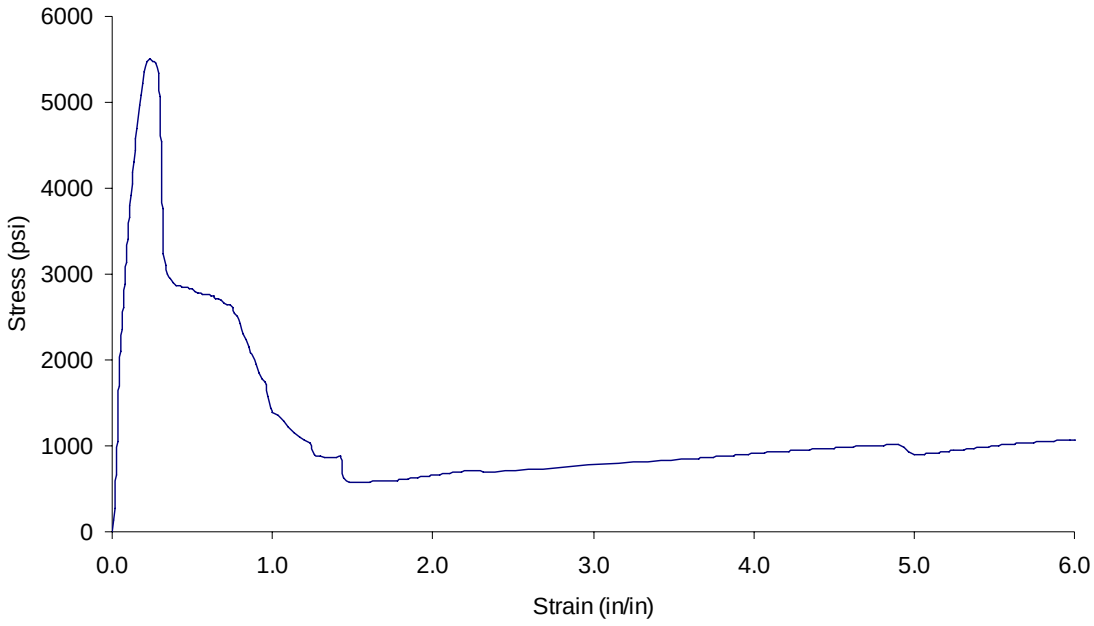

Figure A.32: 0/90˚_T_2_1.5" Stress vs. Strain

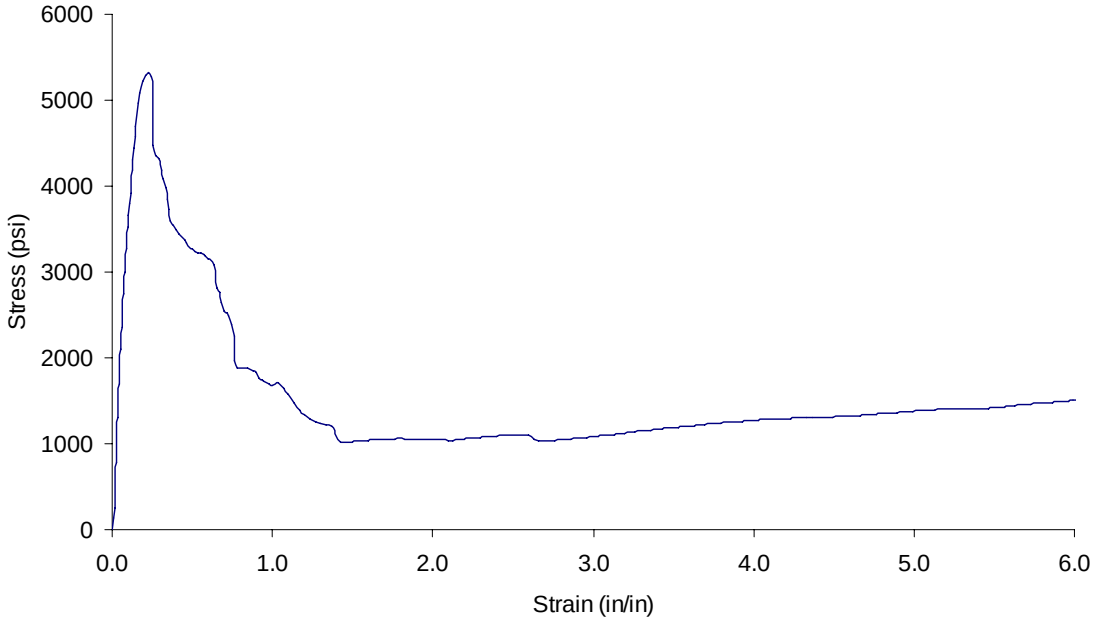

Figure A.33: 0/90˚_T_3_1.5" Stress vs. Strain

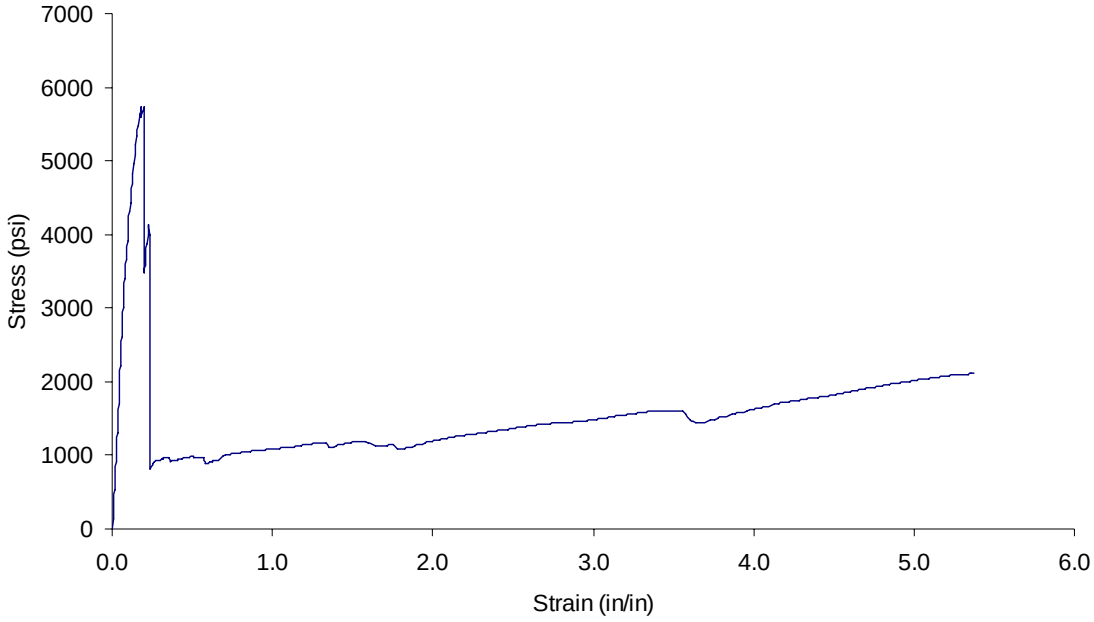

Figure A.34: 0/90˚_T_4_1.5” Stress vs. Strain

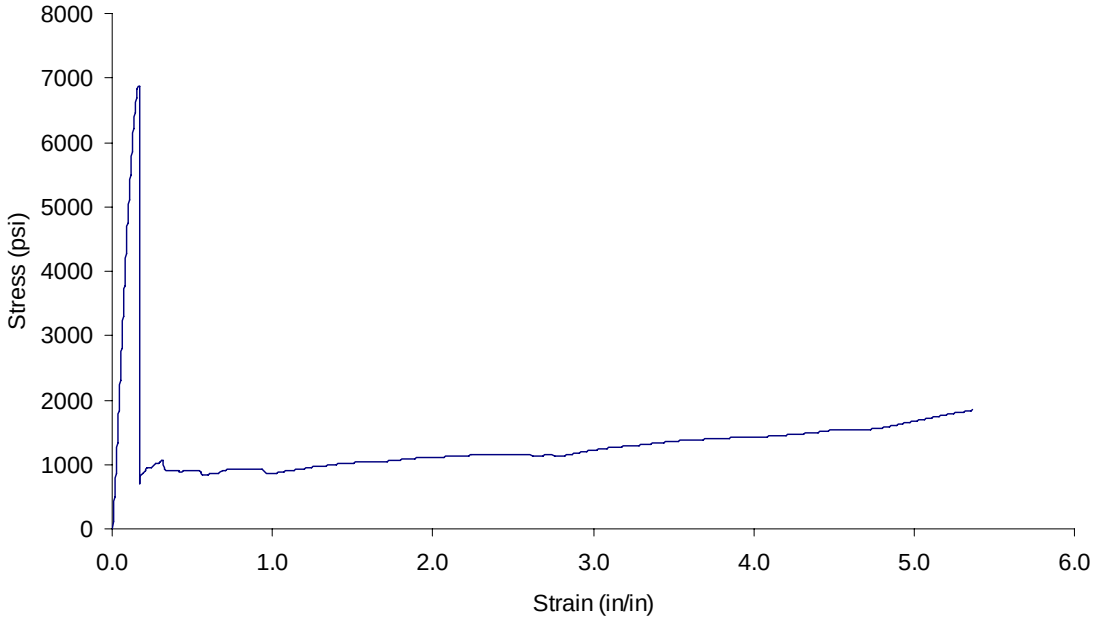

Figure A.35: 0/90˚_T_5_1.5” Stress vs. Strain

REFERENCES

ACI 530(2002), "Building Code Requirements for Masonry Structures," American Concrete Institute, Farmington Hills, MI, 50 pp.

ASTM C67, "Standard Test Methods for Sampling and Testing Brick and Structural Clay Tile, American Society for Testing and Materials.

ASTM C109, "Standard Test Methods for Compressive Strength of Hydraulic Cement Mortars, American Society for Testing and Materials.

ASTM D3039/D3039M-93, Standard Test Methods for Tensile Properties of Polymer Matrix Composite Materials, American Society for Testing and Materials.

ASTM D638, Standard Test Method for Tensile Properties of Plastics, American Society for Testing and Materials

Albert, Michael L., Elwi, A.E., and Cheng, J.J.R. (2001). "Strengthening of unreinforced masonry walls using FRPs." *Journal of Composites for Construction*, 5(2), 76-84

Almusallam, T.H., Al-Salloum, Y.A., Alsayed, S.H., Mosallam, A.S. (2001). "Behavior of unreinforced masonry walls (URM) strengthened with FRP composite materials." *International SAMPE Symposium and Exhibition (Proceedings)*, v 46 I, 473-484

Barbero, Ever J., Davalos, Julio F., Kiger, Sam A., and Shore, James S. (1997) "Reinforcement with Advanced Composite Materials for Blast Loads." *Proceedings of the 1997 Structures Congress – Building to Last*, v 1, 663-667

Crawford, John E., Malvar, Javier L., Wesevich, James W., Valancius, Joseph, and Reynolds, Aaron D. (1997) "Retrofit of Reinforced Concrete Structures to Resist Blast Effects." *ACI Structural Journal*, 94(4), Jul-Aug, 371-377

Davidson, James S., Porter, Jonathan R., Dinan, Robert J., Hammons, Michael I., and Connell, James D. (2004) "Explosive Testing of Polymer Retrofit Masonry Walls." *Journal of Composites for Construction*, 18(2), 100-106

Davidson, James S., Fisher, Jeff W., Hammons, Michael I., Porter, Jonathan R., and Dinan, Robert J. (2005) "Failure Mechanisms of Polymer-Reinforced Concrete Masonry Walls Subjected to Blast." *Journal of Structural Engineering*, 131(8), 1-12

Ehsani, M.R., Saadatmanesh, H., and Velazquez-Dimas, J.I. (1999). "Behavior of retrofitted URM walls under simulated earthquake loading." *Journal of Composites for Construction*, 3(3), 134-142

Erki, M.A. and Meier, U. (1999). "Impact Loading of Concrete Beams Externally Strengthened with CFRP Laminates." *Journal of Composites for Construction*, 3(3), 117-124

Fatt, M.S. Hoo, Ouyang, X., and Dinan, R.J. (2004). "Blast Response of Walls Retrofitted with Elastomer Coatings." *Structures and Materials*, v 15, *Structures under Shock and Impact VIII*, 129-138

Gilstrap, J.M., Dolan, C.W., and Christensen, J. Bradley. (1995). "Evaluation of Kevlar fabric reinforcement for masonry walls." *Proceedings of Engineering Mechanics*, v 1, 106-109

Gilstrap, J.M., and Dolan, C.W. (1998). "Out-of-Plane bending of FRP reinforced masonry walls." *Composites Science and Technology*, 58, 1277-1284

Hamilton, III, H. R. and Dolan, C. W. (2001). "Flexural Capacity of Glass FRP Strengthened Concrete Masonry Walls." *Journal of Composites for Construction*, 5(3), 170-178

Hamoush, Sameer A., McGinley, Mark W., Mlakar, Paul, Scott, David, and Murray, Kenneth (2001). "Out-of-Plane Strengthening of Masonry Walls with Reinforced Composites." *Journal of Composites for Construction*, 5(3), 139-145

Hutchinson, T.C., Nicolaisen, K.N., and Morrill, K.B. (2004). "Blast Retrofit Strategies for Masonry Walls: Exploratory Experimental Study." *Proceedings of the 2004 Structures Congress – Building on the Past: Securing the Future*, 175-182

Jerome, David M. and Ross, C. Allen (1996). "Dynamic Response of Concrete Beams Externally Reinforced with Carbon Fiber Reinforced Plastic (CFRP) Subjected to Impulsive Loads." *ASME, Pressure Vessels and Piping Division Publication*, v 325, *Structures under Extreme Loading Conditions*, 83-94

Jerome, David M. and Ross, C. Allen (1997). "Impact Response of Concrete Beams Externally Reinforced with Fiber Reinforced Plastics." *Proceedings from the 1997 Structures Congress – Building to Last*, v 1, 668-672

Johnson, Carol F., Slawson, Thomas R., and Cummins, Toney K. (2003). "Concrete Masonry Unit (CMU) Static and Dynamic Wall Experiments with Elastomeric Retrofits." US Army Engineer Research and Development Center (EDRC)

Mosallum, A., Haroun, M., Almusallam, T., Faraig, S. (2001). "Experimental Investigation on the Out-of-Plane Response of Unreinforced Brick Walls Retrofitted with FRP Composites." *Proceedings of SAMPE: Symposium and Exhibition*, 1364-1371

Muszynski, Larry C. and Purcell, Michael R. (2003). "Composite Reinforcement to Strengthen Existing Concrete Structures against Air Blast." *Journal of Composites for Construction*, 7(2), 93-97

Patoary, Kabir Md. Hossain and Tan, Kiang Hwee (2003). "Blast resistance of FRP-strengthened masonry walls." *Concrete*, June 2003, 38-39

Ross, C. Allen, Purcell, M.R., and Jerome, Elisabetta L. (1997) "Blast Response of Concrete Beams and Slabs Externally Reinforced with Fiber Reinforced Plastics (FRP)." *Proceedings from the 1997 Structures Congress – Building to Last*, v 1, 673-677

Scott, David W. and Mlakar, Sr., Paul F. (1998). "Dynamic Response of Concrete Members Externally Reinforced with Carbon-Fiber Reinforced Polymeric Materials."

Tan, Kiang Hwee and Patoary, M. K. H. (2004). "Strengthening of Masonry Walls against Out-of-Plane Loads Using Fiber-Reinforced Polymer Reinforcement." *Journal of Composites for Construction*, 8(1), 79-87

Triantafillou, T.C. (1998). "Strengthening of masonry structures using epoxy-bonded FRP laminates." *Journal of Composites for Construction*, 2(2), 96-104

Tumialan, Gustavo J., Nanni, Antonio, Galati, Nestore (2003) "Fiber-reinforced polymer strengthening of unreinforced masonry walls subject to out-of-plane loads." *ACI Structural Journal*, 100(3), May-June, 321-329

Tumialan, Gustavo J., Galati, Nestore, Nanni, Antonio (2003). "Field Assessment of unreinforced masonry walls strengthened with fiber reinforced polymer laminates." *Journal of Structural Engineering*, 129(8), 1047-1056

Ward, Stephen P. (2002) "Retrofitting Existing Masonry Buildings to Resist Explosions." *Masonry Construction the world of Masonry*, 15(12), 34-37